(445 G)
Geotectonics and Well Logging

4th year Geophysics

By:

Dr. Ismail Sayed Ahmed

Dr. Ahmed Mohammed Abdel Gawad

2022/2023

Part 1:

Geotectonics

By:

Dr. Ahmed Mohammed Abdel Gowad

Geotectonics: Introduction

1- Definition of the term geotectonics: What is geotectonics??

The word geotectonics is derived from two Greek words geo-earth, and tectonicon-to build. **Geotectonics** is the study of the geological structural forms of the earth crust and the tectonic movements creating them. In other words: it is the study of the mechanical processes in the Earth's crust and their results. Geotectonics is concerned with structures of deep-seated origin.

Geotectonics can be divided into:

1- Structural geotectonics:

- Studying the morphology of structural forms.
- Studying the mechanism of the development of structural forms.

2- Regional geotectonics:

- Studying the spatial distribution and history of structural forms, which is done by the methods and techniques of regional geological investigations.

3- General geotectonics:

- Studying the geotectonic cycles or stages: the cycles or stages of the development of the tectonic movements.
- Explaining the causes of the tectonic processes.

2-Historical background and the Continental Drift theory:

On the old times, scientists observed many criteria about the earth that needed to be explained:

1- Jigsaw-puzzle fit of the continental edges.

2- Fossil plants and animals are extraordinarily similar across the globe

3- Sequences of rock formations in distant continents are also strikingly alike.

4- Paleoclimate change

5- Earthquakes and volcanoes are concentrated into specific locations.

6- How mountains are formed

At the turn of the 20th century, Austrian geologist Eduard Suess proposed the **theory of Gondwanaland** to account for these similarities: that a giant supercontinent (Gondwanaland)

had once covered much or all of Earth's surface before breaking apart to form continents and ocean basins. A few years later, German meteorologist **Alfred Wegener** suggested an alternative explanation: **continental drift.** Wegener realized that paleoclimate change could be explained if continents had migrated across climate zones and the reconfiguration of land masses altered Earth's climate patterns. Bringing together a large mass of geologic and paleontological data, Wegener postulated that:

1. Throughout most of geologic time there was only one supercontinent called **Pangea** (All-Earth in Greek) and one ocean called **Panthalassa** (All-Sea).
2. Late in the Jurassic, Pangea fragmented, and the parts began to move away from one another, forming two large continents; **Laurasia** in the north and **Gondwana** in the south.
3. Two oceans were also formed, the Panthalassic ocean to the west and the **Tethys Ocean** to the East.
4. Drifting and fragmenting continued. The westward drift of the Americas opened the Atlantic Ocean, and the Indian block drifted across the Equator to merge with Asia. The northward drifting of Africa closed the Tethys Ocean forming the Tethys Sea and opened the Indian ocean.
5. This continued until formed the modern-day continents and oceans. The Mediterranean Sea is the remain of the Tethys Sea.

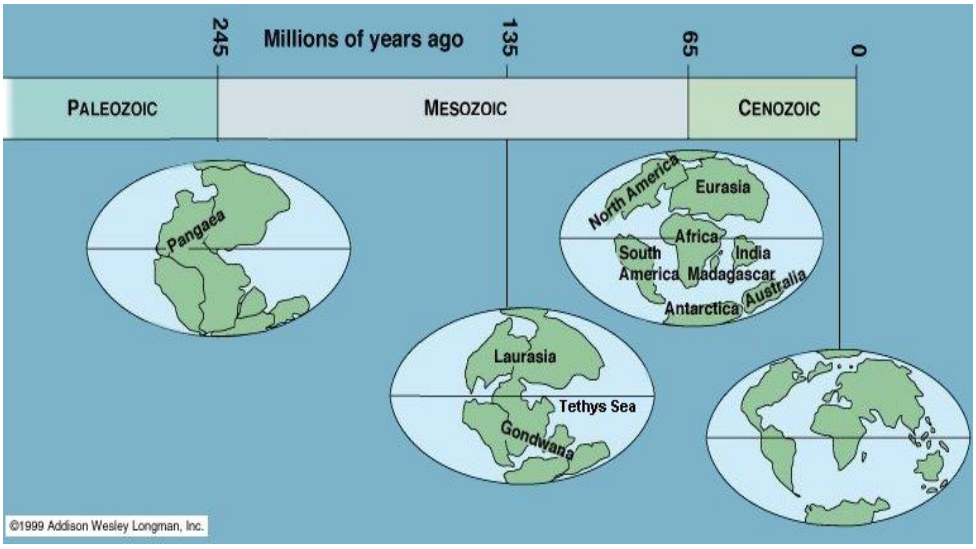

Figure 1: Schematic diagram of the continental drift theory.

In the beginning, Wegner's theory was rejected due to the following reasons:

- The theory didn't explain the powers that moved the continents and how they moved.

- The theory didn’t account for Pratt’s hypothesis of Isostacy adopted by the Americans. Isostasy or isostatic equilibrium is the state of gravitational equilibrium between Earth's crust (or lithosphere) and mantle such that the crust "floats" at an elevation that depends on its thickness and density. There are two theories were made to explain the isostacy: Pratt’s and Airy’s theories (Figure 2). In Pratt's theory, there are lateral changes in rock density across the lithosphere. Assuming that the mantle below is uniformly dense, the less dense crustal blocks float higher to become mountains, whereas the denser blocks form basins and lowlands (high density compensate for low topography and vise versa). On the other hand, Airy's theory assumes that across the lithosphere, the rock density is approximately the same, but the crustal blocks have different thicknesses. Therefore, higher mountains also extend deeper roots into the denser material below and oceans have anti-roots. So, if continental drift were true, then the large compressive forces involved would squeeze the crust to generate thickness differences, ultimately ending up with the Airy version of isostasy.

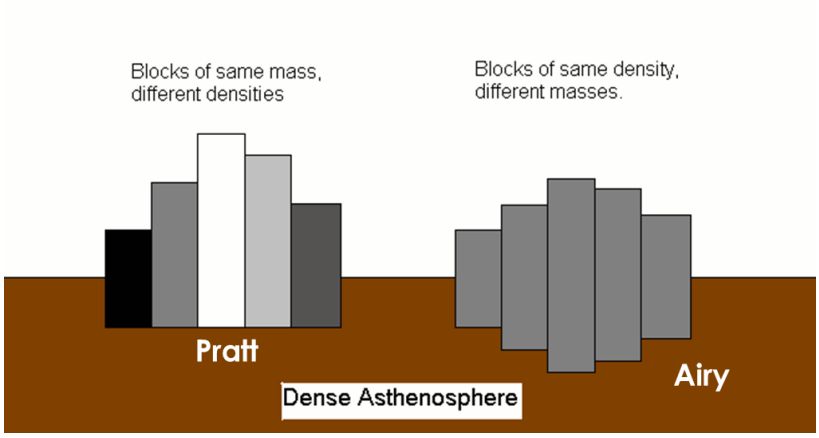

Figure 2: An illustration of Pratt and Airy's theories of isostacy.

- The concept of uniformitarianism. Uniformitarianism was the principle, articulated most famously by British geologist Sir Charles Lyell (1797-1875), that the best way to understand the geological record was by reference to presently observable processes (The present is the key to the past). According to drift theory, however, continents in tropical latitudes did not necessarily have tropical faunas, because the reconfiguration of continents and oceans might change matters altogether. Wegener's theory raised the specter that the present was not the key to the past.

To solve the problem of the forces that causes the continents to drift, the British geologist Arthur Holmes (1890-1965) suggested that the substrate was partially molten (plastic). If it

was plastic, then continents could move within it by convection currents in the mantle (Figure 3).

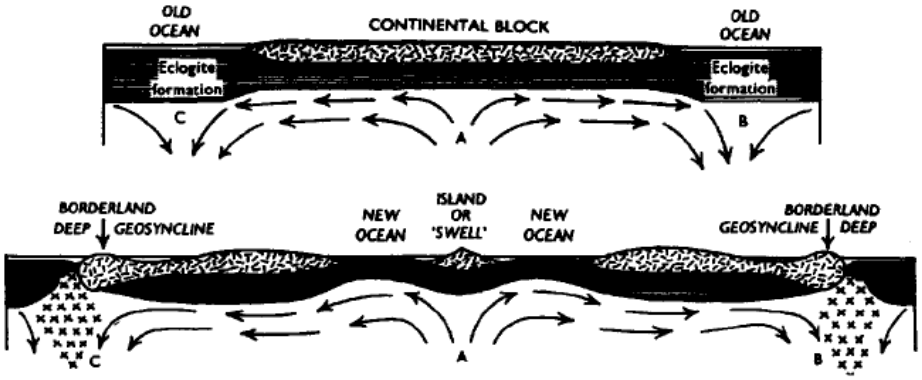

Figure 3: Holmes' model of the convection currents in the mantle.

3- The role of geophysics in supporting the continental drift and the origin of the plate tectonic theory:

A- Gravity anomalies:

Earlier gravity measurements demonstrated an association between negative gravity anomalies (lower gravity values than the surroundings) and regions where the ocean was particularly deep (trenches). These negative gravity anomalies indicated some form of crustal disturbance or deformation, and thus are interpreted to mean that the segments of the lithosphere that underlie trenches are being forced down against buoyant isostatic forces (Figure 4). Apparently, the ocean basins were not static, but actively deforming, at least in certain zones. This was interpreted as that convection currents might be dragging the crust downward into the denser mantle below.

B- Seismology:

This interpretation of gravity data is substantiated by seismological studies. All trenches are associated with zones of earthquake foci. It was found that earthquakes occur close to the trenches, at shallower depths of 55 km or less. With increased distance away from the trenches, earthquakes occur at greater and greater depths—500 km or more. Seismic foci thus define tabular zones approximately 20 km thick that dip landward at about 45° beneath the continents (Figure 5). Analyses of these seismic zones and of individual earthquakes suggest that the seismicity results from the slippage of a lithospheric plate with its associated crust into the asthenosphere.

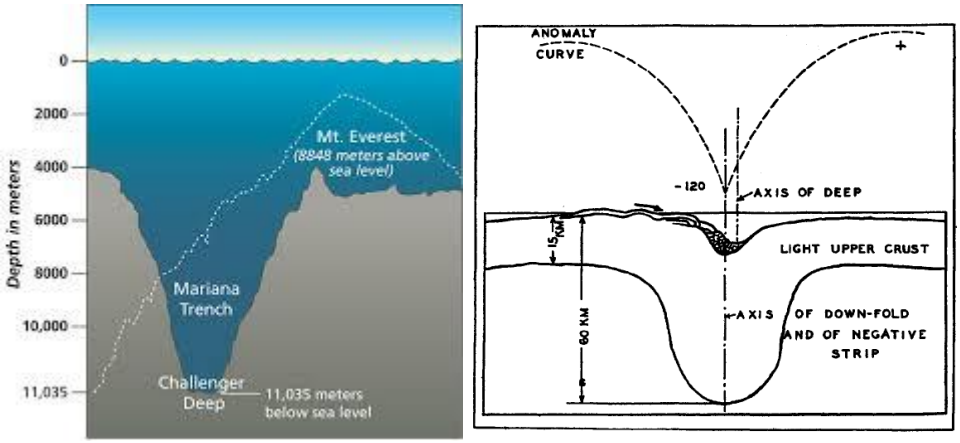

Figure 4: The negative gravity anomalies measured above oceanic trenches.

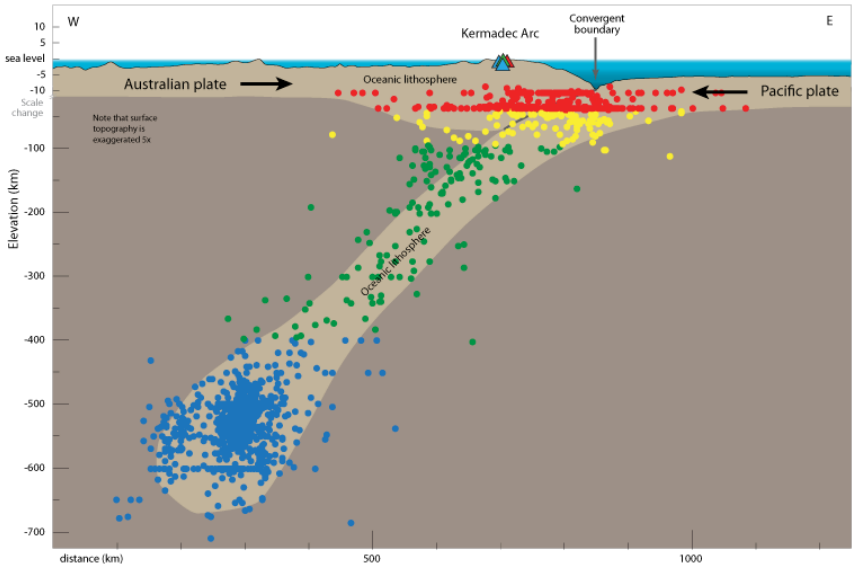

Figure 5: The distribution of earthquake foci along the subducted slab.

C- Paleomagnetism and heat flow studies:

The history of variations in the magnetic field might be recorded in rock by the property of **remanent magnetism**—the rock keeps the properties of the magnetic field even after the removal of the magnetic field. In the early 20th century, Pierre Curie had discovered that rocks cooled in a magnetic field take on the polarity of that field (the temperature at which this occurs eventually became known as the Curie point). Therefore, if the magnetic field varied, these variations might be recorded in rocks, particularly volcanic rocks at the time of their formation. So, remanent magnetism held a record of the variations in the earth's magnetic field, and that these variations showed that rocks had not remained stationary relative to Earth's magnetic field over the course of geological history. This assumption suggests that

the land masses had moved relative to the poles (continental drift). The paleomagnetic data were considered as evidence for continental drift.

In addition, magnetic field reversal also supported the idea and become a key factor in proving the continental drift through paleomagnetic studies. Earth's magnetic field periodically reversed its polarity. A distinctive pattern of normal and reversely magnetized rocks represented anomalies formed a series of stripes, roughly parallel to the shoreline. Published in black and white, they looked a bit like zebra stripes. Magnetic reversals plus sea floor spreading added up to a testable hypothesis; if the sea floor spreads while Earth's magnetic field reverses, then the basalts forming the ocean floor will record these events in the form of a series of parallel "stripes" of normal and reversely magnetized rocks. This anomaly pattern is called **magnetic zebra pattern** (Figure 6).

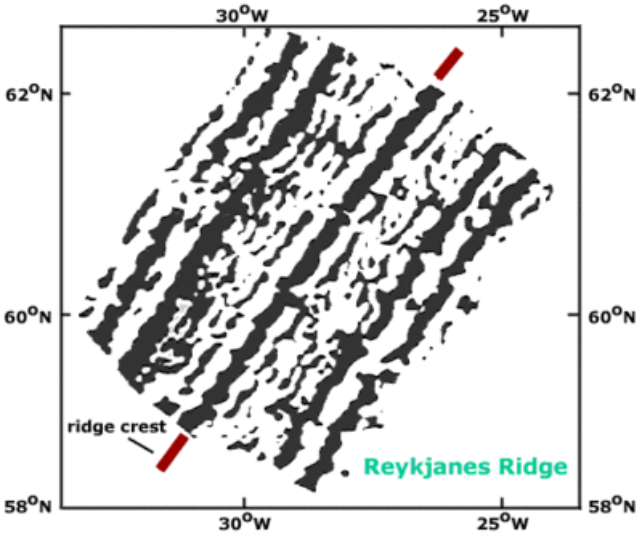

Figure 6: Map of magnetic anomalies in the ocean just south of Iceland. Positive anomalies, where the magnetic field is stronger than average, are marked black while negative anomalies, where the field is weaker, are white. The axis of the mid-Atlantic ridge, here known as the Reykjanes Ridge, is marked in red. Note that the striped pattern is roughly symmetrical about the ridge.

D- Bathymetric studies:

Other studies focused on bathymetric data—measurements of the depth of the sea floor. These measurements were used to create a **physiographic map**, a map of what the sea floor would look like drained of water, based on quantitative measurements. This map revealed the most important feature: a mountain chain running down the middle of the ocean floor, crosscut by an enormous series of east-west fractures that dislocated the ridge all along its length. A fracture zone also ran down the middle of the mid-ocean ridge, and the geologists noted that the shape of this central fracture zone suggested it was a rift, a place where the ocean floor was being pulled apart (Figure 7). Accordingly, the sea floor was split down the middle, the two sides were moving apart, and the rocks on either side preserved a symmetrical pattern of the periodic reversals of Earth's magnetic field (Figure 8).

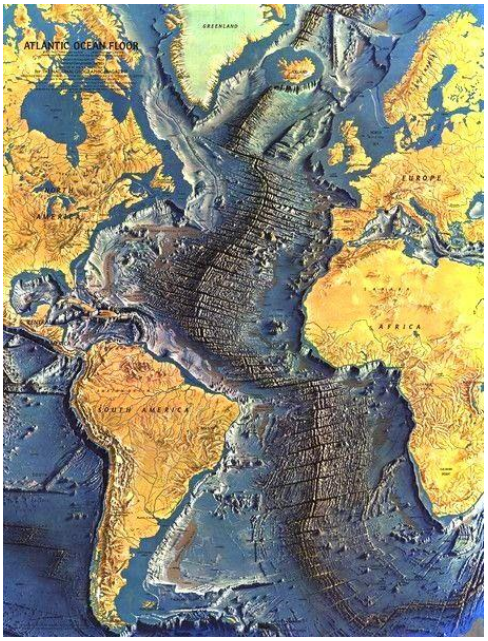

Figure 7: The physiographic map showing the mid-oceanic ridges at the Atlantic Ocean floor.

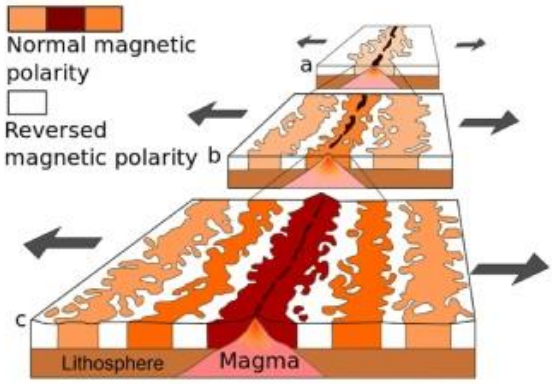

Figure 8: Ocean floor spreading and the production of the magnetic reversals.

A global picture now emerged. Oceans split apart at their centers, where new ocean floor is created by submarine volcanic eruptions. The crust then moves laterally across the ocean basins. Ultimately, it collides with continents along their margins (edges), where the ocean crust sinks underneath, back into Earth's mantle. As it does, it compresses the continental margins, generating folded mountain belts and magmas that rise to the surface as volcanoes, and deep earthquakes as the cold, dense ocean slab sinks farther and farther back into the earth (Figure 9). A map of the world divided into plates was constructed (Figure 10). The result became known as **plate tectonic theory**, and it was now the unifying theory of the earth sciences.

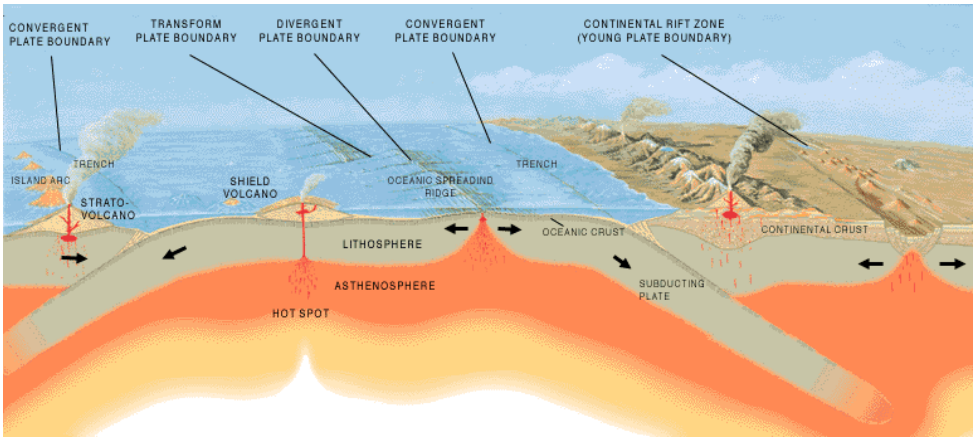

Figure 9: A generalized diagram showing the lithospheric situation associated with the formation of convergent, divergent, and transform plate boundaries (By: USGS).

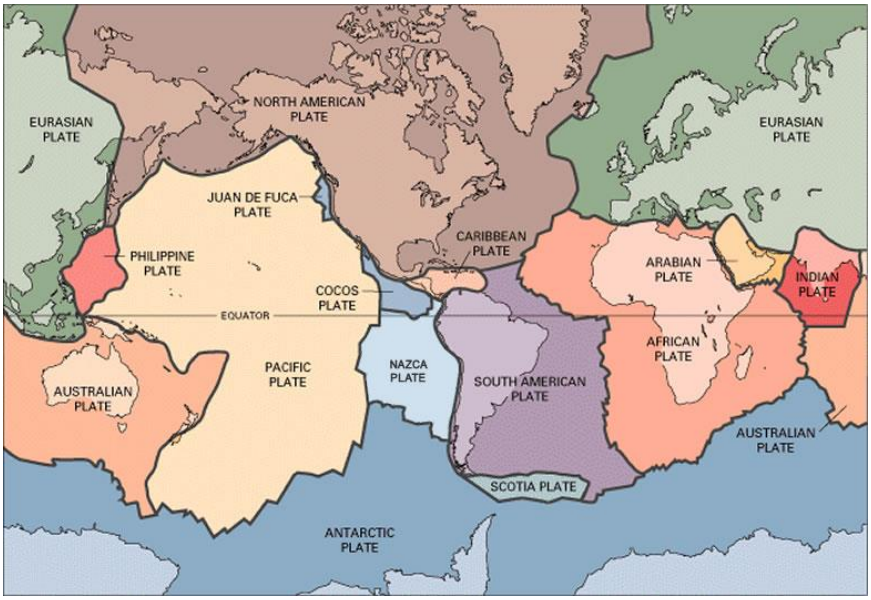

Figure 10: A generalized map of Earth's major tectonic plates. (By: USGS).

3- The Plate tectonic theory:

Plate tectonics is the theory that Earth's outer shell is divided into several plates that glide over the mantle. The plates act like a hard and rigid shell compared to Earth's mantle. This strong outer layer is called the **lithosphere**. The lithosphere includes the crust and outer part of the mantle. Below the lithosphere is the **asthenosphere**, which is ductile or partially ductile, allowing the lithosphere to move around. There are 12 major plates on Earth, each of which slide around at a rate of centimeters per year, pulling away from, scraping against or crashing into each other. Each type of interaction between the plates produces a characteristic "tectonic feature", like mountain ranges, volcanoes and (or) rift valleys.

A- What are the tectonic plates?

The outermost two layers of the Earth, the lithosphere and asthenosphere, are directly involved in plate tectonics. A tectonic plate (also called **lithospheric plate**) is a massive, irregularly shaped slab of solid rock, generally composed of both continental and oceanic lithosphere. Plate size can vary greatly, from a few hundred to thousands of kilometers across; the Pacific and Antarctic Plates are among the largest. Plate thickness also varies greatly, ranging from less than 15 km for young oceanic lithosphere to about 200 km or more for ancient continental lithosphere (for example, the interior parts of North and South America). The lithosphere (Greek shell of rock) ranges in thickness from 70 to 150 km or more, thicker below the continents, thinner below the oceans. It consists of two components – the crust (oceanic or continental), and the lithospheric part of the mantle. The lithospheric mantle behaves in brittle fashion and contrasts in this regard from the underlying "plastic-like" asthenosphere (Greek weak shell). The asthenosphere behaves in ductile fashion and locally contains pockets of molten rock. Beneath the asthenosphere is the rest of the mantle, which is completely solid – but can also flow (on geological time scales) because of the intense temperatures and pressures involved.

Earth's crust, which forms the uppermost 5–60 % of the plates, is generally divided into two types, continental and oceanic.

The continental crust is characterized by:

- an average thickness of 30–40 km but ranges up to 70 km under mountain ranges.
- Older in age.
- consists of relatively light (less dense) material that consists of acidic (SiO_2 > 65% weight), granitic and metamorphic rocks (granites, granodiorites, gneisses, schists); hence the expression that continental crust is granitic.
- Primary mineral components include K- and Na-feldspar, quartz, and mica, especially in the upper portions of the crust. In deeper parts of continental crust, the amount of basic (poorer in SiO_2) minerals such as hornblende and amphibole increase, and rock types include diorite and gabbro.
- The average density of the continental crust is 2.7–2.8 g/cm3

Oceanic crust is characterized by:

- markedly thinner with typical thicknesses of 5–8 km and forms the ocean floor.
- The top of oceanic crust lies an average 4–5 km deeper than that of the continental crust.

- Younger.
- consists of basic basaltic rocks (~50 % SiO2), mostly basalts and gabbros;
- density averages about 3.0 g/cm3; higher density than the continental crust as the content of the minerals containing Fe, Mg and Ca (heavy metals) are higher.
- calcium-rich feldspar and pyroxene are the most important minerals.

The composition of the oceanic crust is illustrated in figure 11.

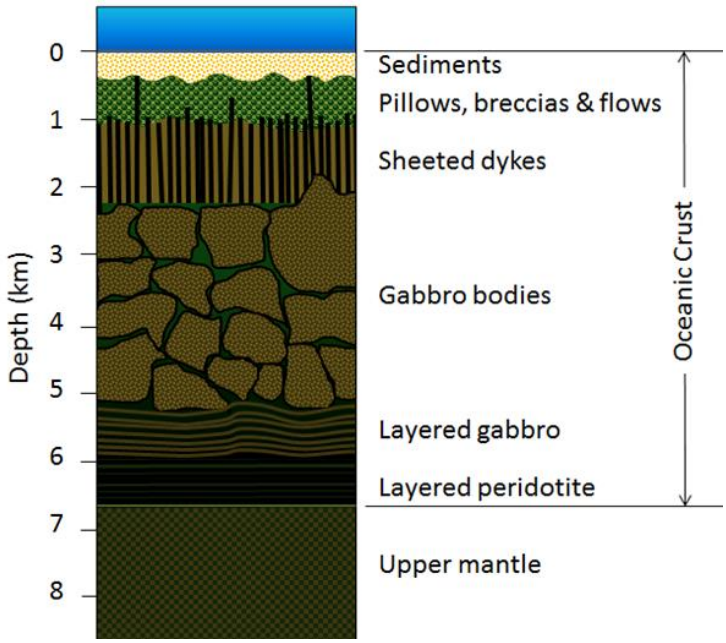

Figure 11: The rock composition of the oceanic crust.

The rock sequence that is characterized to the oceanic crust is called **ophiolite sequence**. It is a sequence of rocks consisting of deep-sea marine sediments overlying (from top to bottom) pillow basalts, sheeted dikes, gabbro, dunite, and peridotite (Figure 11). Ophiolite sequences are indicators of sea-floor spreading. As lava spills out into the cold ocean water it forms pillow basalts; magma that cools before reaching the surface forms sheeted dikes (dikes that appear to be vertically stratified because of the way the magma cools). Magma cooling deeper in the crust forms gabbro, dunite, and peridotite. The rocks with the basaltic composition in the ophiolite sequence are called **MORB** (**Mid-Ocean Ridge Basalt**).

B- Plate motion:

Geologists have hypothesized that the movement of tectonic plates is related to convection currents in the earth's mantle (Figure 12). Convection currents are the transfer of heat by the mass movement of heated particles into an area of cooler fluid. They describe the rising, spread, and sinking of molten material caused by the application of heat. The Earth's solid

crust acts as a heat insulator for the hot interior of the planet. Magma is the molten rock below the crust, in the mantle. Tremendous heat and pressure within the earth cause the hot magma to flow in convection currents. These currents cause the movement of the tectonic plates that make up the earth's crust.

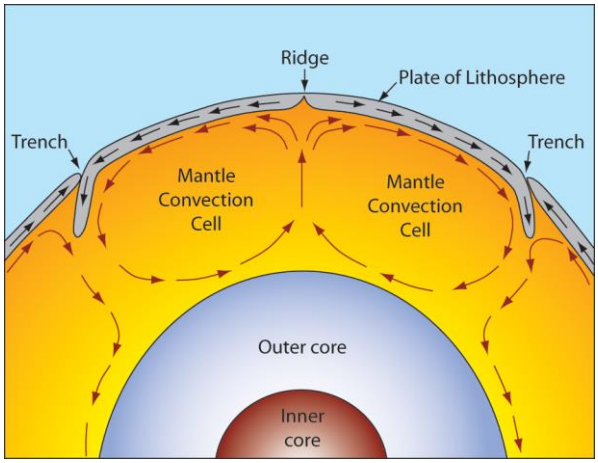

Figure 12: An illustration of the convection currents that drive the motion of the tectonic plates.

C- Plate boundaries:

Firstly, there are three types of plate boundary, each related to the movement along the boundary (Figure 13):

- Divergent boundaries are where plates move away from each other
- Convergent boundaries are where the plates move towards each other
- Transform boundaries are where the plates slide past each other.

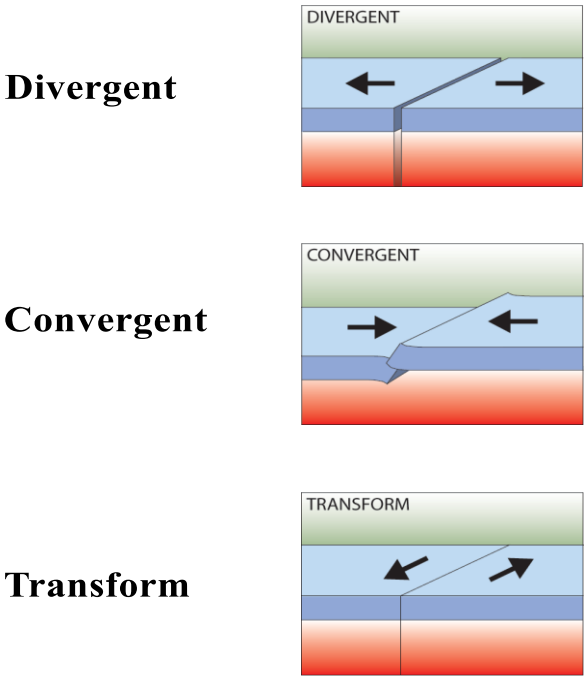

Figure 13: Types of plate boundaries.

1- Divergent boundaries:

A divergent boundary is a linear feature between two tectonic plates that are moving away from each other. These areas are formed in the middle of continents or on the ocean floor.

As the plates pull apart, hot molten material can rise up to the surface causing volcanic activity (Figure 14). Where a divergent boundary forms on a continent it is called a **rift** or **continental rift**, e.g. African Rift Valley. While, where a divergent boundary forms under the ocean it is called an **ocean ridge.**

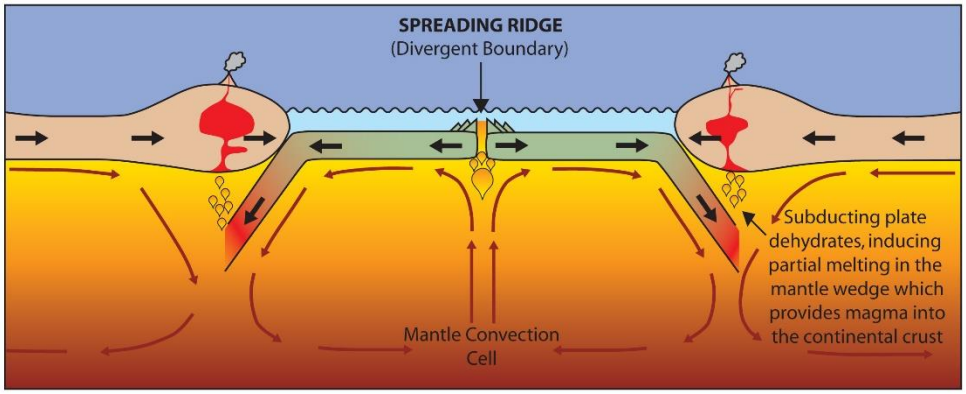

Figure 14: The mechanism of the divergent plate boundaries.

2- Convergent boundaries:

Convergent boundaries are where the plates move towards each other. There are three types of convergent boundary, each defined by what type of crust (continental or oceanic) is coming together: continent-continent collision, continent-oceanic crust collision or ocean-ocean collision.

A- Continent-continent collision:

This occurs when continental crust pushes against continental crust. Because both plates have the same properties, neither of them wants to sink beneath the other side, and as a result the two plates push against each other and the crust folds and cracks, pushing up (and down into the mantle) high mountain ranges. For example, the European Alps and Himalayas formed this way (Figure 15).

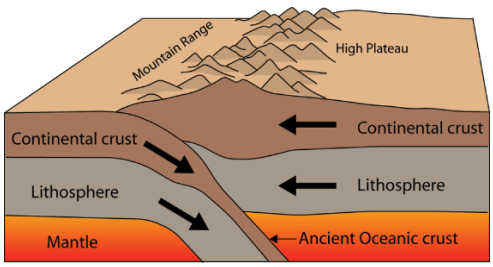

Figure 15: Schematic diagram of the continent-continent collision.

B- Continent-ocean collision (Subduction):

At a convergent boundary where continental crust pushes against oceanic crust, the oceanic crust, which is thinner and denser than the continental crust, sinks below the continental crust. This is called a **subduction**, and the whole zone where this movement occurs is called **subduction zone.** The oceanic crust descends into the mantle at a rate of centimeters per year. This oceanic crust is called the **subducting slab** (Figure 16). When the subducting slab reaches a depth of around 100 kilometers, it dehydrates and releases water into the overlying mantle wedge. The addition of water into the mantle wedge changes the melting point of the molten material there forming new melt which rises up into the overlying continental crust forming volcanoes. Along the subduction zone between the convergent plates, deep trenches are formed. Due to the extreme pressure exerted on the continental crust, it deforms and subjected to folding causing high mountain ranges.

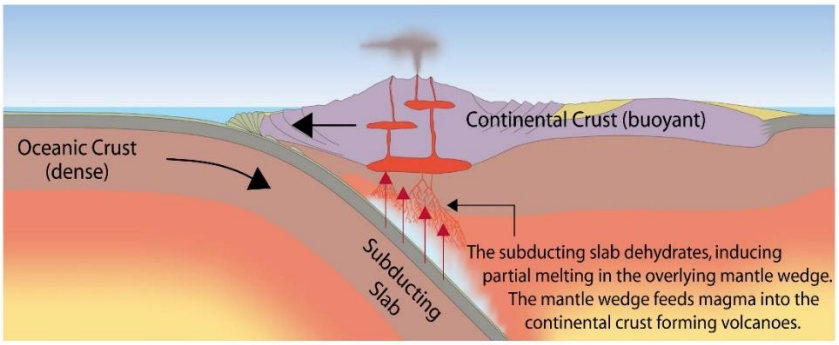

Figure 16: The subduction zone.

C-Ocean-ocean collision:

When two oceanic plates converge, because they are dense, one runs over the top of the other causing it to sink into the mantle and a subduction zone is formed. The subducting plate is bent down into the mantle to form a deep depression in the seafloor called a **trench** (Figure 17). Trenches formed by ocean-ocean collision are the deepest parts of the ocean and remain largely unexplored.

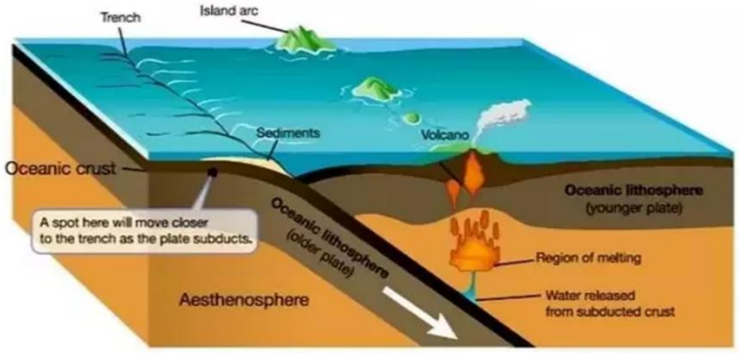

Figure 17: Ocean-ocean plate collision.

3-Transform (Transcurrent) boundaries:

The third type of boundary are transform boundaries, along which plates slide past each other (Figure 18). The San Andreas fault, adjacent to which the US city of San Francisco is built is an example of a transform boundary between the Pacific plate and the North American plate.

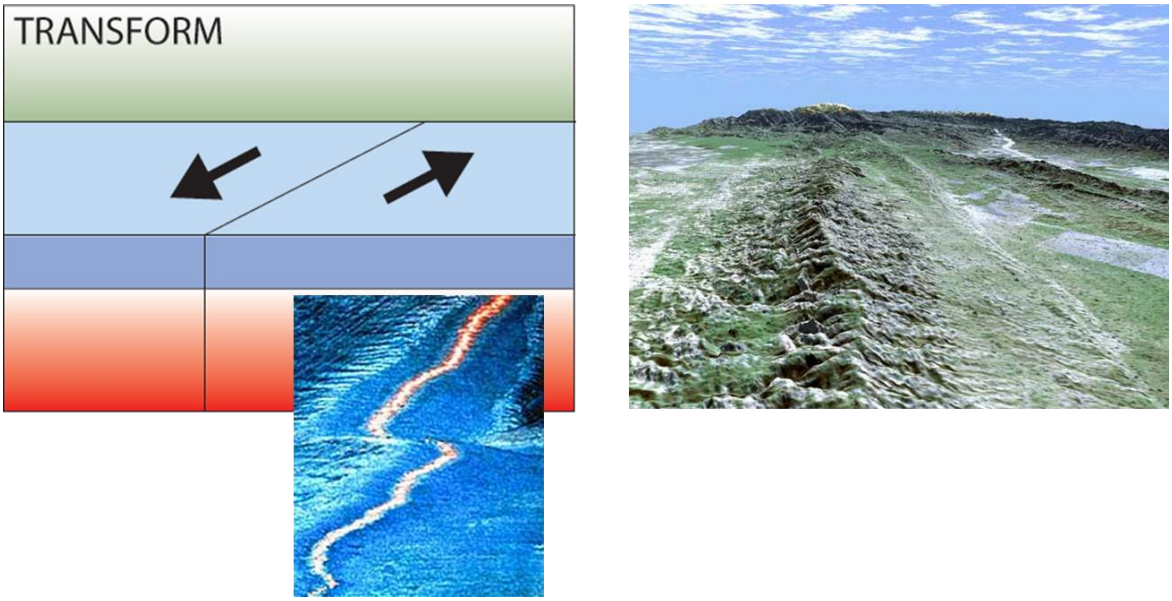

Figure 18: An illustration of the Transform boundaries.

Continental Margins

Nearly all of the presently existing plates contain areas with both continental and oceanic crust. The fact that most plates contain both crustal types means that some boundaries between oceans and continents occur within a given plate; hence, two types of continental margins exist (Fig. 1):

1- Passive continental margins (Fig. 1 upper):

These are the margins that doesn't represent tectonic plate boundaries. In this case, the ocean-continent boundary is an intra-plate feature. Continental and oceanic crust belong to the same plate. Such continental margins are widespread around the Atlantic Ocean.

2- Active continental margins (Fig. 1 lower):

These are the margins where a plate boundary exists between continent and ocean. Two types occur: subduction margins and transform margins.

A- Subduction margins:

In these margins, a part of a plate with oceanic crust is being subducted beneath the continental crust. A deep-sea trench forms along subduction zone plate boundaries. This type of continental margin is today prominent along the Andes and along numerous subduction zones around the Pacific Ocean that are characterized by island arc systems. The margin of the upper plate in these cases is characterized by chains of volcanic arcs, built either on continental crust or on continental pieces that were separated from the neighboring continent.

B- Transform margins:

In these margins, the oceanic plate slides laterally along the continental margin.

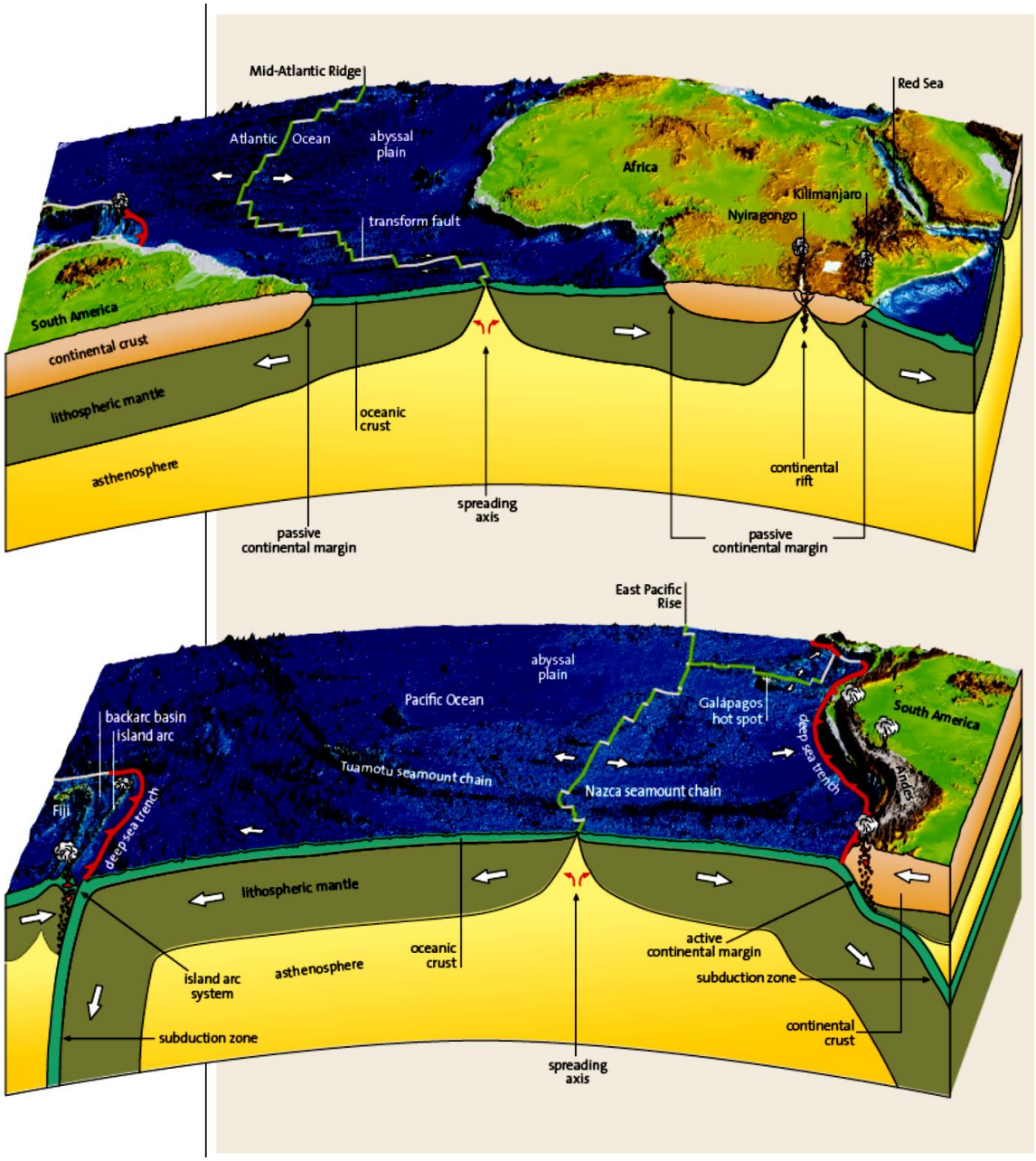

Figure 1: Block diagrams of the outer shells of the Earth in the Atlantic and the Pacific region. Shown are the three types of plate boundaries, passive and active continental margins, island arcs, volcanic chains.

Paleomagnetism

Paleomagnetism is the study of ancient pole positions and makes use of remanent magnetization to reconstruct the direction and strength of the geomagnetic field in the past. The origin of the Earth's magnetic field is not completely understood but is thought to be associated with electrical currents produced by the coupling of convective effects and rotation in the spinning liquid metallic outer core of iron and nickel. This mechanism is termed the dynamo effect. Certain minerals in rocks keep a record of the direction and intensity of the magnetic field when they form. This record provides information on the past behavior of Earth's magnetic field and the past location of tectonic plates. Minerals and the rocks in which they are contained acquire a magnetic signature as a given mineral cools below a certain temperature, its **Curie temperature** (named after the physicist Pierre Curie). Below the Curie temperature, a given mineral acquires the magnetic signature of the Earth's magnetic field that was present at that time. As an example, magnetite has a Curie temperature of 580°C. Three signatures of magnetism are generally infused into magnetic minerals: inclination, which reflects latitude; declination, which reflects direction to the poles; and normal or reversed polarity, which indicates magnetic reversals (by convention, the current situation is defined as "normal"). Magnetic signatures in minerals are maintained for hundreds of millions of years, although some overprinting from subsequent geologic events does occur so that samples must be "cleaned" to eliminate younger events. Also, the perturbing effect of the current magnetic field must be compensated for during the analysis of the sample.

Fields of the paleomagnetism:

1- Polar drift:

Polar drift means the small-scale changes in the direction and intensity of the Earth's magnetic field caused by variations in the flow of molten iron in Earth's outer core. The magnetic pole moves around the geographic pole (the rotational pole of the Earth) in an irregular manner. The North Magnetic Pole is approximately 965 kilometres from the geographic north pole. The pole drifts considerably each day, and since 2007 it moves about 55 to 60 km per year as a result of this phenomenon. This is called **magnetic pole wandering**. Although the magnetic pole wanders it does not move far from geographic pole. The path by which a paleo pole moves through time is called **paleomagnetic polar wandering** and is only caused by plate tectonics (Figure 2). However, averaged over a period

of several thousand years the two poles coincide. Therefore, the orientation of earlier geographic poles can be detected using paleomagnetics if the mean value is calculated from enough samples.

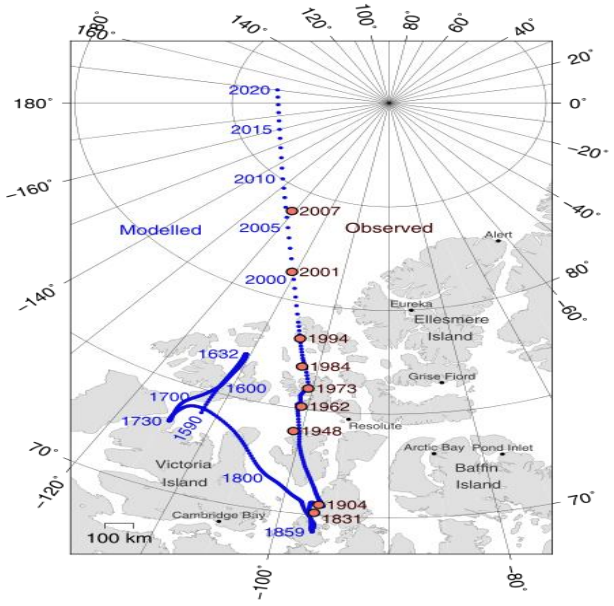

Figure 2: Positions of North Magnetic Pole of the Earth. Red circles mark magnetic north pole positions as determined by direct observation, blue circles mark positions modelled using the GUFM model (1590–1890) and the IGRF-12 model (1900–2020) in 1-year increments.

2- Magnetic reversal:

At very irregular intervals over periods of variable duration, the polarity reverses and the earlier South Pole becomes the North Pole and the other way round. This is called **magnetic reversal** and it is the process by which the North pole is transformed into a South pole and the South pole becomes a North pole. The Earth's field has alternated between periods of normal polarity, in which the predominant direction of the field was the same as the present direction, and reverse polarity, in which it was the opposite.

3- Magnetic polarity stratigraphy (Magnetostratigraphy):

Paleomagnetism has led to a new type of stratigraphy based on the aperiodic reversal of polarity of the geomagnetic field. Magnetic polarity stratigraphy is the ordering of sedimentary or igneous rock strata into intervals characterized by the direction of magnetization of the rocks, being either normal polarity or reverse polarity. This new stratigraphy is used to providing chronology for interpretation of oceanic magnetic anomalies and calibrating the geologic time. When measurable magnetic properties of rocks vary stratigraphically they may be the basis for related but different kinds of stratigraphic units known collectively as **magnetostratigraphic units (magnetozones).**

The method works by collecting oriented samples at measured intervals throughout the section. The samples are analyzed to determine their **characteristic remanent magnetization** (ChRM), that is, the polarity of Earth's magnetic field at the time a rock was formed. This technique is typically used to date sequences that generally lack fossils or interbedded igneous rock.

To understand the magnetostratigraphy, principles of the remenant magnetization should be studied.

Remenat magnetization (also called Natural Remenant Magnetization-NRM):

It is the permanent magnetism in rocks, resulting from the orientation of the Earth's magnetic field at the time of rock formation in a past geological age. It is the source of information for the paleomagnetic studies of polar wandering and continental drift. Remanent magnetism can derive from several natural processes. The most important component of remanence is that acquired when a rock formed. This is called its **primary component or characteristic remanent magnetization (ChRM).** Any later component is called a **secondary component.** Based on the processes by which remenant magnization is acquired, there are several types of primary remenant magnetization.

Types of primary remenant magnetizations:

1- Thermoremenant magnetization (TRM):

It is acquired in igneous rocks during cooling through the Curie temperature of the magnetic minerals. Iron-titanium oxide minerals in basalt and other igneous rocks may preserve the direction of the Earth's magnetic field when the rocks cool through the Curie temperatures of those minerals. The Curie temperature of magnetite, a spinel-group iron oxide, is about 580°C, whereas most basalt and gabbro are completely crystallized at temperatures below 900°C. Hence, the mineral grains are not rotated physically to align with the Earth's field, but rather they may record the orientation of that field.

2- Detrital remenant magnetization (DRM):

It is acquired in the sedimentary rocks when the magnetic grains in sediments may align with the magnetic field during or soon after deposition. It has two types:

- Depositional detrital remenant magnetization (dDRM):

If the magnetization is acquired as the grains are deposited.

- Post-depositional detrital remenant magnetization (pDRM):

If it is acquired soon after deposition

3- Chemical remenant magnetization (CRM):

It is acquired in the rocks when the magnetic grains grow during chemical reactions and record the direction of the magnetic field at the time of their formation. A common form of chemical remanent magnetization is held by the mineral hematite. Hematite forms through chemical oxidation reactions of other minerals in the rock including magnetite. Clastic sedimentary rocks (such as sandstones) are red because of hematite that formed during sedimentary diagenesis. The CRM signatures in these beds can be quite useful and they are common targets in magnetostratigraphy studies.

All these became the basis for the geomagnetic polarity time scale (GPTS) which is useful for the calibration of geologic time.

Geomagnetic polarity time scale:

It is record of the onset and duration of the episodes of reversal of the Earth's magnetic polarity, or geomagnetic polarity reversals. The GPTS was developed by studying rocks from around the world, containing magnetic minerals whose orientation was opposite to that of the current magnetic field. By comparing the patterns of magnetic reversals with those of rocks of known age, the approximate ages of rocks can be established. This is particularly useful for basalts of the oceanic crust, which record the Earth's magnetic field as they solidify from molten lava symmetrically about the midocean ridges. The time scale has been accurately extended back to the Upper Jurassic, the age of oldest existing oceanic crust. It is found that the mean time between reversals being roughly 200,000 years.

In dividing the time units according to the paleomagnetic polarity, intervals of constant polarity (normal or reverse) are called **chrons**. These chrons are divided into **subchrons**. **Excursions** are very short events take place within these intervals and are shorter than chrons. During these excursions, the magnetic pole departs greatly from the usual geographic pole, sometimes achieving the reverse direction for a short time. Excursions also involve dramatic decreases in intensity. They involve a rapid collapse of the field. Studies of the geomagnetic field in the last 1 million years have found 14 excursions, large changes in direction lasting 5-10 thousand years.

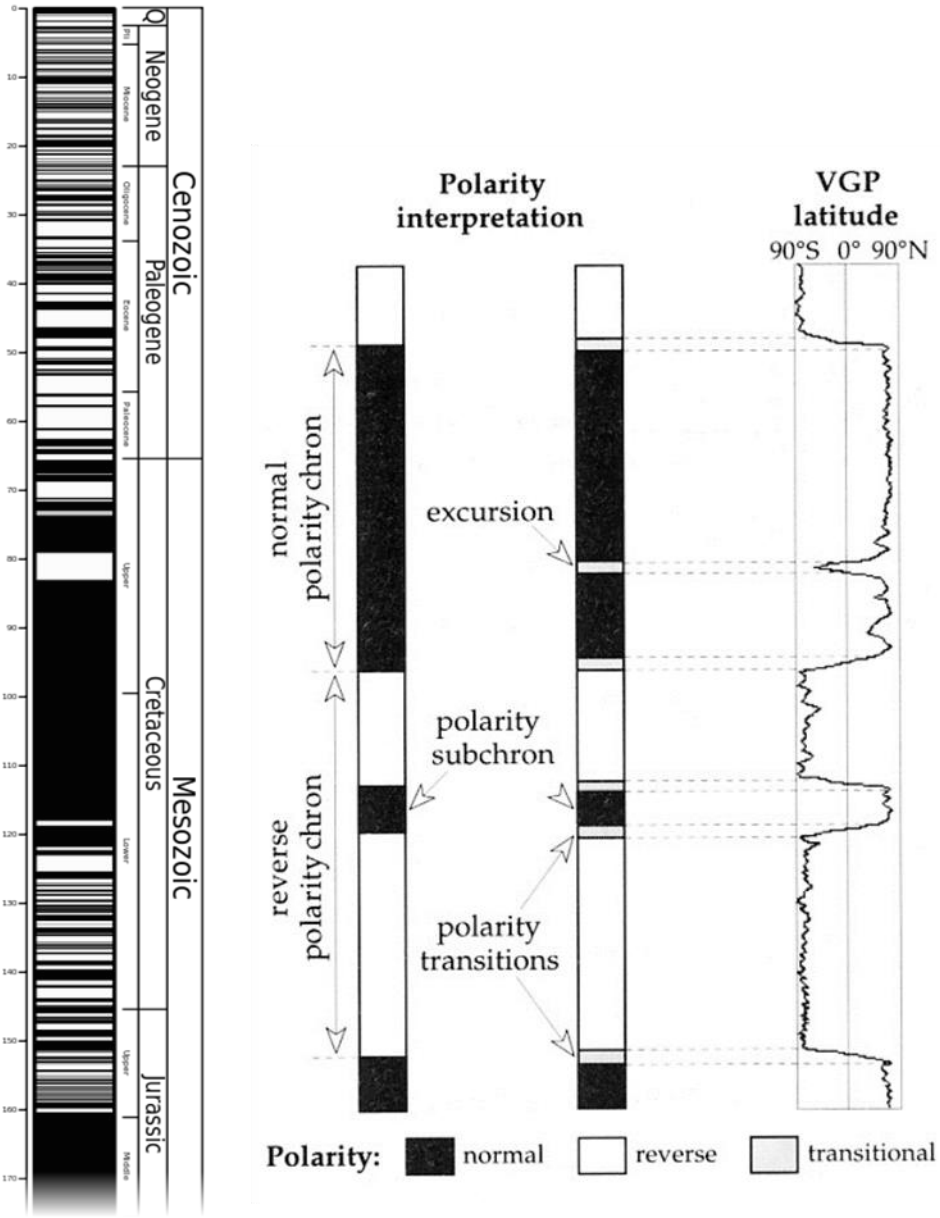

Figure 3: The Geomagnetic Polarity Time Scale

These patterns of normal and reverse magnetization are found parallel and symmetrically aligned to the oceanic ridges forming a distinctive anomaly pattern called **magnetic zebra stripes** (Fig. 4). Based on the characteristic patterns of normal and reversed magnetization, the stripes can be dated by comparing them with known sequences. This is very strong proof for seafloor spreading because the method shows that variable magnetic stripes of oceanic crust are formed parallel to the ridges and that they become older with increasing distance to the ridge (Fig. 5). Magnetic reversals in oceanic rocks only yield data back to approximately 180 Ma, the Early Jurassic (Fig.6) – all older oceanic crust has been subducted. A paramount reason for this fact is that older ocean crust is colder and more dense, and therefore subducts

more readily; for example, if 20 Ma ocean crust and 150 Ma ocean crust collide, the older will be subducted.

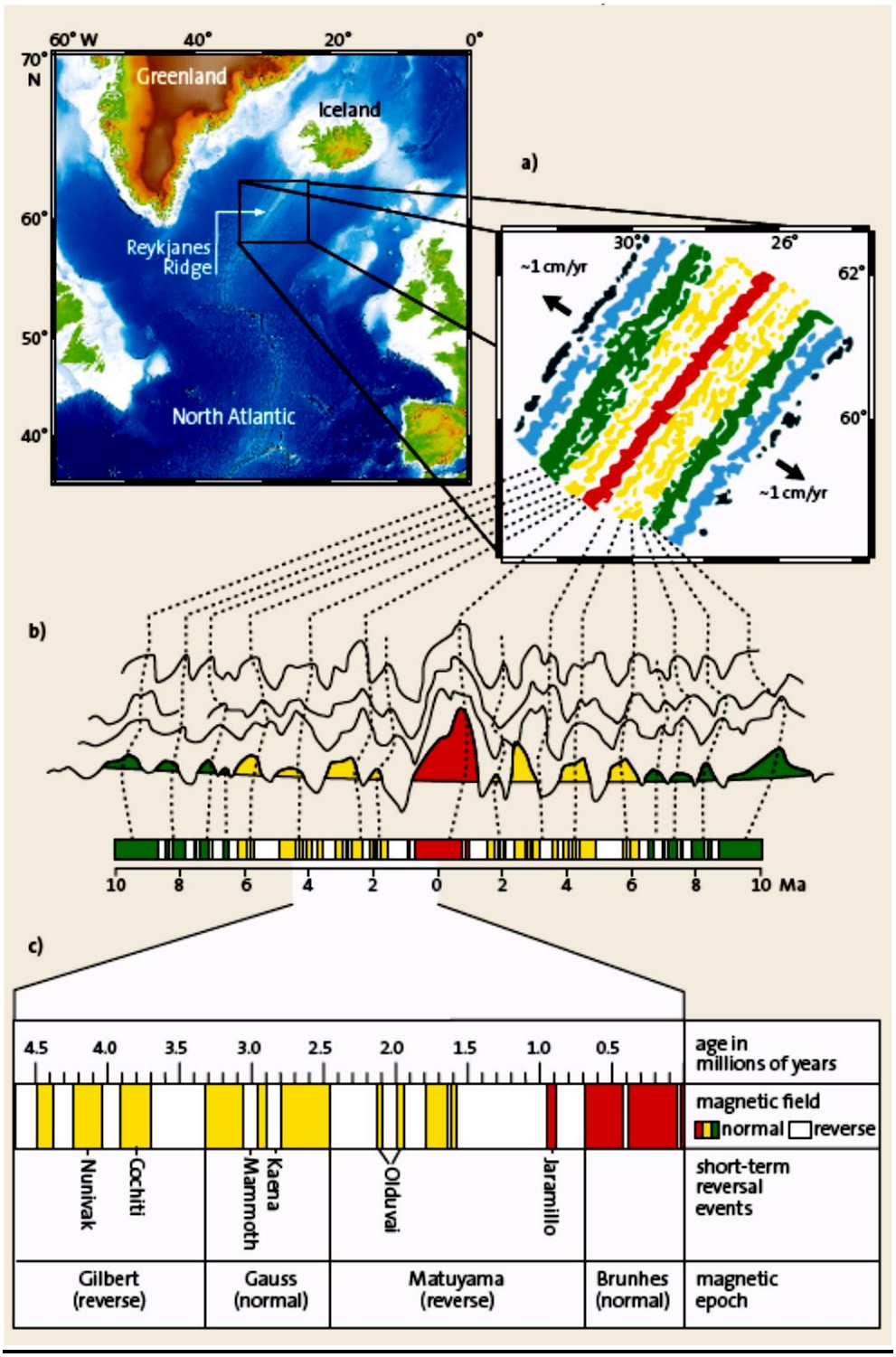

Figure 4: a) Stripe pattern of magnetic polarities on the ocean floor at the Reykjanes Ridge, part of the Mid-Atlantic Ridge southwest of Iceland (Heirtzler et al., 1966). b) Curves representing the magnetic field strength measured along the track of ships crossing the ridge. Normal (in colors) and reverse magnetization can be obtained from these curves. c) Graph showing detailed magnetic stripe pattern for the last 4.5 Ma. By comparison with measured profiles, the ocean floor can be dated.

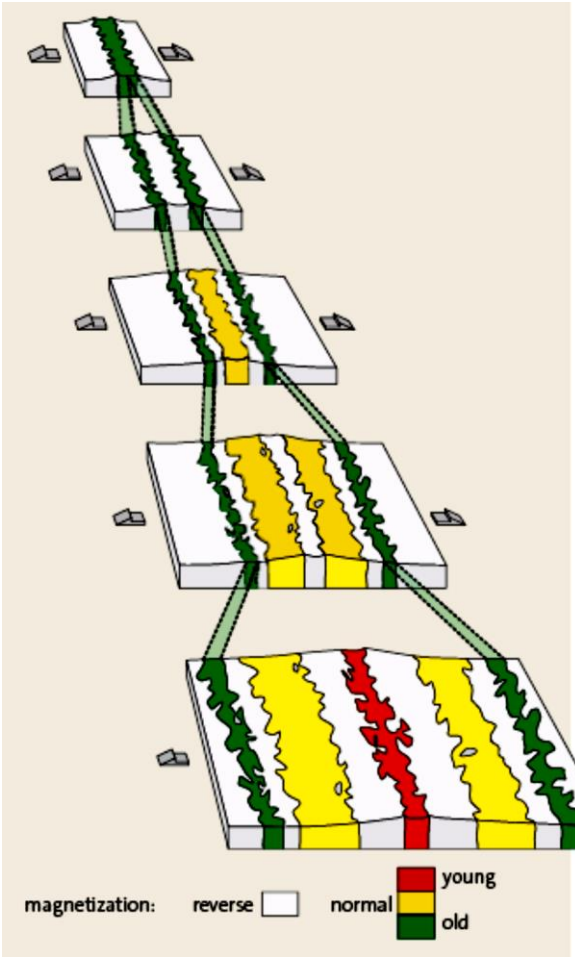

Figure 5: Simplified sketch showing development of the magnetic stripe pattern along the spreading axis. The pattern is caused by repeated reversals of the Earth's magnetic field. Irregularities of the stripes are caused by submarine extrusion of basaltic lavas that adapt to the existing, commonly rough topography.

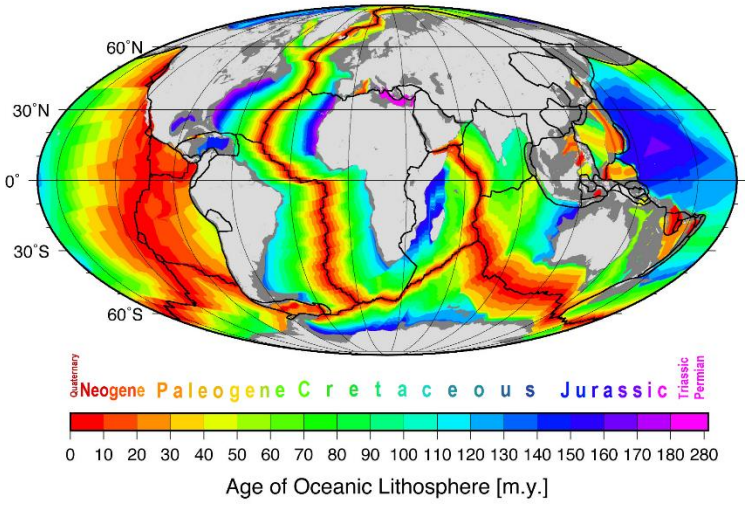

Figure 6: Map showing distribution of ages of oceanic crust. The oldest oceanic crust is of Jurassic age and is located in the NW Pacific (ca. 185 Ma) and near the edges of the Central Atlantic (ca. 175 Ma). Small fragments of older oceanic crust are captured between continental blocks in the Mediterranean Sea.

Geotectonics: Seismotectonics

What is seismotectonics?

Seismotectonics can be defined as the study of the relationship between the earthquakes and active tectonics. The spatial distribution of earthquakes can be used to determine the location of plate boundaries, as relative movements of the plates along the plate boundaries induce earthquakes.

Earthquakes are studied as the main field of seismology. Seismology is the study of vibrations within the Earth. These vibrations are caused by various events, including earthquakes, extraterrestrial impacts, explosions, storm waves hitting the shore, and tidal effects.

Earthquakes:

Stages of an earthquake:

1- Elastic Buildup:

The first stage of an earthquake is the gradual buildup of elastic strain, which occurs over thousands of years. When both sides of the fault move due to plate motion, the elastic strain builds up in the rocks slowly, compressing the rock particles together that the rock deform or bend.

2-Dilatancy:

With continuous plate motion, stress and strain become localized. The rocks are cracking to increase the amount of space they occupy. This process is called dilatancy. As small cracks form, the water inside the pores of the rocks is forced out and air is let in. The process allows the rocks to hold even more elastic strain.

3- Earthquake:

Because the rocks can no longer resist the elastic strain, a sudden fault rupture occurs releasing the accumulated stress. The stored energy in the rocks is forced out and released in the form of heat and seismic waves.

The above stages (shown in fig. 1) where the elastic strain is sustained and then released are called the **elastic rebound theory**.

4-Aftershocks:

The aftershocks which are smaller earthquakes or ruptures, release the remaining elastic strain. Aftershocks can occur years after the initial earthquake. Depending on the size of the main

earthquake, the size and frequency of aftershocks can be significant. Eventually the strain decreases, allowing normal conditions under the surface to return.

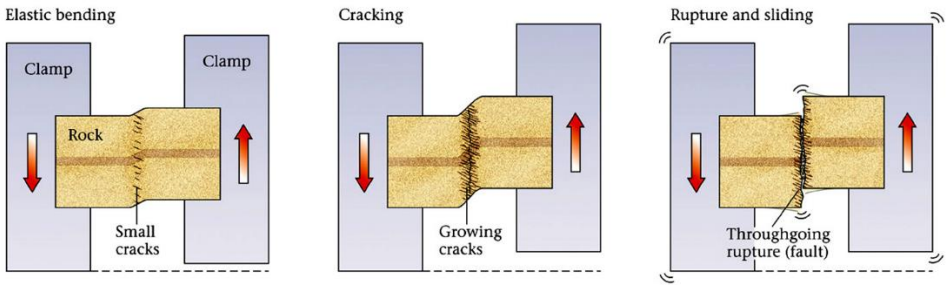

Figure 1: Stages of an earthquake

Seismic waves:

At the moment when the earthquake occurred, the energy is released in the form of seismic waves. There are two categories of earthquake waves. Body waves can travel deep into the Earth. Surface waves can only travel very near the surface of the Earth. Only body waves can give us any information about the deep interior of the Earth. Earthquake waves as moving out like rays (arrows) or as wave fronts (spherical shells) (Fig. 2). Surface wave rays travel out in all horizontal directions (like the arrows on the top of the block pictured below), like ripples moving out from a pebble dropped into a pond.

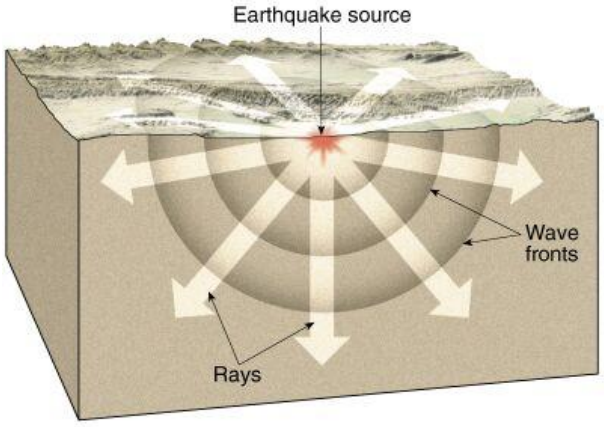

Figure 2: Earthquake waves.

Two different types of seismic body waves are generated by the sudden movement on a fault: P-waves and S-waves. The velocity of the waves depends on wave type and the properties of the rock; the denser the rock, the faster the waves travel. In the Earth's crust P-waves travel at around 6-7 km/s, while S-waves travel at around 3.5-4 km/s. P-waves travel fastest. They consist of successive contractions and expansions, just like sound waves in air. The motion of

the particles in the rocks that the waves travel through is parallel to the direction of the wave (Figure 2). S-waves are slower than P-waves. They are transverse waves, which means that the particle motion is at right angles to the direction of travel (Fig. 3). S-waves cannot travel through air or liquids.

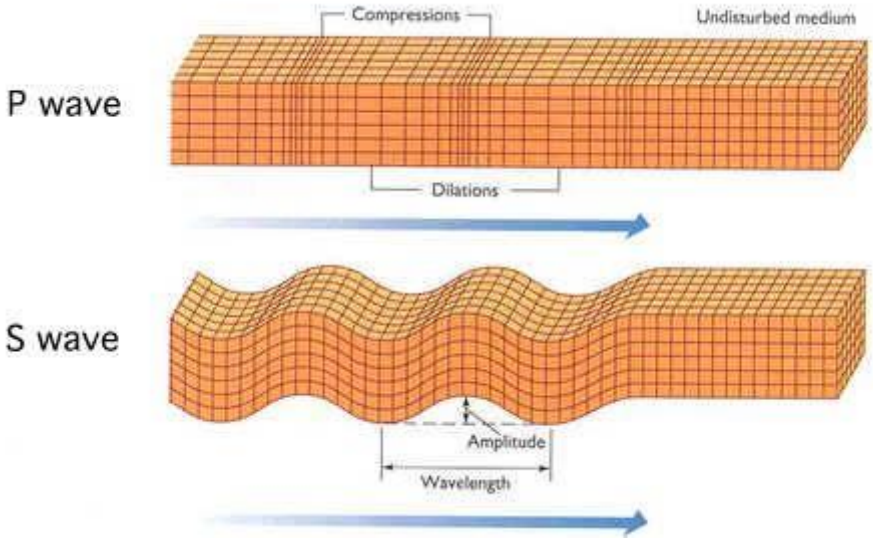

Figure 3: An illustration of P and S wave propagation.

Earthquake components:

The coordinates of an earthquake point source are known as the ***hypocenter (focus)***. The hypocenter is usually given in terms of latitude, longitude, and depth below the surface (***Focal depth***). The ***epicenter*** is the surface projection of the hypocenter (the latitude and the longitude). ***Epicentral distance*** is the distance separating the epicenter and the recording seismic station. The **seismogenic layer** or **seismogenic zone** covers the range of depths within the crust or lithosphere in which most earthquakes originate.

Earthquake size is the amount of the energy released by an earthquake and is described by the **earthquake magnitude**. The magnitude is depending on the area of the fault plane that ruptures and generate the earthquake. As the area of the fault increased, the earthquake magnitude increased. **Earthquake swarms** are events where a local area experiences sequences of many different -sized earthquakes striking in a relatively short period of time. While **earthquake cluster** is any group of earthquakes of similar type and magnitude in a given area over a period of months. Fig. 4 below shows the earthquake zone components.

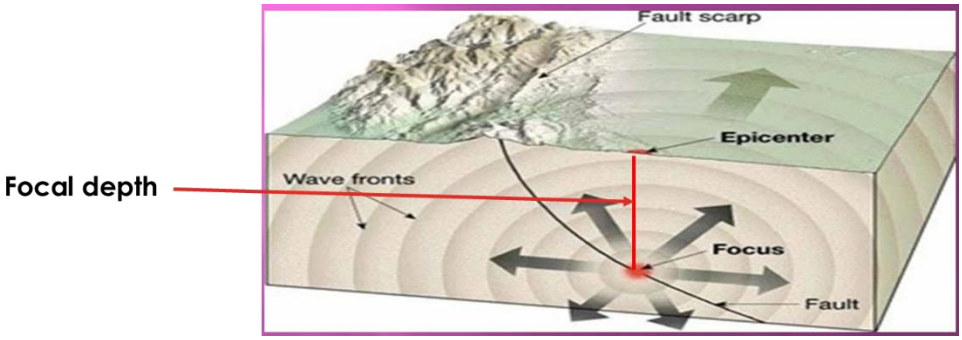

Figure 4: Earthquake zone components.

Reading a seismogram:

Reading and interpreting a seismogram is very important in establishing the earth velocity structure and determining the various types of the seismic sources. The components in a seismogram are shown in figure 5.

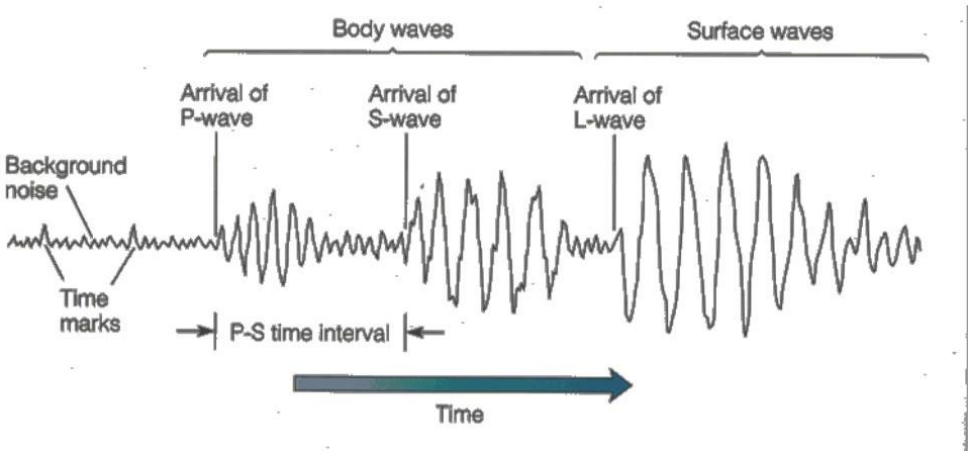

Figure 5: An example of a seismogram.

The basic character of seismograms depends strongly on the epicentral distance. There are four general classifications of seismograms based on epicentral distance:

(1) ***Local-distance seismograms*** are defined as travel paths of less than 100 km. Seismic recordings at local distances are strongly affected by shallow crustal structure, and relatively simple direct *P* and *S* phases.

(2) ***Regional-distance seismograms*** are defined as $100 < X < 1000$ km, where X is epicentral distance in kilometers. Regional-distance seismograms are dominated by seismic energy refracted along or reflected several times from the crust-mantle boundary. The corresponding waveforms tend to be complex because many phases arrive close in time.

(3) ***Upper-mantle-distance seismograms*** are dominated by seismic energy that turns in the depth range of 70 to 700 km below the surface.

(4) *Teleseismic seismograms*. The direct *P*- and S-wave arrivals recorded at teleseismic distances are relatively simple, indicating a smooth velocity distribution between 700 and 2886 km depth.

Seismic waves on seismograms:

For body-wave, there are two phases:

a) *Direct arrivals:* They travel the minimum-time path between source and receiver and are usually just labeled *P* or S. At epicentral distances greater than a few tens of kilometers in the Earth, direct arrivals usually leave the source *downward*, or away from the surface, and the increasing velocities at depth eventually refract the wave back to the surface. Figure (6 a) shows two direct rays leaving a seismic source.

b) Depth phases: they are upgoing rays that travel from the source up to the free surface, reflect, and travel on to the receiver. They are called pP, sP, sS,,, (Figure 6 b). Seismic phases that reflect at a boundary within the Earth are subscripted with a symbol representing the boundary. For example, P-wave energy that travels to the core and reflects is called *PcP*, the *c* indicating reflection at the core. Moho reflections are labeled *PmP*, *PmS*, *SmP*, or *SmS*. P wave that travels to the core, traverses it, and reemerges as a P wave is denoted as *PKP*. The P wave that traverses the inner core (which is solid) is denoted with an *I*, *e.g.*, *PKIKP*

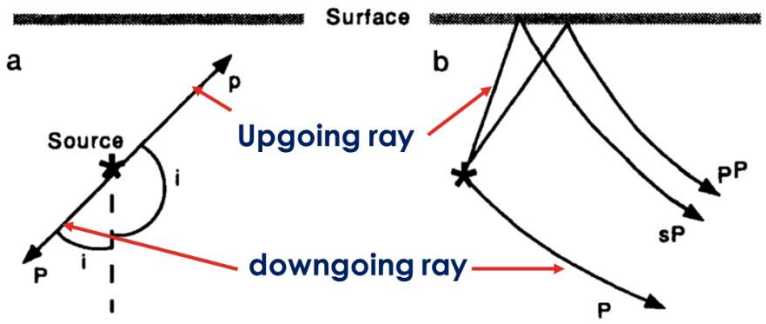

Figure 6: (a) Geometry of upgoing and downgoing rays, (b) Geometry of depth phases.

Earthquakes and plate boundaries:

Looking at the distribution map of earthquake epicenters, it shows that earthquakes are mainly restricted to narrow zones around the globe (Fig. 7), the present plate boundaries.

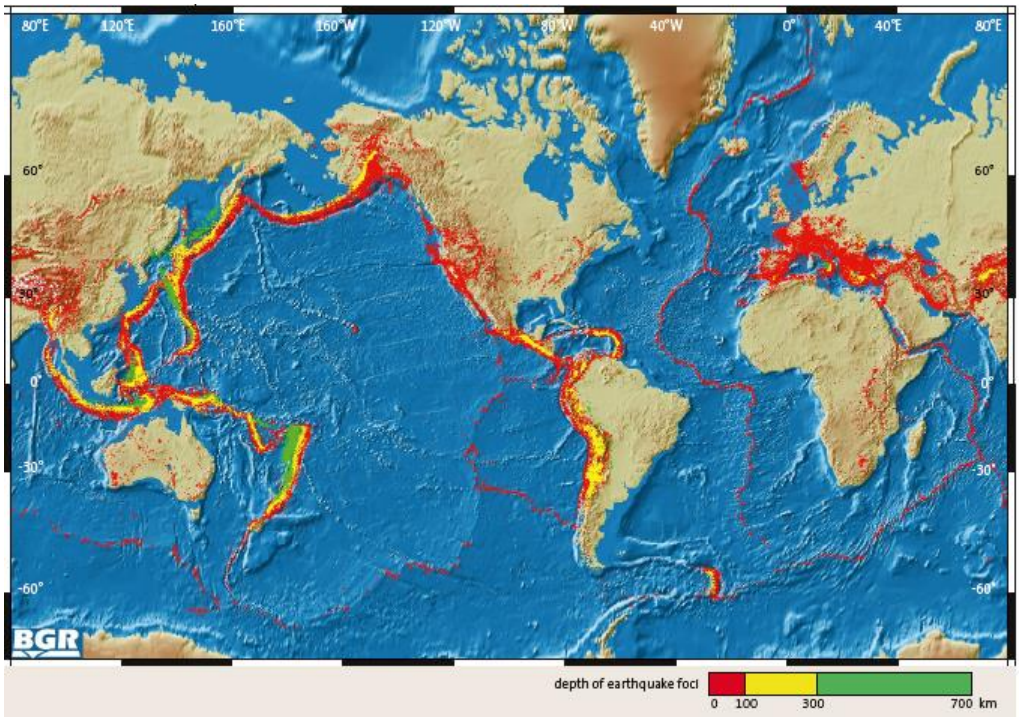

Figure 7: Global distribution of earthquake centers with epicenters mapped according to their depth. Note how the epicenters define plate boundaries; also note that most earthquakes occur within 100 km of the surface except along subduction zones where they deepen under the upper plate.

According to the earthquake distribution relative to the plate boundaries, there are two types of seismicity:

1- Interplate seismicity (or earthquakes): which is concerned with the seismicity occurred directly at the boundaries between two tectonic plates.

2- Intraplate seismicity (or earthquakes): which is concerned with the seismicity occurred within the plates away from the plate boundaries.

In general, divergent and transform plate boundaries are characterized by shallow seismicity (focal depths less than 30 km), while subduction zones and regions of continental collision can have much deeper seismicity (focal depths exceed 100 km).

1- Divergent Boundaries:

As the mid-oceanic ridges and continental rifts are tensional environments, most of the earthquakes involve normal faulting.

A- Midoceanic ridges:

Focal depths and magnitude of the earthquakes at the mid-ocean ridges are controlled by two factors:

- **Spreading rates:** the rate at which new oceanic lithosphere is formed and describes the relative motion between the two plates.

- **Thermal structure of the lithosphere:** the temperature relationships within the lithosphere. As lithosphere moves away from the ridge, it cools and becomes denser.

In this case, there are two situations:

1- Fast spreading rates:

Oceanic ridges that are spreading rapidly have a broad, smooth topographic signature. The lithospheric thickness is very small near the ridge as it cools rapidly, which means that the available "width" of a fault plane is also small. This condition results in shallow, moderate- to small-sized earthquakes. As the spreading rate increases, the maximum centroid depth shallows.

Since earthquake magnitude correlates with fault dimensions, it is concluded that as the spreading rate increases, the maximum expected magnitude of an earthquake near the ridge decreases. Fast spreading centers have few earthquakes, all of small magnitude.

2- Slow spreading rates:

Slow spreading centers are capable of generating much larger earthquakes with much deeper hypocenters. Slow spreading rates means that the lithosphere cools slowly, and thus increasing both the thickness and density of the ocean crust. Increasing the density led to increasing the ocean depth as the denser new formed thicker lithosphere sinks in the asthenosphere as it becomes heavier. In this case, the fault planes are wider with more depths, giving rise to higher-magnitude earthquakes with more focal depths.

Most normal-faulting earthquakes associated with oceanic ridges do not occur exactly at the plate boundary but are on faults associated with a feature known as the axial valley (Fig. 8). They are mostly occurred in earthquake swarms.

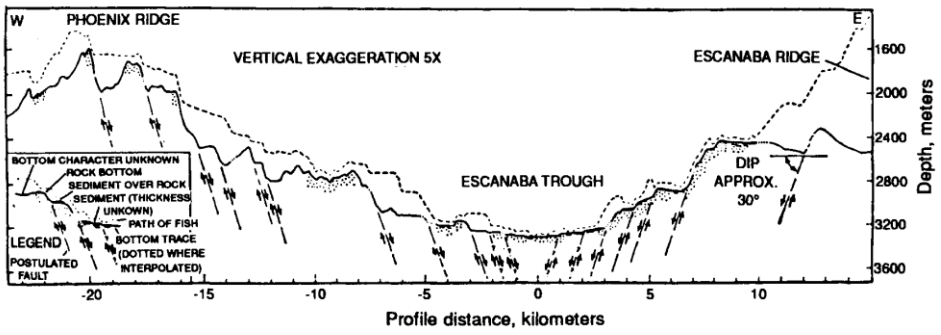

Figure 8: The axial valley, which is approximately 30 km across, is bounded by a series of normal faults.

B-Continental Rifts:

In general, continental rifts have slow spreading rates and thus are much wider, and the seismicity is more widespread than at oceanic ridges. The maximum magnitude expected in a continental divergent setting will be significantly larger than that along an oceanic ridge.

2- Transform boundaries:

Transcurrent (or transform) boundaries, between horizontally shearing plates, are of two types: (1) *transform faults,* which offset ridge segments, and (2) strike-slip faults that connect various combinations of divergent and convergent plate boundaries. The size of earthquakes on a transform fault largely depends on two factors:

(1) the length of offset between ridges.

(2) spreading rates.

If a transform fault is long, connecting slowly spreading ridges, a substantial seismogenic source region is available. In most cases the largest expected magnitude for transform events is 7.0-7.5. Strike slip faults are much longer and wider. As the area of the rupture can be so great, it is quite common for large transform boundaries earthquakes to involve multiple subevents.

3- Convergent boundaries:

A- Subduction zones:

Two categories of seismic activity occur in subduction zones:

1- The First category:

This category is related to the interaction between the two converging plates, which results in a large contact zone between two plates on which frictional sliding must take place, producing interplate seismicity. In this category, earthquakes are occurring along deep seismic belts along the subducted plates are known as **Wadati-Benioff zones.** The earthquakes are variable along different ranges of depth along these zones, as follows:

a) The largest number of earthquakes and largest energy release occur in the upper 200 km, which is the region of interplate interaction and slab bending. Normal frictional sliding processes dominate at this depth.
b) The earthquake activity is at a minimum between 200 and 400 km depth, where the subducting lithosphere is interacting with *weak* asthenosphere.

c) Below 400 km, the number of earthquakes increases with depth and some slabs strongly distort.

d) All earthquake activity ceases by a depth of 700 km as mentioned earlier. This is because during the downdip extension of the subducted plate below this depth, the lower part of subducted plate is totally melted on the asthenosphere or if not melted, this lower part is cut from the rest of the plate and sinks within the asthenosphere by the effect of the gravity and increasing compression on its weight (Fig. 9).

e) Some subduction zones show a very interesting variation at depths of 50 to 200 km. In these zones, the Wadati-Benioff zone is made up of two distinct planes. Each plane is defined by a thin, well-defined cluster of epicenters; the planes are separated by 30-40 km. This is called **double Waldati-Benioff zone** (Fig. 10). This explained as bending a thin plate causes extension in the outer arc of the bend, while the underside of the plate is in compression. The earthquakes in double Wadati- Benioff zones are small, rarely exceeding magnitude 5.5.

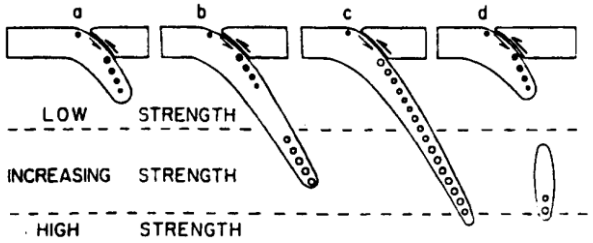

Figure 9: Downdip extension of the subducted plate (Isacks and Molnar, 1971)

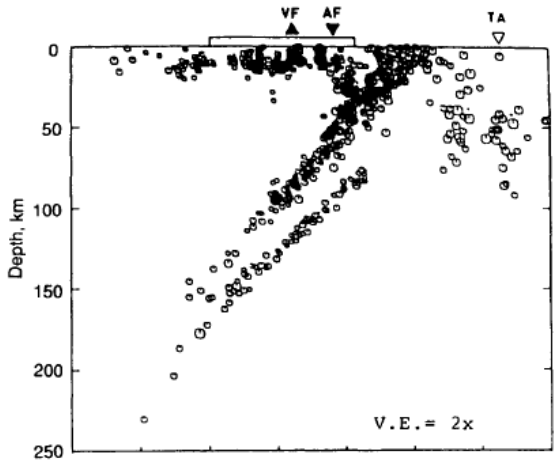

Figure 10: Double Wadati-Benioff zone observed in northeast Japan. (Hasegawa et al., 1978)

Some subduction zones have strong shallow seismicity while others have small-sized ones. This occurs because the different subduction zones have different **seismic coupling**. Seismic coupling is measure of the seismogenic mechanical interaction between the subducting and

overriding lithospheric plates (Fig. 11). Strongly coupled subduction zone will have a greater seismicity compared with less coupled zones.

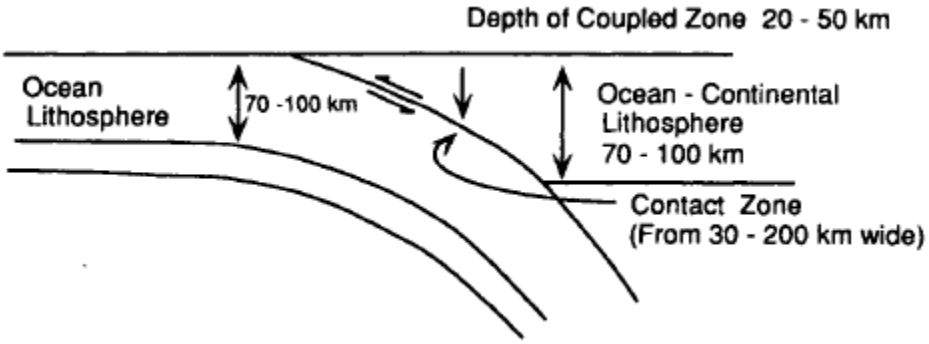

Figure 11: Schematic cross section through the shallow portion of a subduction zone.

What causes the variability in coupling?

1- Age of the lithosphere.

2- rate of convergence

The maximum observed earthquake size increases with increasing convergence rate and decreasing lithospheric age.

3- The presence of a back arc:

Back arc formed when spreading centers formed behind the subduction zone. When they occurred, the seismic coupling is reduced.

4- The dip angle of the subducted plate:

Shallow dip of the uppermost part of the slab (between 10° and 2°) increases the coupling.

5- The topography of the subducted slap:

Smooth topography increases the coupling.

It is noted that seismic coupling decreases with time. Shallow-dipping, broad, strongly coupled zones produce extensive ruptures. The thrust zone may be weakened and partially decoupled by repeated fracturing, yielding smaller rupture lengths.

2- The second category:

This category is related to the internal deformation of the overriding plate as well as the internal deformation within the subducting plate that results from the slab's interaction with surrounding mantle. Within the overriding plate, seismicity is intraplate and is formed due to deformation by extreme pressure.

Within the subducting plate relatively few earthquakes occur that are associated with the bending of the plate. For trenches in which the subducting and overriding plates are weakly coupled, these intraplate events can be very large. Tensional stress produced in these

environments results in large normal-faulting earthquakes, which may actually "break" the subducting lithosphere (Fig.12).

Figure 12: Schematic figure of large normal-faulting in subduction zones. In regions with weak interplate coupling, the normal faulting can involve great earthquakes, effectively detaching the deep plate.

B- Continent-continent collision:

The seismotectonics of a continent-continent collision are complicated. Usually, faulting is dominated by thrusting, which is a manifestation of the lithospheric shortening. In many of the collisions, well developed, low-angle thrusts occur beneath the suture zone. These low-angle faults can generate very large earthquakes (M > 8.5).

Earth velocity structure:

It is also known as the seismic velocity profile of the earth. It is determined by measuring travel times of earthquake waves to seismograph stations. A large number of body-wave travel times and surface-waves were modeled in constructing the Preliminary Reference Earth Model (PREM). In this model, the entire Earth can be approximately viewed as a layered, 1D stratified, chemically differentiated planet composed of crust, mantle, and core. These major layers are separated by boundaries (the Moho and the core-mantle boundary) across which seismically detectable material properties have strong contrasts. When seismic waves pass between geologic layers with contrasting seismic velocities reflections, refraction (bending), and the production of new wave phases (e.g., an S wave produced from a P wave) often result. Sudden jumps in seismic velocities across a boundary are known as ***seismic discontinuities***.

Seismically, the earth velocity structures include:

1- Crustal structure (Vp 1.5 to 8.1 km/s):

The boundary separating crustal rocks from mantle rocks is called the ***Moho*** and is a ubiquitous boundary of highly variable character. The Moho likely involves a chemical contrast and transitions in rheological properties, phase transitions in shallow mineral structures, and petrographic fabrics of the rocks. Seismically, the shallow rocks of the crust have slower seismic

velocities than the deeper rocks, and this the crust is considered a low-velocity layer over the higher-velocity mantle.

2- Upper mantle structure (about 70 km to 670 km depth and Vp of about 8 to 11 km/s):

Stratification of the mantle is represented by seismic discontinuities that probably represent mineralogical phase transformations that involve no bulk change in composition but reflect a transition to denser lattice structures with increasing pressure. The mantle also has localized boundaries at various depths associated with laterally varying thermal and chemical structure:

A- The lid:

It is the region of the upper 250 km of the mantle, just below the Moho and with high seismic velocities *(P* velocities of 8.0-8.5 km/s). It is particularly heterogeneous, with strong regional variations associated with surface tectonic provinces. It is called the *lid* because it overlies a lower-velocity region. The lid is thought to represent the rheological transition from the high-viscosity lithosphere to the low-viscosity asthenosphere.

B- The Low velocity zone (LVZ):

It is a region of reduced velocity beneath the lid. It is thought to represent the upper portion of the rheologically defined asthenosphere, where low strength decreases the velocity. The LVZ extends in depth from 100 to 200 km below the lid.

C- The transition zone:

Occurred at depths near 400 and 650 in the lower part of the upper mantle.

The seismic discontinuities between the LVZ and transition zone and between the transition zone and the lower mantle is thought to be due to phase changes in the constituent minerals of the mantle. In this phase transformation, material with uniform composition collapses to a denser crystal structure with increasing pressure. Most of the minerals in the upper mantle have an olivine structure which changes to the high-pressure spinel structure at the 450 km discontinuity (beginning of the transition zone) increasing the seismic velocity. The 650 km discontinuity (the base of the transition zone and beginning of the lower mantle) is attributed to another phase transition from spinel to a more close-packed structure possibly stishovite. The earthquakes stop near this boundary. No earthquakes were recorded deeper than about 700 km.

3- Lower-mantle structure (Vp of about 11.5 to 13.5 km/s):

There is an absence of significant boundaries throughout much of the vast region from 710 to 2600 km depth. Thus, the lower mantle is considered homogenous. From 2600 to 2900 km, a

zone called D`` occurred, which is a less homogenous zone that scatters the seismic waves. This could be a thermal boundary layer at the interface with the core.

4- Core structure:

The boundary between the mantle and the core can be estimated accurately due to the absence of S-waves in the reflections from the core as well as a significant dramatic decrease of the P waves (Vp decreased to 8 km/s), suggesting it is a pure liquid. The boundary between the mantle and core is very sharp and is the largest compositional contrast in the interior, separating the molten core alloy from the silicate crystalline mantle. It is called **Gutenberg boundary**.

This outer core structure was discovered when seismologists had noticed that P waves are not recorded at seismograph stations which are from 104^{o} to 140^{o} away from an earthquake (the angle is the angle made by drawing a line from the earthquake to the center of the Earth, and then from there to the seismograph station). This area where the P-wave was not recorded is called **P Shadow Zone**. It is formed because the outer core slowed and bent P waves. An S wave shadow zone was also recognized, meaning no S waves were received at seismographs stations from 104^{o} to 100^{o} from an earthquake; the S wave shadow zone is caused by the outer core, which is liquid iron/nickel (Fig. 13).

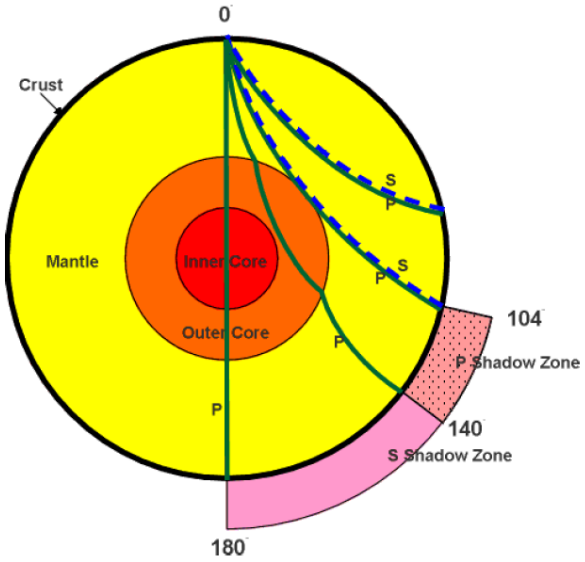

Figure 13: The formation of the P and S shadow zones by the inner and outer core.

Figure 14 shows a model describing the earth velocity structure.

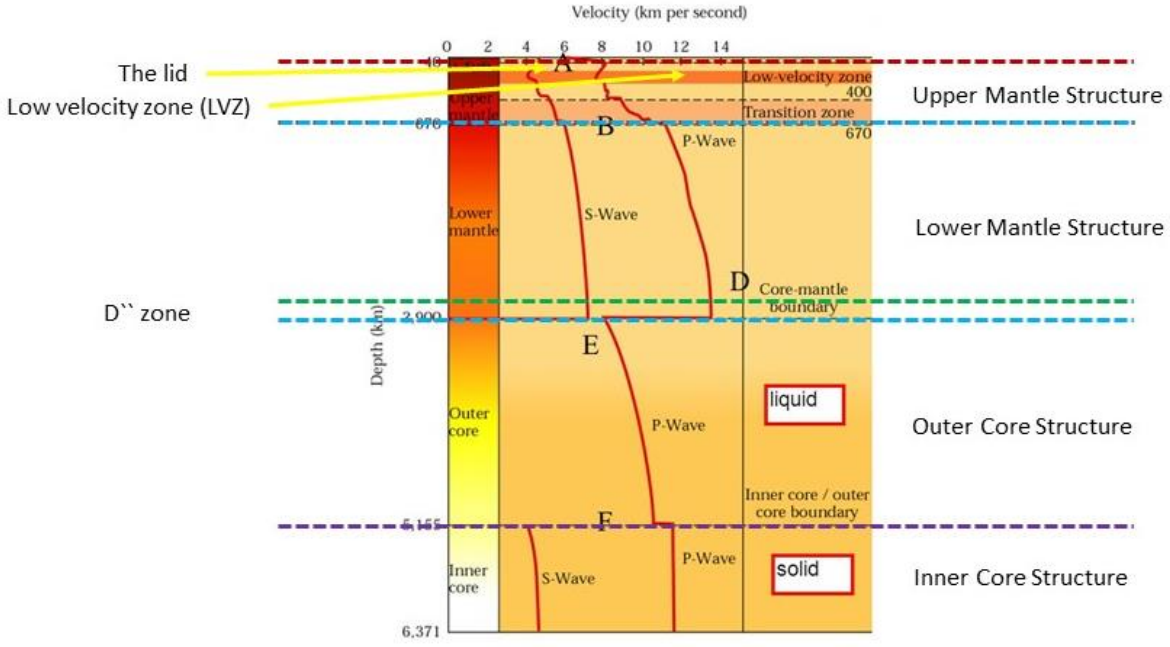

Figure 14: the earth velocity structure model

Wilson Cycle

Wilson cycle describes the cyclical opening and closing of ocean basins caused by movement of the Earth's plates. A Wilson cycle consists of two phases each have three stages as follows (Fig.1):

1- The opening phase:

A- Embryonic stage:

The cycle begins when stable thick continental crust (craton). A mantle plume (hot spot) rises up under the craton, heating it, causing it to swell upward, stretch, expand and thin. Eventually the crust fractures, forming a rift valley.

B- Juvenile stage

With rifting of the continental crust, the broken sides rise forming the ridge, that often fills with fresh water. Rift valleys gradually widen and eventually connect to the ocean and the freshwater lakes become narrow saline gulfs. This is happening now in the Red Sea.

C- Mature stage

With continued lateral spreading of the rift valley, the divergent plate boundary widens and additional oceanic crust is generated.

2- Closing Phase:

D- Declining stage:

In time, cooling and the loss of volatiles increase the density of oceanic plates. Away from the ridge, the other side of the plate sinks into the asthenosphere at subduction zones. Typically an ocean basin widens for about 200 million years before subduction begins. Eventually, the basin begins to close as subduction rates (at trenches) exceed spreading rates (at mid-ocean ridges). For Earth as a whole, spreading must equal subduction—otherwise the planet would be shrinking or expanding.

E- Terminal stage:

Subduction of the intervening oceanic crust causes a narrowing of the sea separating the continents and the ocean basin closes as continents from opposite sides of the ocean basin get closer to one another.

F- Suturing stage:

Collision of the continents is complete, and the intervening sea is gone. The two colliding continental crusts, being less dense than the oceanic crust, do not subduct but rather override one another causing uplift and mountain building. Collision of the continents squeezes out the intervening ocean and causes subduction of oceanic crust.

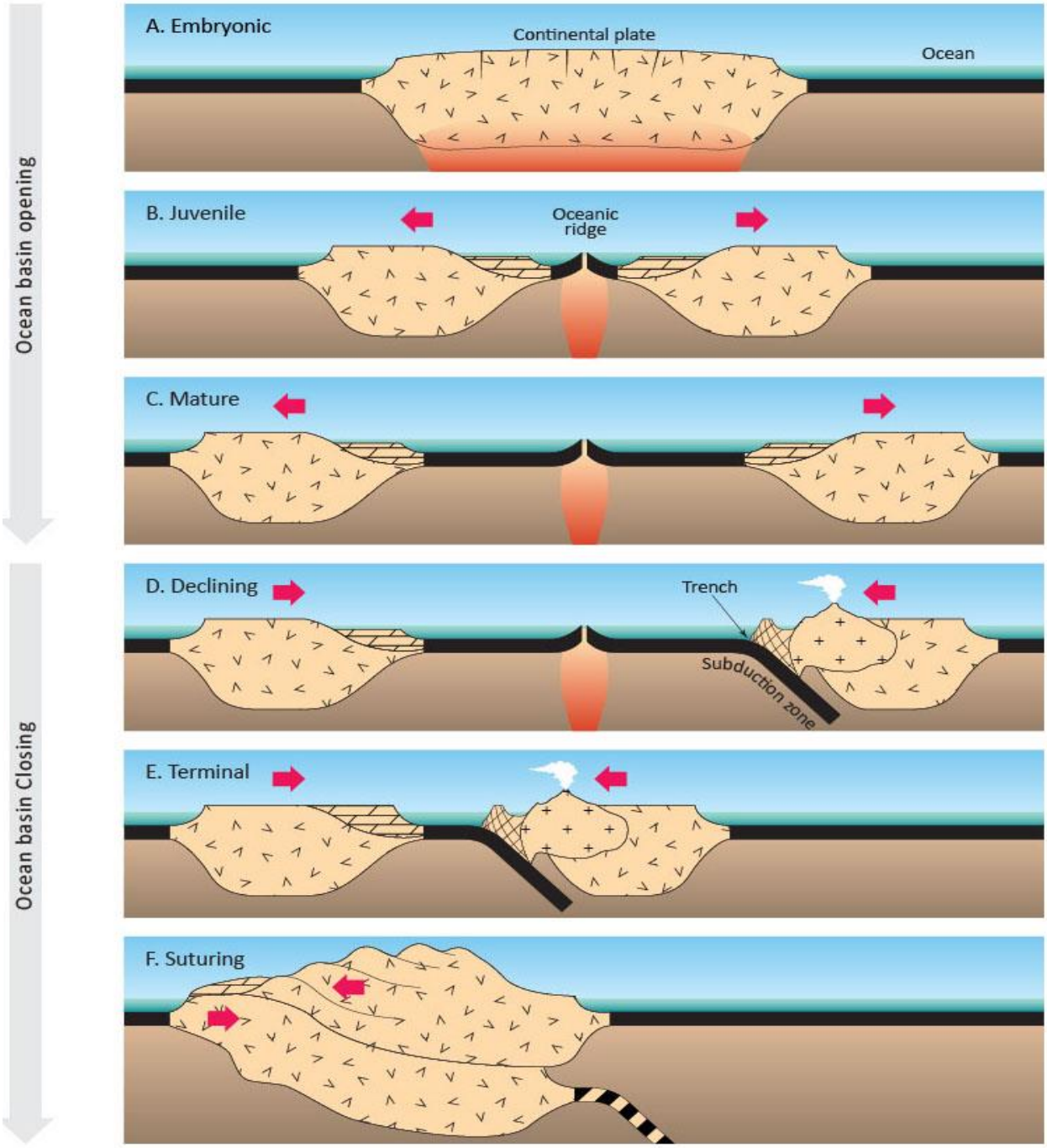

Figure 1: Wilson Cycle.

Continental graben structure (Rift)

Definition and occurrence of continental graben structure

A continental graben structure or rift is a narrow, elongated, fault-bounded structure in the Earth's crust (Fig. 2). Grabens consist of a central axial depression flanked by steep walls and elevated shoulders that plunge steeply into the rift axis and slope gradually towards the exterior (Fig. 3.2). The most famous examples are the East African rift system and the Upper Rhine Graben in Central Europe.

Graben structures occur in:

- regions where the crust and lithospheric mantle are extended, and thinned,
- in oceanic crust along mid-ocean ridge systems.

The components of the graben structure are illustrated in Fig. 2., and include:

1- The graben axial or rift valley:
   It is an elongated topographic depression bordered by fractures (faults)in the center of the graben formed as the central block of the rock subsided due to the lithospheric extension and faulting.
2- Normal faults:
   Formed by the tension forces and they bound the axial valley. The have dip angles of 60-65^{o}.
3- Graben shoulders:
   The blocks of the rocks that are formed by tearing the rock by the faulting and they plunge steeply into the rift axis and slope gradually towards the exterior.

Mechanism of the graben formation:

1- The brittle extension, generated by fracturing associated with earthquake activity in the upper crust, extends downward to a depth of approximately 15 km.
2- At greater depths, ductile flow occurs without fracturing the rocks.
3- Graben subsidence is accommodated along normal faults that dip towards the central graben axis at angles of 60 to 65°: the hanging wall, the block located above any point of

the fault plane, moves downwards with respect to the foot wall and causes the subsidence of the graben.

4- As the lithosphere extends, the asthenosphere tends to rise and heat flow rate increases; as a consequence, melting in the uppermost asthenosphere or overlying lithospheric mantle may occur.
5- The melts penetrate the crust and feed volcanoes at the surface or form magma chambers at depth.
6- Because the magmas are derived directly from the mantle, they are basaltic in composition, hence the close association of basaltic volcanism and graben rifting.
7- When magmas are trapped at depth and accumulate in magma chambers, they potentially undergo additional processes that result in change of magma composition. These processes remove the mafic minerals that have high melting points and sink to the bottom of the magma chamber produce intermediate to granitic melts. These various magmatic processes explain why many rift areas are associated with volcanism and plutonism of various compositions.

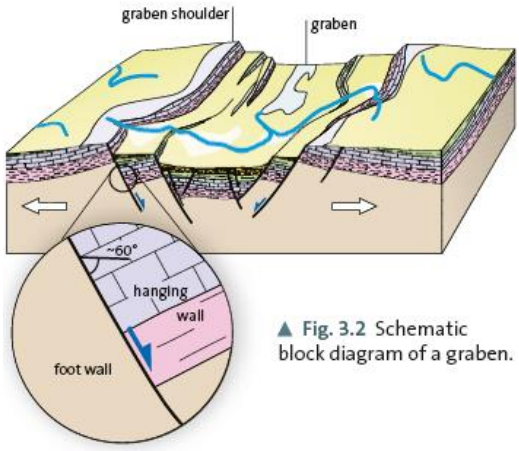

Figure 2: Schematic block diagram of graben structure.

Classification of the graben structures:

Based on the relations between topographic expression and method of formation, there are two classes of grabens, active and passive (Fig.3):

1- Active Graben Structure:

- Active grabens are generated by upwelling of the asthenosphere, commonly over hotspots; the overlying mantle lithosphere and crust respond to this process, and both are thinned.
- The mantle lithosphere and lower crust deform plastically, and the upper crust is faulted to form the graben structure; both are thinned and basaltic volcanism is generated.
- The wide zone of the asthenospheric doming causes the bulge of the Earth's surface at active rifts to also be broad, commonly several hundred kilometers wide.

2- Passive Graben Structure:

- At passive graben structures, extensional forces are the primary cause.
- Initially, the extension is limited to the narrow zone of the rift, both in the deeper crust and in the lithospheric mantle. This process can result in the complete tearing off of the lithospheric mantle which then leads to asthenospheric material rising to the base of the crust.
- The surficial bulge is thus restricted to the narrow graben zone.
- However, extension of the lithosphere may also lead to a wider updoming of the asthenosphere and the lithosphere above. Thus, a passive rift may change into an active rift system and the passive stage is no longer detectable.
- Although most present graben systems seem to be active rifts, it is assumed that both processes, updoming and crustal extension, act together.

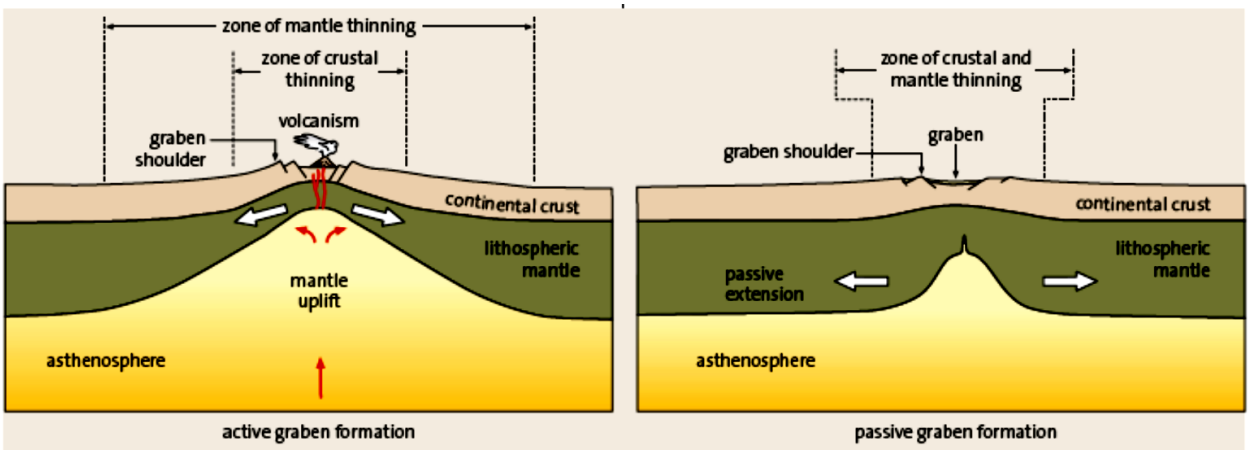

Figure 3: Active and passive Grabens.

Crustal extension is believed to occur in two different modes symmetric and asymmetric. Accordingly, graben structures are also classified into symmetric and asymmetric grabens (Fig.4).

3- Symmetric Graben structure (Symmetric model, McKenzie, 1978):

- The symmetric model is based on many present graben systems.
- It assumes symmetric, brittle extension of the crust along normal faults in the upper 10 to 15 km, and ductile deformation at depth.
- Both the crust and lithosphere thin accordingly and cause the surface of the Earth to subside and generate the graben morphology.
- However, the ascent of hot asthenosphere causes the lower part of the lithospheric mantle to be transformed into asthenosphere. Therefore, lithospheric mantle can be transformed into asthenosphere by an increase in temperature and vice versa.
- The original bulge of the surface, caused by a hot, relatively light bulge of asthenospheric mantle material, leads to erosion at the graben shoulders, a process that also results in a reduction of thickness of the crust.
- Thermal subsidence is developed after the heat source disappears and the mantle bulge cools and increases in density.

4- Asymmetric Graben structure (Asymmetric model, Wernicke, 1981):

- Asymmetric grabens are characterized by a gently dipping master fault, termed a detachment fault, that cuts at low angles through the crust from one flank of the graben down to the base of the lithosphere.
- The overriding upper plate of the detachment is characterized by steeply inclined normal faults that form in response to the extreme amount of brittle crustal extension.
- the crust of the upper plate is extended and thinned at a different location from that of the lithospheric mantle, the lower plate of the detachment.
- This asymmetry gives rise to the following morphology: above the area of crustal thinning, the surface subsides because light crustal material is replaced by denser mantle material; above the area of lithospheric mantle thinning, the surface bulges because lithospheric mantle is replaced by slightly less dense, hotter asthenospheric material.

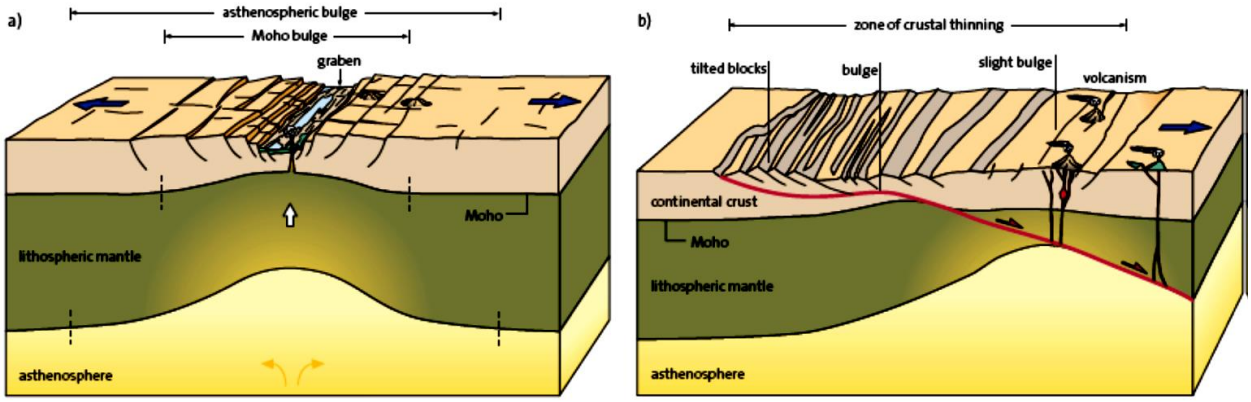

Figure 4: a) Symmetric and b) asymmetric model for the evolution of a graben system.

Sediments and ore deposits in graben structures:

1- Immature terrestrial sediments (fluviatile sediments) are deposited by rivers that source the steep flank of the graben shoulder. Many fluviatile sediments in graben structures are mostly composed of conglomerates rich in rock fragments and arkoses (sandstones that contain abundant feldspar) and have a relatively low percentage of quartz.

2- Lacustrine deposits are rich in clays and, under arid or semi-arid conditions, saline sediments.

3- Marine sediments in graben structures are mostly mudstone, marl (limy mud) or limestone. Strong evaporation in arid climates where partly or completely isolated basins fill with seawater leads to concentration of salt in the water followed by precipitation of salt.

4- Petroleum and natural gas are important deposits in some continental rift systems. Lack of oxygen in the lower part of the water column leads to oxygen-poor sediment which in turn prevents decomposition of organic matter included in the bottom fossils. This generates an enrichment of organic material in the sediment and results in characteristic dark gray or black colors. Basin subsidence lowers organic-rich sediment into the so-called petroleum window, a temperature range between approximately 80 and 170 °C. Here petroleum forms by complicated reactions involving the organic matter. At temperatures over approximately 150 °C, gas deposits are formed.

Hotspots

Magmatic activities at plate boundaries:

Magamatic activities at the plate boundaries produce magmatic belts as magma and related volcanisms are rising by the interaction between the plates.

1- At subduction zones:

   The melting that produces magmatism is caused by complex interrelations between the asthenosphere and the subducting plates plunging into it. These melts intrude into the upper plate and feed volcanic chains above subduction zones

2- At mid-ocean ridges:

   Mid-ocean ridges are the location of major production of basic magmatites, namely basalts and gabbros. High temperature and pressure release beneath the ridges combine to generate partial melting of up to ~20 % the rocks of the mantle (peridotite). Oceanic crust develops from these melts. Mid-ocean ridges generate more than twice the amount of melts than are generated above subduction zones.

Hot spots

Hot spots are places of intraplate magmatism. They are point-sources of magma caused by mantle diapirs and occur on either the continents or oceans (Fig. 5). Diapirs, known as mantle plumes are hot, finger-like zones of rising material within the mantle. When they reach the upper asthenosphere beneath the plates, melting is induced that creates volcanic eruptions and doming of the surface over long time periods.

As plates drift over hot spots, long volcanic chains develop with the hot spot located at the active end; Hawaii is a good example of this.

On continents, hot spots are commonly related to graben structures characterizd by extensive, deep fault systems that cut through the entire thickness of continents. Graben structures are characterized by crustal extension and bordered by faults; such areas cause thinning of the lithosphere and provide the opportunity for magma to rise along fault zones. If extension continues,

new ocean can be formed at these structures. An example for such a newly developing ocean is the northern part of the East African graben system (Afar) and the Red Sea.

Graben structures may be transferred into constructive plate boundaries where the hot spot commonly plays an important role.

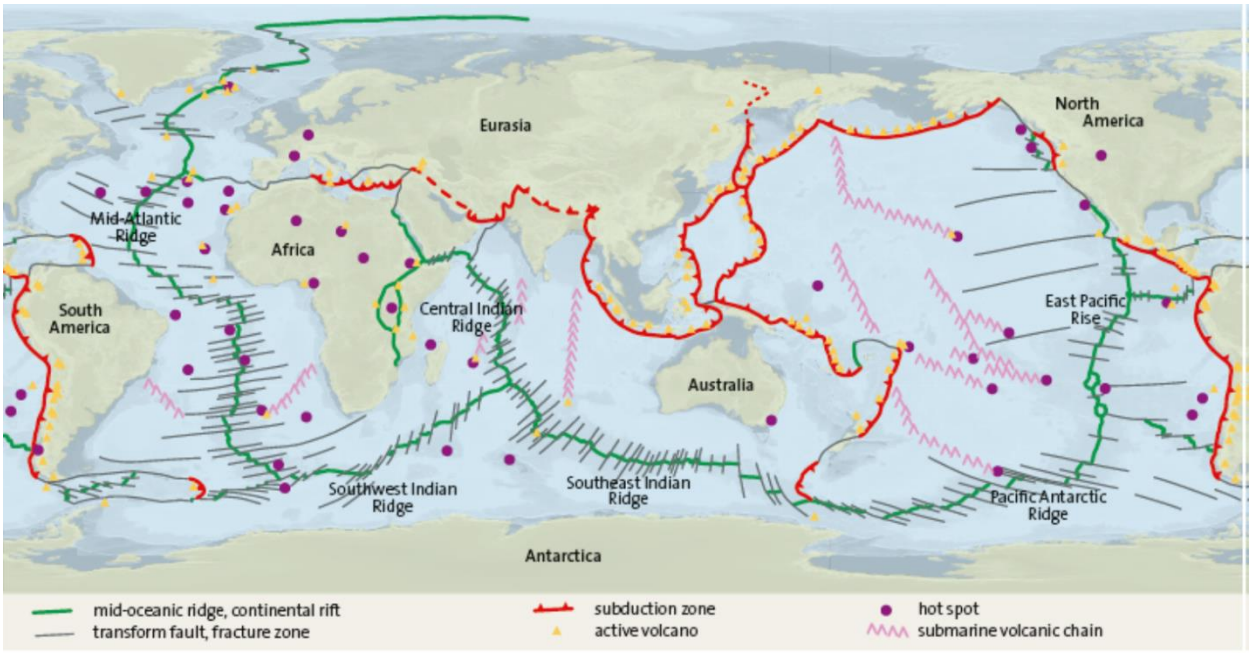

Figure 5: A map of the earth with the location of plate boundaries, active volcanoes and hot spots.

Convergent boundaries

Types of convergent boundaries:

There are four types of convergent plate boundaries (Fig. 1):

1. The first type occurs when ocean lithosphere is subducted below other ocean lithosphere ("intra Oceanic subduction zone") to create a volcanic island arc system built on oceanic crust ("ensimatic island arc"; sima – artificial word made from silicon and magnesium to characterize ocean floor and Earth's mantle).
2. The second type occurs where oceanic lithosphere is subducted beneath continental lithosphere and an island arc underlain by continental crust forms ("ensialic island arc"; sial – silicon and aluminum for continental crust). The island arc of this system is separated from the continent by a marine basin underlain by oceanic crust.
3. The third type of convergent plate boundary represent the active continental margins where oceanic lithosphere is subducted beneath continental lithosphere without a marine basin behind the volcanic arc; rather, the arc is built directly on the adjacent continent.
4. The fourth type of convergent margin occurs along zones of continent-continent collision. If two continental masses collide, they eventually merge. In this case, a standstill subduction occurs within the collision zone. The oceanic part of the subducting plate tears off and continues to drop down, a process referred to as " slab breakoff ". Continent-continent collisions ultimately result in the formation of mountain.

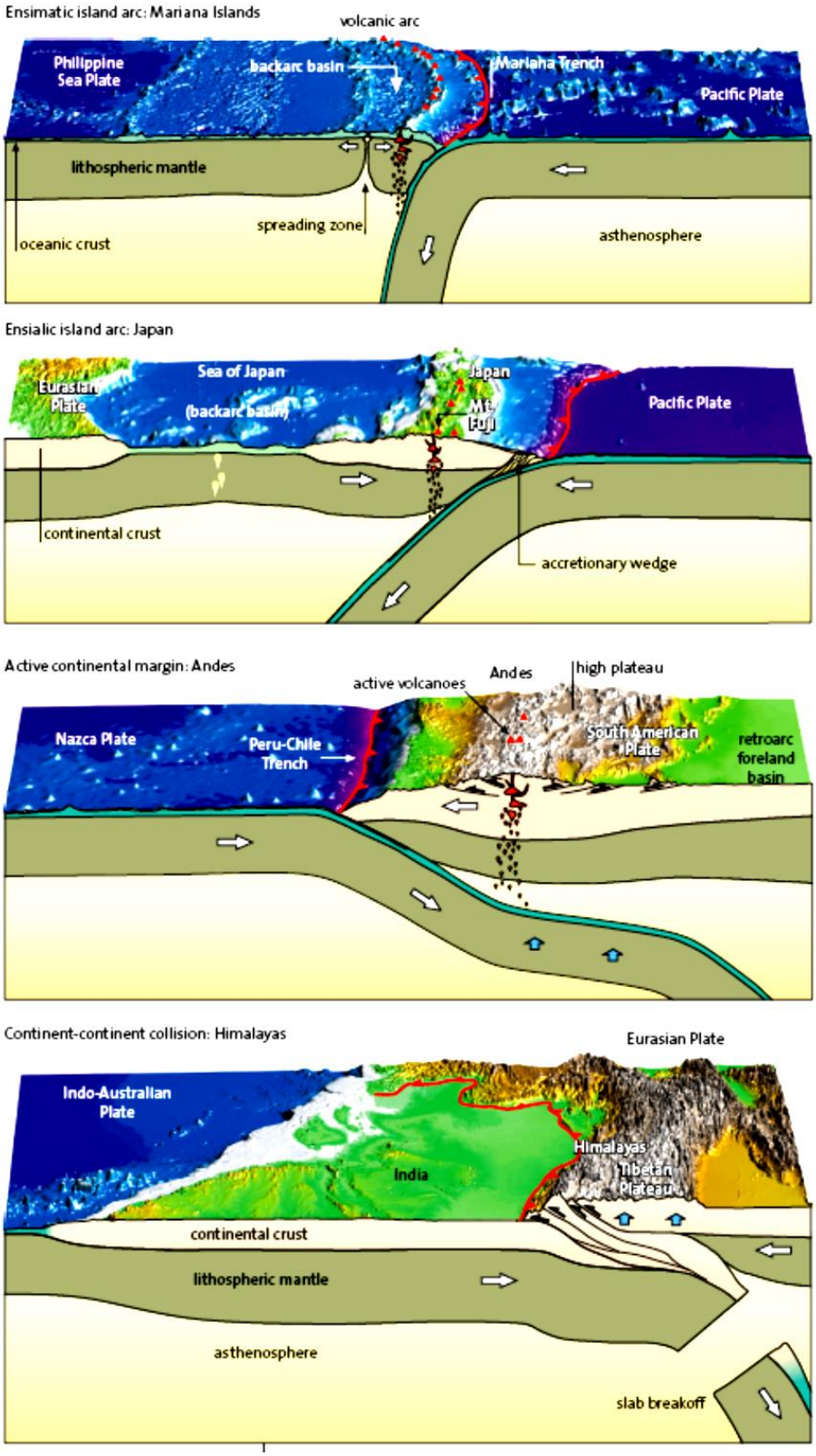

Figure 1: Examples of different types of plate margins with subduction zones. The collision of two continents produces a mountain range like the Himalayas – subduction wanes, leading to slab breakoff.

Features associated with convergent boundaries:

1- Island arcs:

The volcanic zone above the subduction zone, in many cases expressed as an island arc, is the dominating element of this plate boundary system. Island arcs are long chains of active volcanoes with intense seismic activity found along convergent tectonic plate boundaries. Most island arcs originate on oceanic crust and have resulted from the descent of the lithosphere into the mantle along the subduction zone.

The arc area is usually divided into three parallel zones (Fig. 2):

a) **The forearc zone**: the zone from the trench to the arc.

b) **The arc zone** comprises the magmatic belt, and

c) **The backarc zone:** the region behind the arc.

2- Deep sea trenches:

They are elongated narrow deep trenches that are located at the border of the upper plate, resulted by downward bending of the oceanic lithosphere under the margin of the upper plate during subduction. The morphological features of these trenches are (Fig. 2):

A- The trench slope:

The landward side of the deep-sea trench is part of the upper plate and consists of a slope with an average steepness of several degrees.

B- The outer ridge:

The outer ridge follows behind the slope. In most cases, the ridge remains substantially below sea level; however, in several cases, islands emerge above sea level. The outer ridge is not always distinctive.

The morphology of the outer ridge forms as sediments are scraped off of the subducting plate during subduction. As the subducting plate transports its sedimentary fill from the trench towards the arc, some portion of the sediment is subducted and transported down to great depths where it becomes an important factor in the feeding of subduction-related magmas. The remaining portion, or in some cases the entire sedimentary layer and parts of the oceanic crustal basement, can be scraped off at the frontal tip or the bottom of the upper plate and added to a so-called accretionary wedge on the upper plate. An accretionary wedge or accretionary prism forms from sediments accreted onto the non-

subducting tectonic plate at a convergent plate boundary. Most of the material in the accretionary wedge consists of marine sediments scraped off from the downgoing slab of oceanic crust, but in some cases the wedge includes the erosional products of volcanic island arcs formed on the overriding plate.

C- Forearc basin:

The forearc basin lies directly in front of the volcanic arc. Collectively, the deep sea trench, outer ridge, and forearc basin comprise the forearc region. The distance between the plate boundary and magmatic zone has a width of between 100 and 250 km. This region is also called the arc- trench-gap, a magmatic gap that with very few exceptions is void of magmatic activity. Low temperatures in the crust are caused by the coolness of the subducting plate underneath and prevent the formation of magma by melting or the rise of magma from deeper sources.

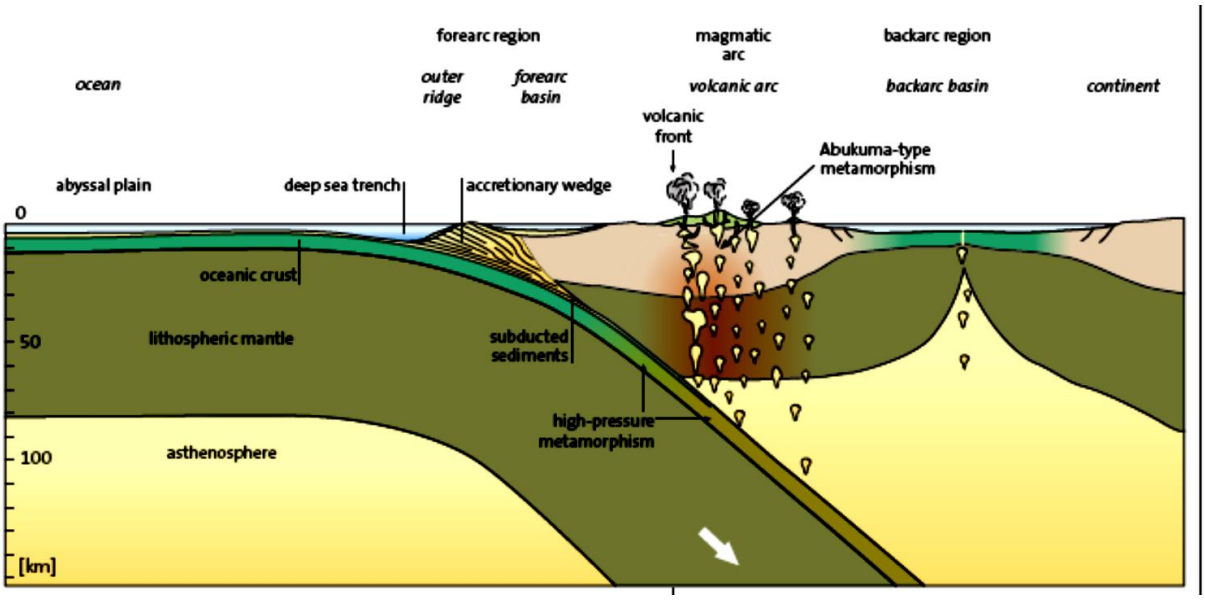

Figure 2: Structure of a plate margin system with subduction zone and ensialic island arc.

Types of subduction zones:

1- Mariana-Type or spontaneous subduction zone:

It is characterized by old and dense lithosphere that is subducted and sinks into the sublithospheric mantle by its own weight. Therefore, it is generally the steepest-dipping subduction. Because oceanic lithosphere becomes denser with increasing age, it can

achieve a density greater than that of the underlying asthenosphere and thus be more easily subducted (spontaneous).

2- Chile-type or forced subduction zone

It is characterized by younger, hotter and less dense lithosphere that dips at a shallower angle (Fig. 7.5). If the age of the oceanic lithosphere is young, subduction can only be initiated by compressional forces; this is forced subduction.

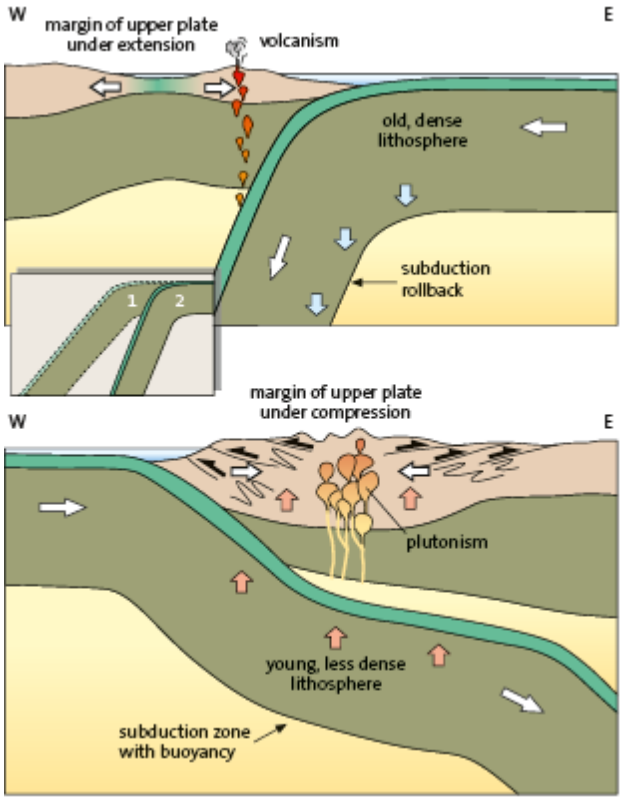

Mountain Building (Orogeny)

Orogeny is the process of forming mountain belts by folding and thrust faulting. Orogeny typically produces orogenic belts or orogens, which are elongated regions of deformation bordering continental cratons (the stable interiors of continents). They are characterized by crust thickened to more than 70 km, in comparison to normal continental crust that is 30–40 km thick.

Orogenies affect localized areas called orogenic zones. Such zones are affected by a regular sequence of events that is essentially the same for each orogenic belt.

The motor of orogeny is subduction. The process of orogeny becomes initiated by subduction of ocean floor and finds its climax in the collision of continents.

An orogenic belt undergoes several phases of sedimentation, magmatism, metamorphism, and deformation as it evolves into a mountain range. The phases that affect an orogenic belt may be separated into two groups, the geosynclinal phases and the tectonic phases.

1- Geosynclinal Phases:

A geosyncline (or geocline) is a very elongated structural trough in which a great thickness of sedimentary and/or volcanic rock has been deposited. The geosyncline forms as a result of the subsidence of a continental margin, perhaps one that formed as a result of the separation of two continents. The subsidence of the geosyncline/geocline is due in part to the weight of the sediments deposited. The geosynclinal phases take place below sea level or near the surface and is characterized by negative vertical motions (subsidence). These phases include:

A- Preorogenic Phase.

The preorogenic phase is characterized by:

- Rapid deposition of thick sequences of sediments in a geosyncline
- These sediments are flysch sediments that are fed into the geosyncline from the adjacent continent, which undergoes rapid erosion.
- Subsidence in the geosyncline is slow.
- Sediments are commonly calcareous, but sands and muds were also deposited.

B- Early Synorogenic Phase:

This phase is characterized by:

- Rapid subsidence and volcanic rocks are erupted from deep fissures originating in the asthenosphere. These rocks include:
  - Spilites (metamorphosed basalt at low temperature) often display pillow structures.
  - Radiolarian cherts (radiolarites)
  - Detrital deposits (flysch and turbidites)

- Serpentinites as part of ophiolites and they form a linear belt along the suture between collided continents.

C- Cata-orogenic Phase:

This phase is characterized by:

- The first folding occurs
- Ophiolite complexes and flysch sediments continue filling geosyncline
- Rising of ridges (also known as geanticlines) that are composed of soft sediments or soft sedimentary rocks as well as old, indurated basement rocks. These ridges are elongated regions that are normally uplifted and shed sediments into the adjacent geosyncline.
- Geosynclinal basins may be divided by several geanticlines into separate subsiding troughs.
- Calcalkaline volcanism (andesites, dacites, and basalts, but rhyolites may be present)

D- Epiorogenic Phase:

This phase is characterized by:

- folding intensifies and there is some thrusting in the geanticlines on the foreland.
- coarse flysch deposition continues in the geosyncline.
- Stratovolcanoes continue to erupt andesitic lavas and ash.
- Subsidence is rapid, and sequences of detrital sediments are laid down along with interbedded volcanic rocks.
- Metamorphism may reach granulite grade in the rocks most deeply buried, and granitization may occur in these sequences.
- The deposits of the main geosyncline basins are intensely folded and metamorphosed, but those of the fore arc basins are less deformed and less metamorphosed.

2- Tectonic Phases

These phases take place above sea level, like in mountain ranges. The tectonic phase is characterized by positive vertical motions (uplift).

A- Late Synorogenic Phase.

This phase is characterized by:

- the ocean floor between two approaching continents disappears as these continents begin to collide.
- On the surface, the new mountain range formed by the collision undergoes folding and thrust faulting while rising.
- In the core of this mountain range, granitic magmas are formed and rise as they are lighter than the surroundings. Some, or perhaps most, of these magmas originate as a result of the partial melting great depths within the mountain range. These granites may be accompanied by pegmatitic dikes and mineralized veins. Basaltic volcanism may also accompany this phase as the mountain range undergoes fracturing.
- Some marginal parts of the mountain range may sink again so that the sea invades these subsiding coastal areas.

B- Postorogenic Phase:

This phase is characterized by:

- The mountain range is now indurated and becomes a part of the continent.
- At this stage, it may undergo epeirogenic uplift and as it is rather brittle, it breaks easily.
- The mountain belt may undergo normal faulting.
- Subaerial erosion by rivers and wind generates detrital sediments such as molasse, and basaltic volcanism may accompany this sedimentation.
- At depth, granitic magmas may again form and rise upward.

C- Nonorogenic Phase:

This phase is characterized by:

- The mountain range is at last integrated into the continent, leveled by erosion, and no longer rejuvenated, the site of the mountain range may become stable and the only movements affecting it will be epeirogenic uplift, subsidence, or tilting
- Weathering and pedogenesis work slowly to generate arkosic detrital sediments and soils.
- Basaltic lavas may rise along great faults and fractures from sources within the asthenosphere.
- Explosive rhyolitic volcanism may also occur at this stage, forming rhyolitic lavas and microgranites very low in dark minerals, often intruded as ring dikes.

The Great Rift Valley

The Great Rift Valley System stretches from the Middle East in the north to Mozambique in the south. The area is geologically active, and features volcanoes, hot springs, geysers, and frequent earthquakes.

The northern part of the system is the Jordan Rift Valley. The Jordan Rift Valley stretches from the Golan Heights, near Palestine's border with Syria and Lebanon, to the Dead Sea, to the Gulf of Aqaba—an inlet of the Red Sea that separates the Sinai Peninsula from the Arabian Peninsula.

Associated with the Jordan Rift Valley to the south is the Red Sea Rift. Millions of years ago, the Arabian Peninsula was connected to Africa. Seafloor spreading caused the Arabian and African plates to rift apart. The Indian Ocean flooded the rift valley between the continents, creating the Red Sea. Today, Africa and Asia are connected by the triangle of the Sinai Peninsula. Eventually, the Red Sea Rift will separate Africa and Asia entirely and connect the Mediterranean and Red Seas.

Southern and linked to the Red Sea is the East African Rift system.

1- The East African Rift System

East African rift system is a presently active system with abundant volcanism. It represents different stages of continent break-up. The East African rift system has not matured enough to have formed a new plate to the east, although the crust is nearly severed at some places forming the Somalian Plate. At its northern end, the Afar Depression, which because of its triangular shape is also called the Afar Triangle, has partly generated new oceanic crust.

Characteristics of the east African system:

1- The rift is a developing divergent tectonic plate boundary where the African Plate is in the process of splitting into two tectonic plates, called the Somali Plate and the Nubian Plate. The eastern portion of Africa, the Somalian plate, is pulling away from the rest of the

continent, that comprises the Nubian plate. The Nubian and Somalian plates are also separating from the Arabian plate in the north, thus creating a 'Y' shaped rifting system. These plates intersect in the Afar region of Ethiopia at what is known as a 'triple junction'.

2- Crustal extension has formed a series of elongate lowland valleys bound by steeply dipping normal faults, separated by regions of comparatively high land.
3- The region is characterized by two broad topographic uplifts (Fig. 1), each underlain by mantle diapirs with broad mushroom-shaped heads:
    a. The northern uplift includes Ethiopia and Yemen and has the afar triangle at its center.
    b. The southern uplift area is in Uganda, Kenya and Tanzania and is marked by the intersection of the Kenya and Central African rifts.
4- The system is divided into eastern and western branches. Both the eastern and western rifts are characterized by volcanic activity, brittle faulting and large asymmetric half graben systems filled with river and lake sediments.
5- The faults of the rift systems are generally parallel to structures of the Precambrian basement, suggesting that the graben structures follow old zones of weakness in the crust.
6- The East African Rift has evolved since the Late Oligocene or Early Miocene, originating at the Afar triple junction and extending southwards over time.
7- The average extension rates in the East African graben system, 0.4–1 mm/yr.
8- The system is not considered to be a plate boundary but rather the result of intraplate tectonics.
9- The entire region is characterized by negative gravity values and local high heat flow.
10- The graben system is underlain by a 1500 km wide bulge of the asthenosphere that nearly cuts through the lithosphere in the Kenya Rift (Fig. 2); a 20 km-wide intrusion has protruded to a depth of only 3 km below the sole of the graben.
11- The east African rift system comprises two graben systems:
    A. The Kenya or Georgory Graben

    The Gregory Rift stretches from the Red Sea and the Arabian Sea to as far south as Mount Kilimanjaro. The Gregory Rift Valley has shoulders that rise more than 3000 m above sea level and 1000 m above the inner part of the graben. Collective vertical displacement along the main graben faults much as 4 km. The graben area is cut by

densely clustered faults that parallel the edges of the graben and define a horst-and-graben structure.

B. The Ethiopian Rift system.

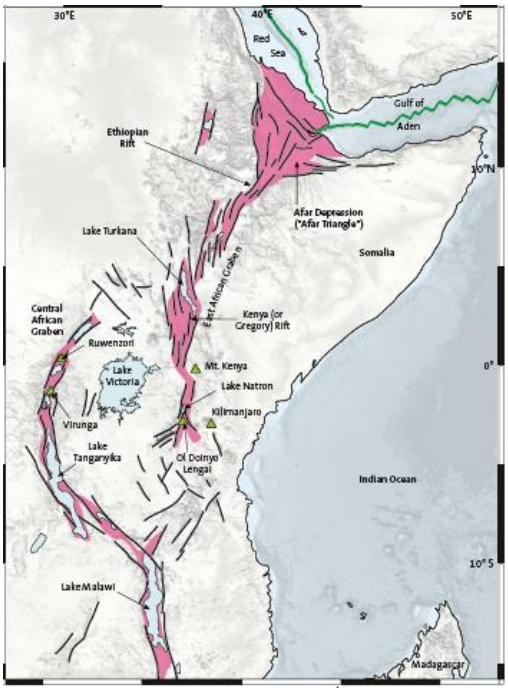

Figure 1: Map of the principal elements of the East African graben system.

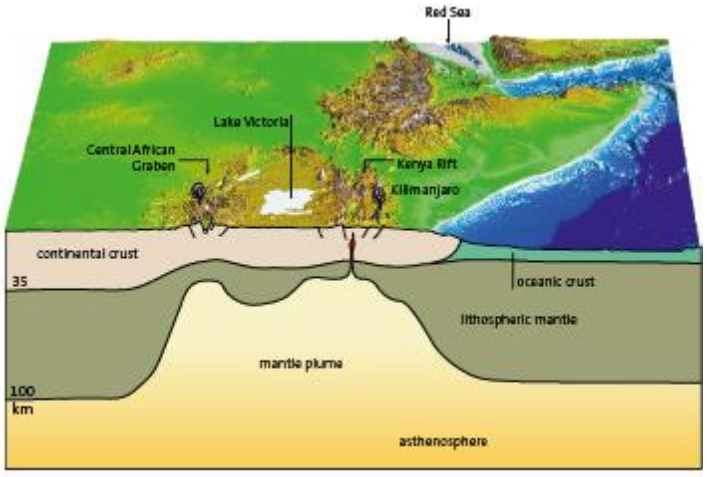

Figure 2: Block diagram of the East African graben system. The lower cross-section through the Central African Rift and the Kenya Rift demonstrates the strong thinning of the lithospheric mantle.

Afar depression

The Afar triangle (Fig. 3) is the triple junction between the African, Arabian and Somalian plates. The Afar Depression is a lowlying triangular area (Fig. 3), at the center of a three-point graben

star, where the East African graben system (Ethiopian Rift), the Red Sea, and the Gulf of Aden meet. Here, the transition from a continental graben to an initiating ocean basin can be observed. Underlying the depression, a mantle diapir rises and overlying continental crust is strongly thinned and fragmented. In fact, between the separated continental fragments, new oceanic crust has been generated. Numerous bundles of faults pervade the depression. Along these faults, basaltic lavas with a tholeiitic composition similar that of mid-ocean ridge basalts, periodically discharge.

Two arms of the Afar Triple Junction continue to widen in the process of seafloor spreading—the arm extending into the Red Sea and the arm extending into the Gulf of Aden. As these rifts continue, the narrow valley created by the Gregory Rift (the arm of the Afar Triple Junction located above sea level) may sink low enough that the Arabian Sea will flood it.

The tectonic and volcanic activity is concentrated along the inner part of the graben system, an area characterized by both horizontal and vertical movements of blocks.

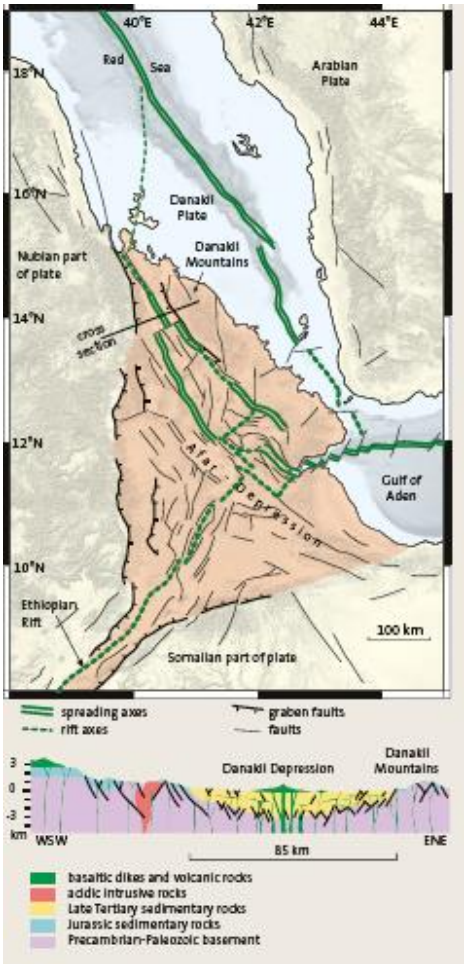

Figure 3: Map showing structural elements of the Afar Depression or Afar Triangle. The region consists of a mosaic of blocks with thinned continental crust including the small “Danakil Plate”. Basaltic rocks lie in the separation of the crust within the narrow spreading axes between the blocks. This relation is shown in the cross section through the Danakil Depression.

2- The Red Sea Rift

The Red Sea is a relatively recent constructive plate boundary that consists of a band of oceanic crust up to 100 km in width that was formed during the Late Tertiary by the separation of Arabia from Africa. The oceanic band contains a central graben that marks the plate boundary and attains a depth of more than 2000 m (Fig. 4). The central graben is not yet developed as a midocean ridge in the true morphological sense. It is asymmetric graben structure (Fig. 5).

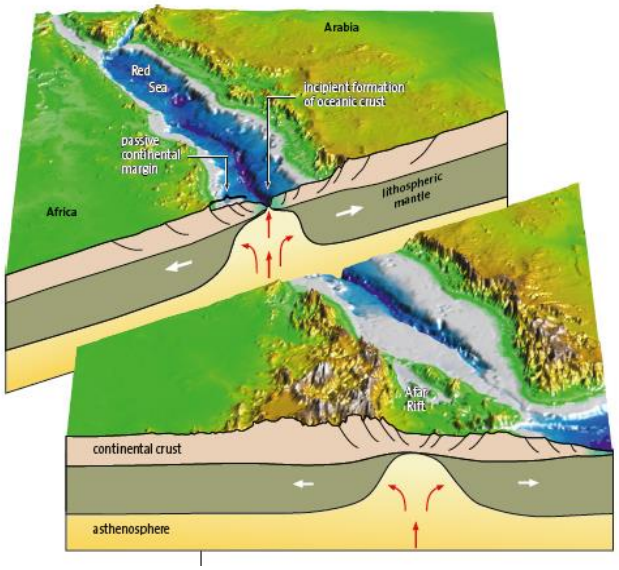

Figure 4: Block diagram of the Red Sea region. Note the graben-in-graben structure, the high elevation of the graben shoulders, and the central graben fissure on oceanic crust in the middle of the Red Sea. The foreground cross-section that passes through the southern Afar Depression indicates that the continental crust is not severed there.

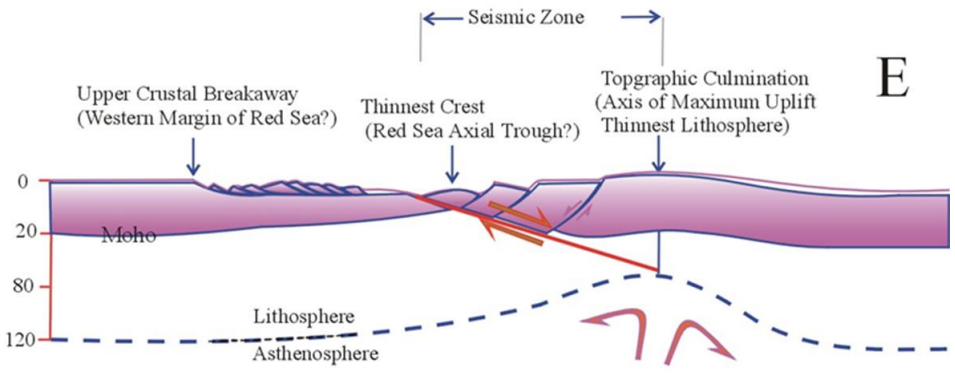

Figure 5: Cross-section across the Red Sea.

Plate divergence in the southern Red Sea is 1.4 cm per year and decreases towards the NW (Fig. 6). In the Gulf of Aqaba it merges into the transform fault of the Jordan Graben. The Gulf of Aden represents a more advanced stage of ocean-basin formation with a mid-ocean ridge, a feature that continues eastward into the Indian. Ocean. Here the spreading rate along the ridge increases to 7 cm per year. Spreading direction of ocean floor in both the Red Sea and Gulf of Aden is in the same, SW-NE, although the spreading axes of both oceans have different orientations.

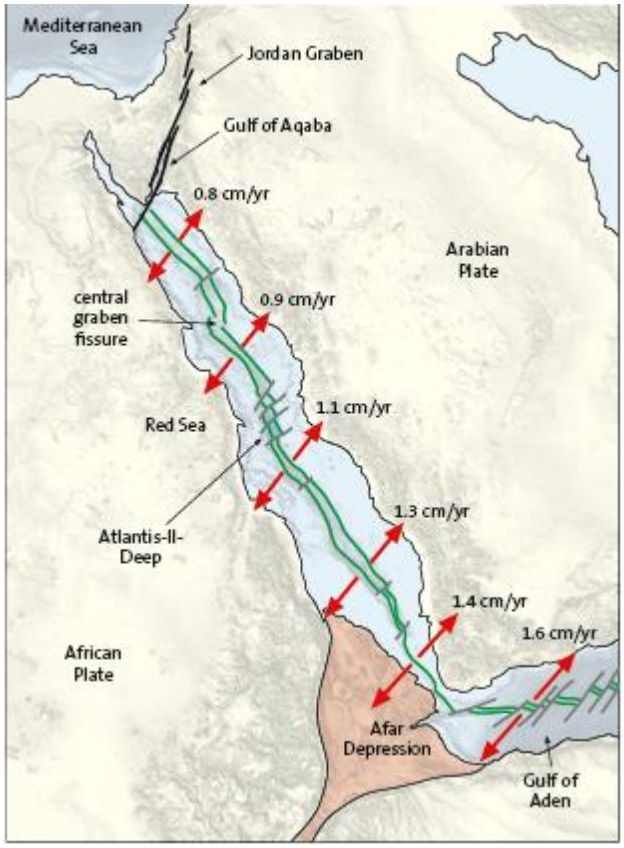

Figure 6: Spreading rates in the Red Sea and the Gulf of Aden (DeMets et al., 1990). The central graben fissure in the Red Sea is marked by a double green line. The Atlantis Deep is one of several depressions that contain metal-rich oozes.

The history of the Red Sea dates back to the middle Cenozoic, as follows:

1. The Red Sea rift was formed due to a major reactivation of a structural weakness zone during the late Oligocene gradually with intense magmatic activity that developed a continental rift. This rift is cut through the Arabian- Nubian Shield, an area of Precambrian

continental crust that is mantled by Upper Cretaceous and Lower Tertiary sedimentary rocks.

2. The formation of the rift graben initiated from the south to north; with violent volcanic activity and basaltic eruptions commenced in the Afar Triangle, a southern extension of the Red Sea.
3. During the Middle to Late Miocene, sea water intruded the graben system from the Mediterranean Sea; the graben-restricted sea had a blind end to the south.
4. Restricted water exchange, high rates of evaporation in the arid region, and low inflow of freshwater generated more than 3 km of salt deposits.
5. Sea floor spreading with a rate of 1–2 cm/yr started in the southern Red Sea in the Pliocene at approximately 5 Ma.
6. At the same time the Red Sea opened to the Gulf of Aden and the Indian Ocean.
7. Due to the total separation between the continental blocks of Africa and Arabia, the tectonic activity shifted from the edges of the graben to the new spreading zone in its center, the zone where new oceanic crust was generated along a narrow, newly formed central graben; this formed the present graben-in- graben structure (Fig. above). The outer graben shoulders are presently tectonically inactive.

References

1. Frisch W, Meschede M, Blakey RC (2011) Plate Tectonics: Continental Drift and Mountain Building, 1st edn. Springer Berlin Heidelberg, Berlin, Heidelberg
2. Oreskes, N. (2003). Plate Tectonics: An Insider's History of the Modern Theory of the Earth (H. Le Grand, Ed.) (1st ed.). CRC Press.
3. Heirtzler JR, LePichon X, Baron JG (1966): Magnetic anomalies over the Reykjanes ridge. Deep-Sea Res 13: 427–443
4. Termier H., Termier G. (1987) Orogenic cycles. In: Structural Geology and Tectonics. Encyclopedia of Earth Science. Springer, Berlin, Heidelberg. https://doi.org/10.1007/3-540-31080-0_76
5. Abbas Mansour (1999) : Review on the Red Sea
6. Wikipedia
7. National Geographic Society
8. United States Geological Survey (USGS).

Chapter 11

Geophysical Well Logging

11.1. INTRODUCTION

11.1.1. Uses of Well Logging

Well logging involves measuring the physical properties of surrounding rocks with a sensor located in a borehole. The record of the measurements as a function of depth is called a *well log*.

Geophysical well logging has become a standard operation in petroleum exploration. Identification of geological formations and formation fluids, correlation between holes, and evaluation of the productive capabilities of reservoir formations are usually the principal objectives.

Except for the natural γ-ray log, which is used routinely in uranium exploration, well logging is still not used extensively in the search for metallic minerals. Some argue that the complete recovery of cores in diamond drilling eliminates the need for logging holes because the information is laid out in the core box. It is unfortunate that this attitude still prevails because well logging is cheap compared to drilling and would be valuable in correlation and identification of mineral-associated anomalies, particularly when core is lost or difficult to identify.

Geophysical well-logging methods include mechanical methods, passive and a number of active electrical methods (including self-potential, resistivity, induction, induced polarization), several nuclear methods (natural γ-ray detection and observations from induced nuclear reactions), acoustic logging, and measurement of magnetic and thermal properties. The emphasis in what follows will be on logging for petroleum (Pickett, 1970) because this is the major application.

11.1.2. History of Well Logging

The first borehole log, run on September 5, 1927 by the Schlumberger brothers in the Pechelbron oil field in France (Segesman, 1980 and Snyder and Fleming, 1985, upon whom this history is mainly based), measured formation resistivity. The first log (called *electric coring*) in the United States was in 1929 when Doll noted spontaneous potentials (SP) and that negative SP was associated with permeable formations. Beginning about 1932, two logs were usually run, resistivity and SP. Around this time Schlumberger also began using different electrode configurations and spacings to reduce distortions. About 1936 photographic recording of measurements replaced manual reading of meters and tabulating of data. The first efforts to measure dip in a borehole came in 1933, using an array of electrodes, and the first uses of a recording thermometer and teleclinometer (to measure borehole deviation and direction) were also about this time.

In 1941, Archie developed empirical equations relating resistivity measurements to porosity and water saturation and in 1945, Guyod published a discussion of well-log interpretation. In 1949, Wyllie related electrochemical SP effects to differences between the resistivities of mud filtrate and formation water and to chemical activities.

The induction log, developed in 1949, allowed the measurement of electrical resistivity (actually its reciprocal, conductivity) without requiring fresh water mud; it was an outgrowth of World War II research. A number of other electrical logs, such as microresistivity and focused logs, were developed in the 1950s.

Natural γ-ray logging, introduced about 1939, permitted distinguishing shales from other formations by their higher natural radioactivity. A neutron log was described in 1941; it utilized a downhole neutron source and measured the γ rays emitted upon the capture of the neutrons, a response depending mainly on a formation's hydrogen content. Logs depending on other nuclear reactions followed in the 1950s. Gamma-gamma (density) logs for determining density began about 1957. The first continuously recording dipmeter in 1950 utilized a three-arm mechanical scratcher for correlating irregularities in the borehole wall.

The measurement of seismic velocity in boreholes was first done in the 1930s and continuous velocity logging began about 1953. However, sonic logging

did not become used widely until Wyllie's time-average equation related seismic velocity to porosity (Wyllie, Gregory, and Gardner, 1958).

Although digital tape recording of log data became available about 1961, well-log processing did not progress much until the 1970s. Downhole digitizing of measurements, multiplexing of different measurements, and telemetering the data to the surface have increased greatly the number of measurements that are feasible. Processing made it practical to combine the readings of different logs so that the plotted values give the needed information more directly.

11.1.3. General Aspects of Well Logging

Well bores are generally drilled by circulating a fresh-water suspension (*drilling mud*) down through the drill pipe and back to the surface through the annular region between the drill pipe and the rock. Occassionally salt-water mud, oil, or air is the circulating medium. The circulating drilling fluid removes rock cuttings from the bottom of the borehole.

The fluids in a rock's pore spaces (*interstitial fluids*) are normally under a pressure about that of a column of water extending to the surface. Their pressure is roughly in balance with that of the borehole fluid. If the borehole pressure were less, the pressure differential would tend to expel the interstitial fluids into the borehole. Sufficient solids are added to the mud to make the pressure of the fluid column approximately equal to that of the formation fluids. Mud densities range between 1.1 and 2.0 g/cm^3. Exact balance is rarely achieved, however, and the usual tendency is for the mud to be under slightly greater pressure. This causes the borehole fluid (*mud filtrate*) to enter porous formations and push the indigenous fluid back from the borehole, a process called *invasion*. In the invasion process the mud solids plaster the borehole wall to form a *mud cake* whereas the fluid portion (mud filtrate) enters the formation interstices. The mud cake quickly becomes sufficiently thick (up to 2 to 3 cm) to prevent further entry of borehole fluid into the formation. However, the mechanical aspects of drilling abrade the mud sheath, which is then repeatedly renewed by additional filtrate invasion.

Boreholes are ordinarily cased with steel pipe (*casing*) several times during drilling to provide permanent protection against collapse of the borehole, loss of borehole fluid into "thief" formations, or formation fluid entering the borehole. This is necessary because different formations have different interstitial fluid pressures relative to the borehole fluid pressure, so that the borehole fluid density cannot be adjusted to be appropriate for all of them. *Open-hole logs* are usually run just before the setting of casing. Consequently, most well logs consist of portions run at different times. Some logs (*cased-hole logs*) measure through casing and cement.

The cable used to lower and raise the sonde in the borehole usually contains seven conductors. It is wrapped (*armored*) with a steel mesh to prevent abrasion. Ordinarily the well *tool* (the part containing the sensors being called the *sonde*) is lowered to the bottom of the borehole and logging is done as the sonde is pulled up the hole. Depths are determined more reliably coming out of the hole than if measured going into the hole because the sonde may not sink at a constant rate.

Borehole diameters are usually 6 to 10 in. (15 to 25 cm), occasionally up to 16 in. (40 cm), in petroleum exploration and 1 to 4 in. (2.5 to 10 cm) in mineral exploration. Boreholes are often not uniform (Fig. 11.1a) either along their axis or in cross section, tending to be slightly egg-shaped (Fig. 11.1b). Some formations, especially shales, absorb fresh water from the borehole, soften, and then slough off material to make enlarged portions called *caves*. Usually a sonde rests against the side of the borehole. Some logs employ an *eccentering arm* to press the sonde against the borehole wall and some employ a *centralizer* to keep it in the center of the borehole. Sondes have to be built to withstand the very high pressures (1,000 to 1,500 atm or 100 to 150 MPa) and temperatures (100 to 250°C) in a deep borehole.

Sonde depth is determined by an odometer counting the revolutions of a measuring wheel over which the cable passes. Depths are usually referred to the kelly bushing (KB) on the drilling rig floor. In addition, magnetic marks located every 100 ft (30 m) along the cable are sensed to check the odometer readings. The sonde is lowered to the bottom of the hole and then slowly raised until the sonde begins to move. The cable depth is then compared with the drill depth record; a cable stretch correction usually has to be made. Occasionally during logging the sonde may stick temporarily and then jerk free, producing a yo-yo motion. Usually several sensors are recorded on each log run and a γ-ray record is made on every logging run to correlate between recorded depths on different runs. Portions logged on previous runs are usually repeated on a subsequent run as a check. A *memorizer* in the recording cab corrects the depth differences between sensors located at different places on long sondes (which may be up to 30 m in length). Bottom-hole temperature is obtained by a maximum-reading thermometer attached to the sonde.

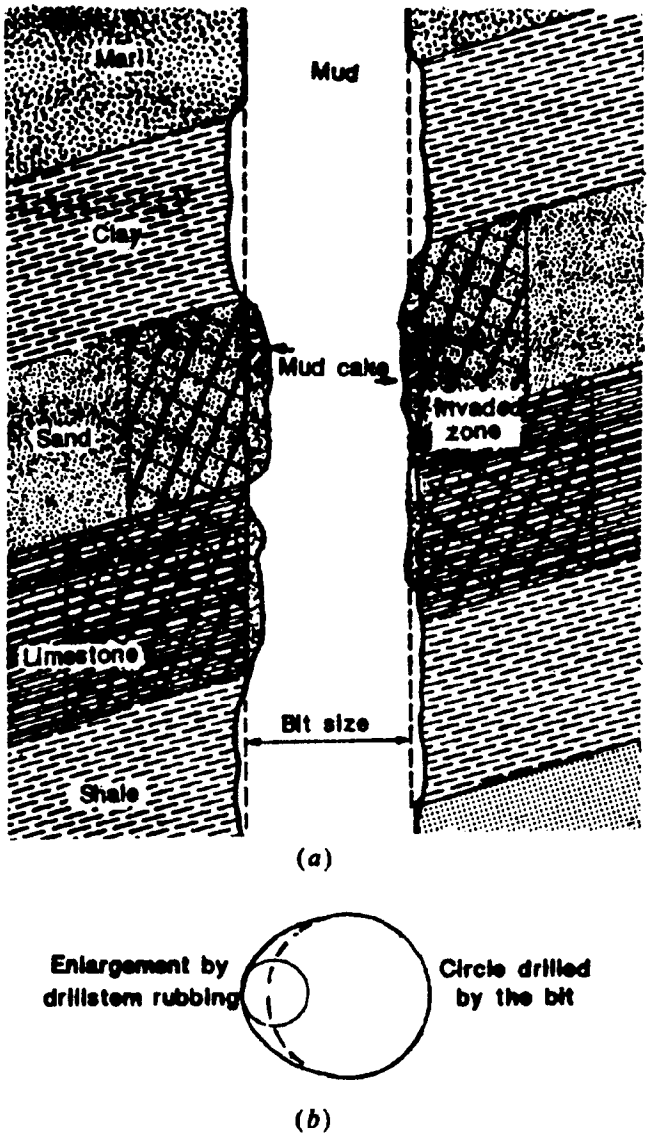

Figure 11.1. Borehole shape. (a) Conceptual vertical slice through a borehole showing caving and mud buildup on permeable formations. (From Tittman, 1986.) (b) Egg-shaped cross section of borehole showing most probable location of a sonde equipped with an "eccentering" arm.

11.1.4. Rock Property Measurements

The objective of well logging is to measure in situ the properties of the undisturbed rocks and the fluids that they contain. However, the act of drilling a hole disturbs them. Appreciation of the invasion process is essential to interpreting well logs because the rock region that exerts the greatest effect on log readings is the portion nearest the logging sonde, the portion altered most by the drilling process.

The relative contribution of formations at various distances from the logging tools varies with different sensor configurations (Fig. 11.2). The effective *depth of penetration* (*investigation*), a qualitative term, is the distance from the borehole that contains the material whose properties dominate the measurements (Roy and Dhar, 1971; Moran, 1972). *Deep penetration* implies that the dominant contribution is from formations that have not been disturbed by invasion. At the other extreme, *very shallow penetration* implies that the properties of the mud cake or of the borehole mud dominate the measurements, depending on whether the logging tool is pressed against the borehole wall or is centered in the borehole. *Intermediate penetration* implies domination by the area invaded by mud filtrate in porous formations. Electric log measurements using different electrode arrangements may give different results because the mud and filtrate are usually more resistive than the indigenous formation whose water is usually highly saline and conductive.

Well logging for petroleum usually has the primary objective of identifying potential reservoir rocks, determining their porosity and permeability, and determining the nature and proportions of the fluids present. *Porosity* is the fractional portion of rock volume occupied by pore space, often expressed as a percentage. Reservoir rocks usually have from 10 to 30% porosity although rocks of lesser porosity can also be hydrocarbon reservoirs. The product of porosity, area, and average thickness of a reservoir gives the volume of fluids that the reservoir contains. Porosity can be determined from resistivity, acoustic velocity (sonic), density, and neutron logs. Each may be subject to distortions and hence better determinations can be made from combinations of logs than from individual logs.

In most reservoirs hydrocarbons fill only part of the pore space, that fraction being the *hydrocarbon saturation*. Where water is the only other fluid present (the usual situation), the water saturation plus the hydrocarbon saturation equals 1. The water saturation is calculated from the Archie equations (11.1), (11.2), and (11.3) and porosity measurements, and it often provides the distinguishing trait of formations that are capable of commercial hydrocarbon production.

Besides porosity, an equally important property is the degree to which the pores are interconnected, that is, the *permeability*. Permeability is usually measured in darcys; a *darcy* is the permeability that will allow a flow of one milliliter per second of fluid of one centipoise viscosity through one square centimeter under a pressure gradient of one atmosphere per centimeter. Commercial reservoirs generally have permeabilities ranging from a darcy to a few millidarcys. Permeability is estimated from logs using empirical rules but only with order of magnitude accuracy. The SP curve is usually a reasonably good indicator of permeability.

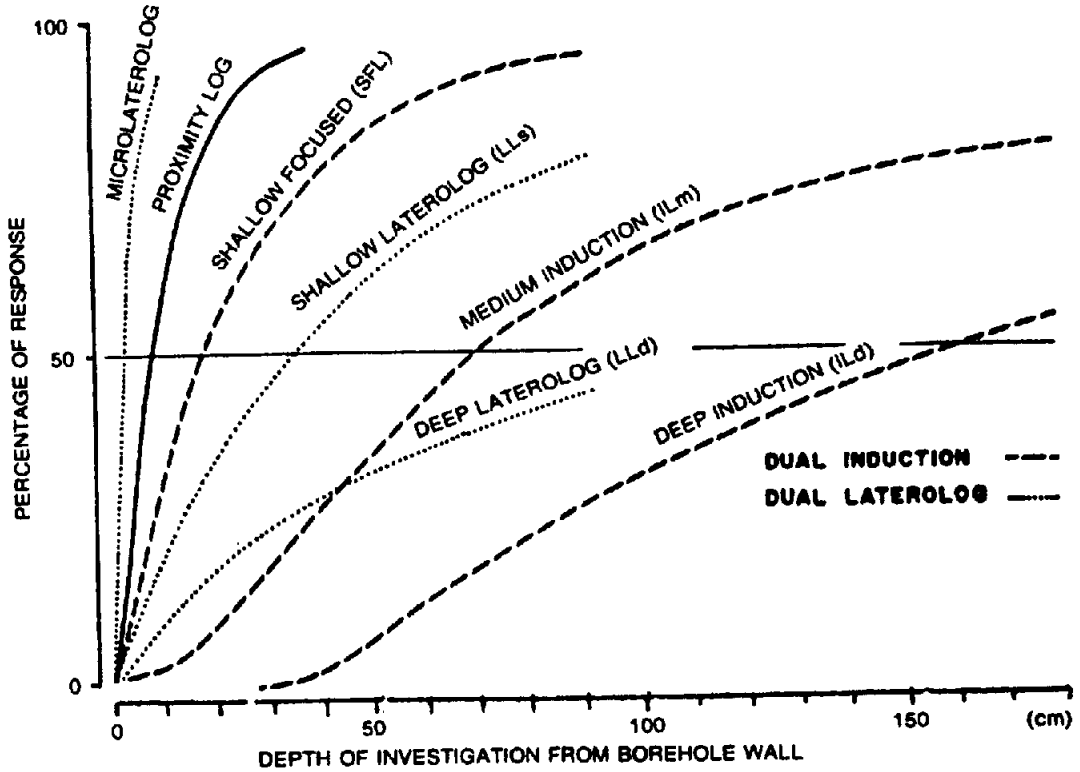

Figure 11.2. Percent of response attributable to rocks within different distances from the borehole for infinite homogeneous medium. (After Schlumberger, 1972).

Formation identification and correlation between wells is often as important as the determination of porosity and estimation of permeability. Particular formations may yield distinctive patterns making it possible to correlate not only major lithologic breaks but many points within formations themselves. Faults and unconformities often can be located fairly precisely by noting a missing section (or repeated section, in the case of reverse faults) in one well compared with others nearby. Stratigraphic details often can be worked out from log-shape patterns. As logs from more wells in an area become available, the amount of detail that can be extracted increases.

11.2. RESISTIVITY METHODS

11.2.1. Introduction to Resistivity Logging

The physical properties of rocks and minerals measured in electrical well logging are principally electrical resistivity and self-potential (SP). The induced-polarization effect has not yet developed as a routine logging technique in petroleum application (see however §11.6).

In most petroleum exploration logging, several logs are recorded on the same logging run (Fig. 11.3). Resistivity and SP logs are generally recorded as adjacent curves. Because most electrical measurements can be made only where the hole has not been cased, logs are commonly run over different parts of the borehole at different times. Also, because the primary objective of logging usually is to evaluate the productive potential of reservoir sands, logging is often done soon after sands are drilled, before drilling deeper; otherwise the sands may change their log characteristics as a result of standing open to drilling fluid with the consequent invasion of mud filtrate.

Resistivities of various rocks and minerals are given in Tables 5.1 to 5.4 (§5.4.1). Sedimentary minerals normally encountered in oil wells are generally poor conductors, having resistivities in the range 10^3 to 10^{10} Ωm. The minerals common in sedimentary rocks (silicates, oxides, and carbonates) are practically all nonconductors. However, most sedimentary rocks contain water in which various salts are dissolved; in solution these disassociate into cations (Na^+, Ca^{++}, Mg^{++}, and so on) and anions (Cl^-, SO_4^{--}, and so on). The movement of ions in the interstitial fluid provides the formation's conductivity.

Metamorphic and igneous rocks may contain minerals (usually disseminated), such as pyrite, chalcopyrite, graphite, magnetite, galena, and so on, which contribute to their conductivity. As in sediments, however, interstitial water is often the controlling factor on resistivity.

Three equations used in petroleum work relate the resistivities of rocks and interstitial fluids, porosity, and the fraction of water filling the pore spaces. These are modifications of the empirical formula of

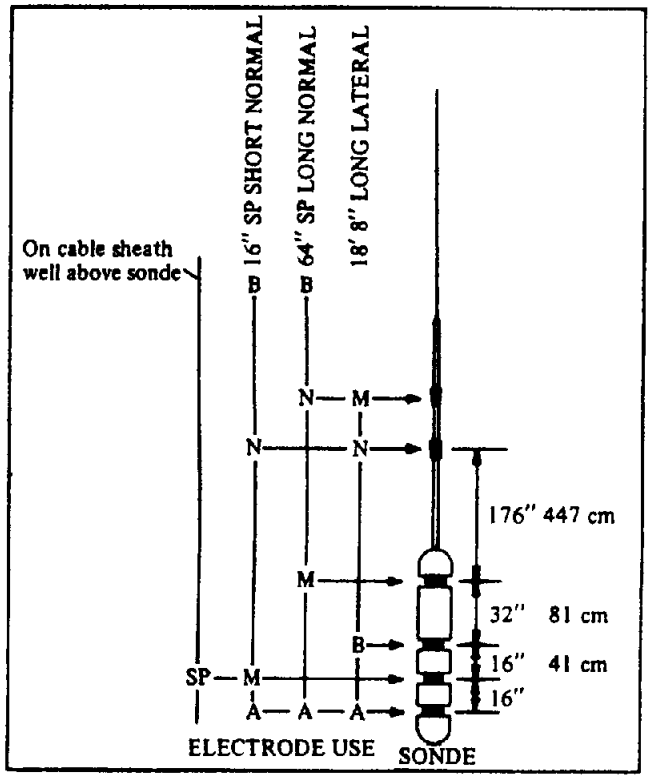

Figure 11.3. Showing how electrodes on a sonde can be used to record different electrical logs. A and B are current electrodes, M and N are potential electrodes. (After Labo, 1987.)

Archie (1942) [see Eq. (5.7)]. The first expresses the bulk water-wet resistivity of a rock sample, ρ_0, and the resistivity of the water contained in its pores, ρ_W, in terms of a *formation resistivity factor F*:

$$F = \rho_0/\rho_W \qquad (11.1)$$

(In formation evaluation the symbol R is usually used for resistivity; however, we shall use ρ to be consistent with Chapters 5 to 9.) Values of ρ_0 can be determined from resistivity logs, those of ρ_W from prior experience in the area, formation water samples, SP logs, or resistivity log crossplots (Schlumberger, 1987, pp. 28–31).

Archie showed that the formation factor is a function of the porosity and, to a lesser degree, of the permeability of the sample. His second relation is

$$F = 1/\phi^m \qquad (11.2a)$$

where ϕ is the porosity of the material and m is a *cementation factor* whose value lies between 1.3 and 2.5. An alternative form of this expression, called the *Humble formula*, applicable to many granular rocks, is

$$F = 0.62/\phi^{2.15} \qquad (11.2b)$$

Another form, the *Shell formula*, is used for low-porosity carbonates:

$$F = 1/\phi^{(1.87+0.019/\phi)} \qquad (11.2c)$$

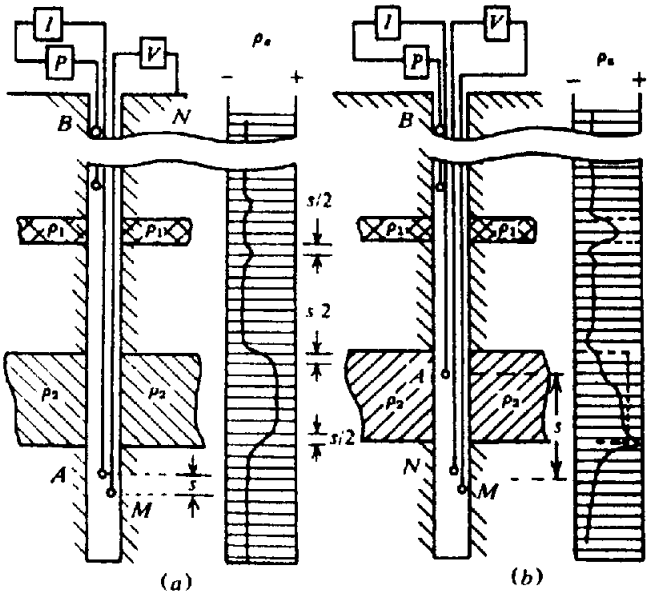

Figure 11.4. Electrode configurations and log curves; ρ_1, ρ_2 indicate resistive beds. P is the power source, I is the ammeter, V is the voltmeter, s is the spacing. (a) Two-electrode (normal) arrangement. (b) Three-electrode (lateral) arrangement; the upper B electrode is on the cable sheath well above the sonde.

If the rock pores are not completely filled with water but contain gas and/or oil also, the effective resistivity is larger than ρ_0. The third empirical equation of Archie accounts for partial *water saturation* of the rock. If S_w is the fraction of the pore volume filled with water,

$$S_w = (\rho_0/\rho_t)^{1/n} \qquad (11.3)$$

where ρ_t is the true resistivity of the sample, derived by applying corrections for logging tool dimensions and configuration, borehole diameter, mud resistivity, and so on, to the measured (or apparent) resistivity ρ_a, and n is the *saturation exponent* that lies between 1.5 and 3.0; it is usually assumed to be 2 where there is no evidence to the contrary. Determination of S_w under a variety of circumstances is discussed by Schlumberger (1987, pp. 95–125).

11.2.2. Normal Resistivity Logging

The basic methods of resistivity logging are similar to those used in surface resistivity prospecting. A low-frequency alternating current is applied between current electrodes and the potential is measured between two or more potential electrodes. The record is then a plot of potential variation (or its equivalent, apparent resistivity) versus depth.

Figure 11.4a shows a *normal* electrode configuration. One current electrode (A) and one potential electrode (M) on the logging sonde are closely spaced

downhole [16 in. (0.4 m) apart for the *short normal*, 64 in. (1.6 m) for the *long normal*] and the other two electrodes (B, N) are either fixed near the top of the hole or a long distance away in the borehole. From Equation (8.26) and Figure 8.3, we get for the apparent resistivity ρ_a in homogeneous ground,

$$\rho_a = (4\pi\Delta V/I)(1/AM - 1/BM - 1/AN + 1/BN)^{-1} \quad (11.4)$$

[The factor is 4π here rather than 2π as in Equation (8.26) because this equation holds in the interior of the medium rather than at the surface of a semiinfinite medium.] Because the distance AM is much smaller than any of the other three dimensions, this becomes

$$\rho_a \approx (4\pi\Delta V/I)(AM) \quad (11.5)$$

The measured apparent resistivity depends mainly on the resistivities of the beds in the vicinity of A and M. Measurements will also be affected by the mud in the borehole and by the penetration of the drilling fluid into formations.

The resistivity log of Figure 11.4a is symmetrical with respect to beds where the resistivity differs from that above and below. The interfaces are marked sharply (but not necessarily at their true locations), particularly in the short-normal curve. High resistivity beds appear thinner than their actual thickness whereas conductive beds appear thicker. The effective penetration into the formations is about twice the electrode spacing and varies inversely as the hole diameter.

The definition and sharpness of normal logs decreases with an increase in the hole diameter and with a decrease in mud resistivity. The effects of adjacent beds and the invasion of porous zones by drilling fluid are also significant. These effects used to be reduced by the use of correction charts called *departure curves*, but today corrections are generally made by computer algorithms.

The short-normal spread is sometimes suitable for measuring the resistivity of porous zones flushed by mud filtrate (flushed zone) and hence for determining formation porosity. It is most useful in geological correlation between wells, because the interfaces between beds are usually well defined. The long normal measures an intermediate resistivity, which, in theory at least, permits calculation of both the invaded-zone resistivity, ρ_i, and an estimate of the true formation resistivity, ρ_t. Old electrical logs provided poor measurements of ρ_t because of poor vertical resolution and hole effects.

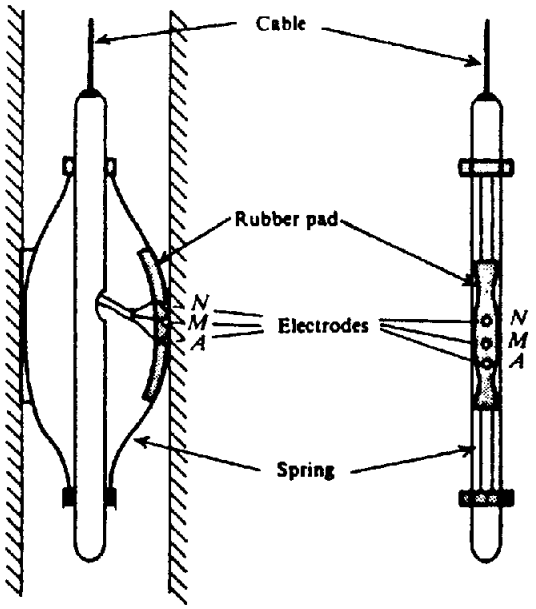

Figure 11.5. Microlog wall-resistivity arrangement.

11.2.3. Lateral Arrangement

A three-electrode sonde yields a *lateral curve*, illustrated in Figure 11.4b. The downhole potential electrodes are usually separated by 32 in. (81 cm) with their center 18 ft 8 in. (5.7 m) from the near current electrode; this latter distance is called the *spacing*. They measure a resistivity of the form

$$\rho_a = (4\pi\Delta V/I)(AM)(AN)/(MN) \quad (11.6)$$

where (AM), (AN), and (MN) are distances between the respective electrodes.

The most striking feature of lateral curves is their asymmetry; in Figure 11.4b this is particularly apparent at the upper and lower boundaries of the thick bed. If the current and potential electrodes are interchanged, the asymmetry is reversed. Lateral curves are distorted by borehole effects similar to those described in the preceding section, as well as by the electrode geometry. The depth of investigation is large and is often taken as approximately equal to the spacing. For homogeneous beds of thickness greater than about 12 m, the lateral curve measures formation resistivity ρ_t unaffected by the invaded zone. A combination of lateral and normal logs permits approximate determination of ρ_i and ρ_t, as well as the extent of fluid invasion. Despite its deep investigation, the long lateral (now obsolete) was of little use except in thick beds.

11.2.4. Microlog

The *microlog* (*wall resistivity log*) is used as a detector of mud cake and for measuring mud resistivity. Mud cake is a qualitative indication that formations

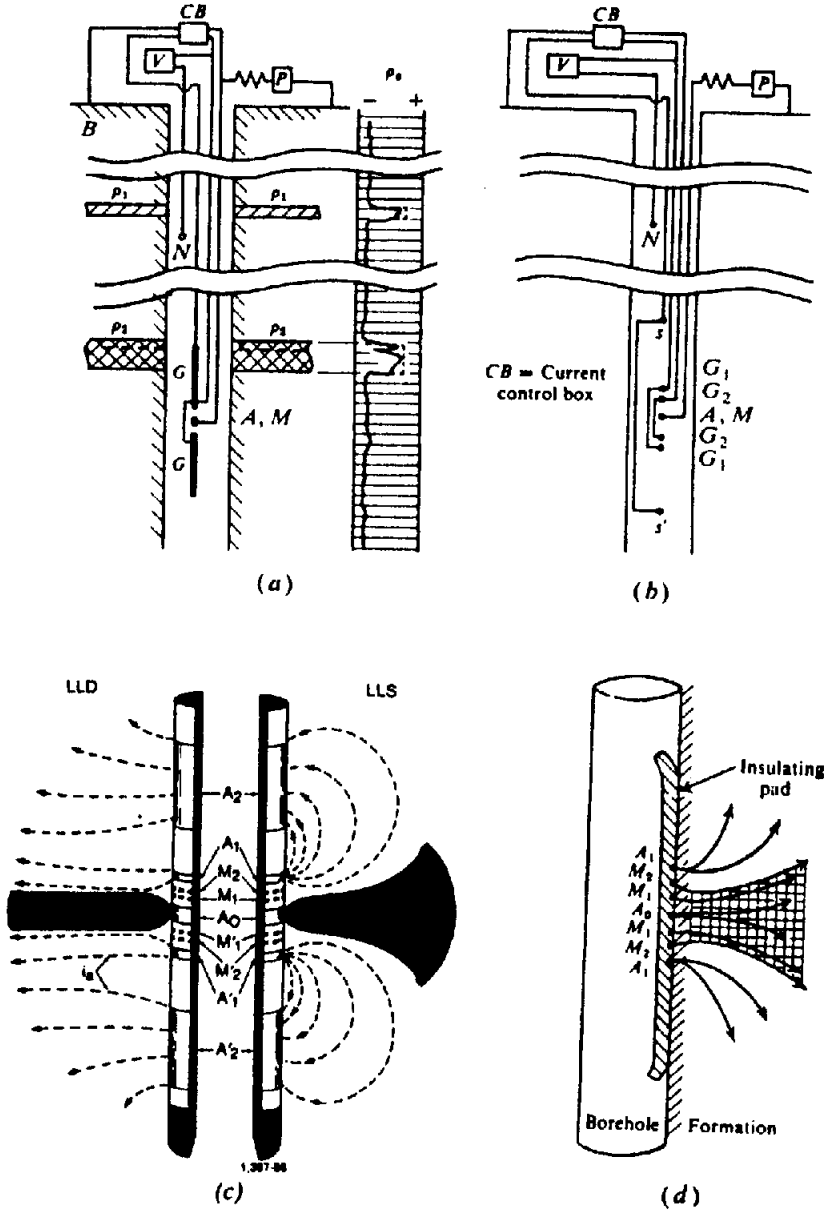

Figure 11.6. Focused current logs. (Courtesy Schlumberger.) (a) Guard log (Laterolog-3). (b) Laterolog-7. (c) Dual laterolog showing how deep and shallow penetration modes of operation can be achieved by reversing the polarity of the A_2 electrodes. (d) Microlaterolog with schematic current flow lines. The shading in (c) and cross-hatching in (d) indicate the current concentration.

are permeable because mud cake forms only on formations that are invaded. However, it may not form in a carbonate section with vugular or fracture porosity. The microlog is illustrated in Figure 11.5. The button-size electrodes are imbedded in an insulating pad that is pressed against the borehole wall by means of an expansion device which is also used to measure hole diameter.

Because the electrodes are against the wall, the effects of hole diameter, mud resistivity, and adjacent beds are negligible. Because the electrodes are very closely spaced (1.5 and 2 in., that is, 38 and 51 mm, apart), very thin beds can be sharply defined, but the depth of penetration is small, less than 10 cm. Differences between resistivities measured with different electrodes is called *separation*, which depends on the thickness of the mud cake. The microlog also measures mud resistivity when the electrode is not pressed against the borehole wall.

11.2.5. Focused-Current Logs

The normal and lateral resistivity devices are too large to measure thin beds, whereas the microlog is influenced by mud cake, and all are ineffective with saline muds. The possibility of using a sharply focused current was realized in the *guard log* or *Laterolog-3*, illustrated in Figure 11.6a (Doll, 1951; Moran and Chemali, 1979; Jackson, 1981).

To measure resistivity, ρ_t, with a vertical resolution of a few centimeters and in the vicinity of thin beds and conductive muds, the current is focused into a horizontal disk that penetrates the formation laterally instead of flowing up the walls. The focusing is achieved by maintaining electrodes G at the same potential as the A, M electrode.

Depth of penetration, taken as the distance at which the current begins to defocus appreciably, is approximately three times the length of the guards. Thus a long guard produces great penetration, but the lower guard prevents logging to the bottom of the hole.

The system known as *Laterolog-7* (Fig. 11.6b) achieves a focused current sheet about 80 cm thick by maintaining the G electrodes at the same potential. Depth of penetration is about 3 m if the spacing between A, M and the nearest guard point is 1.2 m. This arrangement gives essentially the same results as the guard log except that measurements can be made closer to the bottom of the hole.

Both shallow (LLs) and deep (LLd) measurements are made by a *dual laterolog* sonde (Fig. 11.6c); the figure is split to illustrate the two modes of operation. By reversing the polarity of the A_2 electrodes, the focused current bends back after a short distance, producing a focused beam with shallow penetration.

The focusing principle is used with very small electrode spacing in the *microlaterolog*, or *trumpet log*, illustrated in Figure 11.6d (Doll, 1953). The electrodes are mounted like the microlog on a rubber pad that is pressed against the borehole wall. The electrodes are concentric rings 9/16 in. (1.4 cm) apart. Electrodes M_1 and M_2 are maintained at the same potential so that an essentially constant beam of current is produced. The depth of penetration is about 8 cm. This device is used to measure the resistivity of the flushed zone; it also calipers the hole diameter.

11.2.6. Induction Log

The induction log involves the same principle as FDEM prospecting. It is effective with high-resistivity oil-based muds, in an air-filled borehole, and in fresh muds. A schematic diagram is shown in Figure 11.7. A simplified explanation is that the EM field produced by a transmitter coil (with time factor $e^{j\omega t}$) induces circular eddy currents in conductive formations; their time dependence is the time derivative of $e^{j\omega t}$, that is, $j\omega e^{j\omega t}$. These eddy currents in turn induce secondary voltages in the receiver coil proportional to $-\sigma\omega^2 e^{j\omega t}$ where σ is the conductivity. The transmitter coil also induces directly into the receiver coil a voltage whose time dependence is 90°

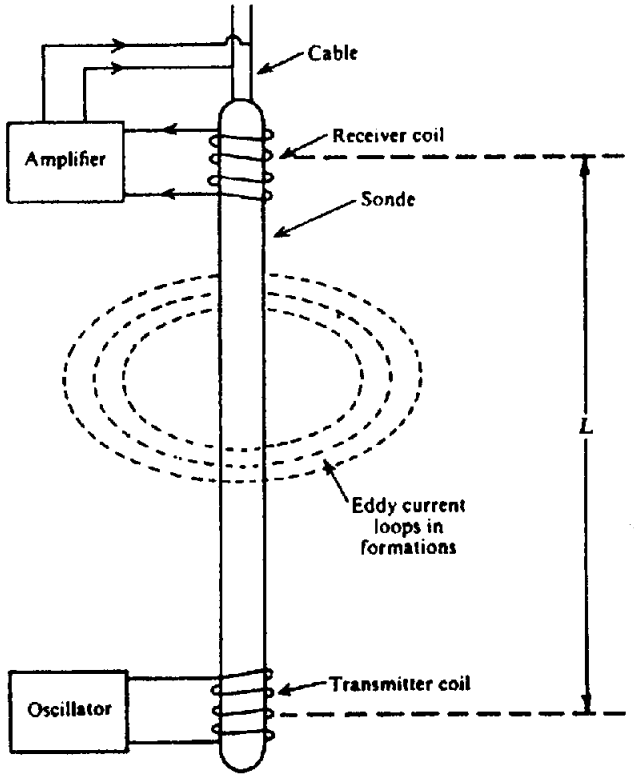

Figure 11.7. Induction log schematic. The tool itself is made of nonconducting material.

out-of-phase (in quadrature) with the secondary current. Most of this mutual-inductance voltage can be compensated (bucked out), or a phase-sensitive discriminator can be used, so that the secondary voltage can be detected by itself.

The induced secondary voltage is the sum of all the eddy-current loops $s(r, z)$ weighted by geometrical factors to allow for their radial distance from the borehole $g(r)$ and distance above or below the sonde $g(z)$; this can be expressed approximately as

$$V \approx K \int\int g(r)\, g(z)\, dr\, dz \qquad (11.7)$$

Graphs of $g(r)$ and $g(z)$ are shown in Figure 11.8; the radial dependence is greatest at a radius of about $L/2$ where L is the distance between transmitter and receiver coils, and $g(z)$ is nearly constant over the range $|z/L| < 0.5$ but falls off rapidly beyond them. However, the conductivity of formations has such a broad range that a highly conductive bed well beyond the tool may still have a significant effect. Less conductive nearby beds have little effect.

The current in an additional coil midway between transmitter and receiver coils can be adjusted so that the secondary voltage in the receiver coil cancels out some of the contribution from the very shallow zone, producing the effect shown dashed in Figure 11.8a. Auxiliary coils are also used to focus the effective

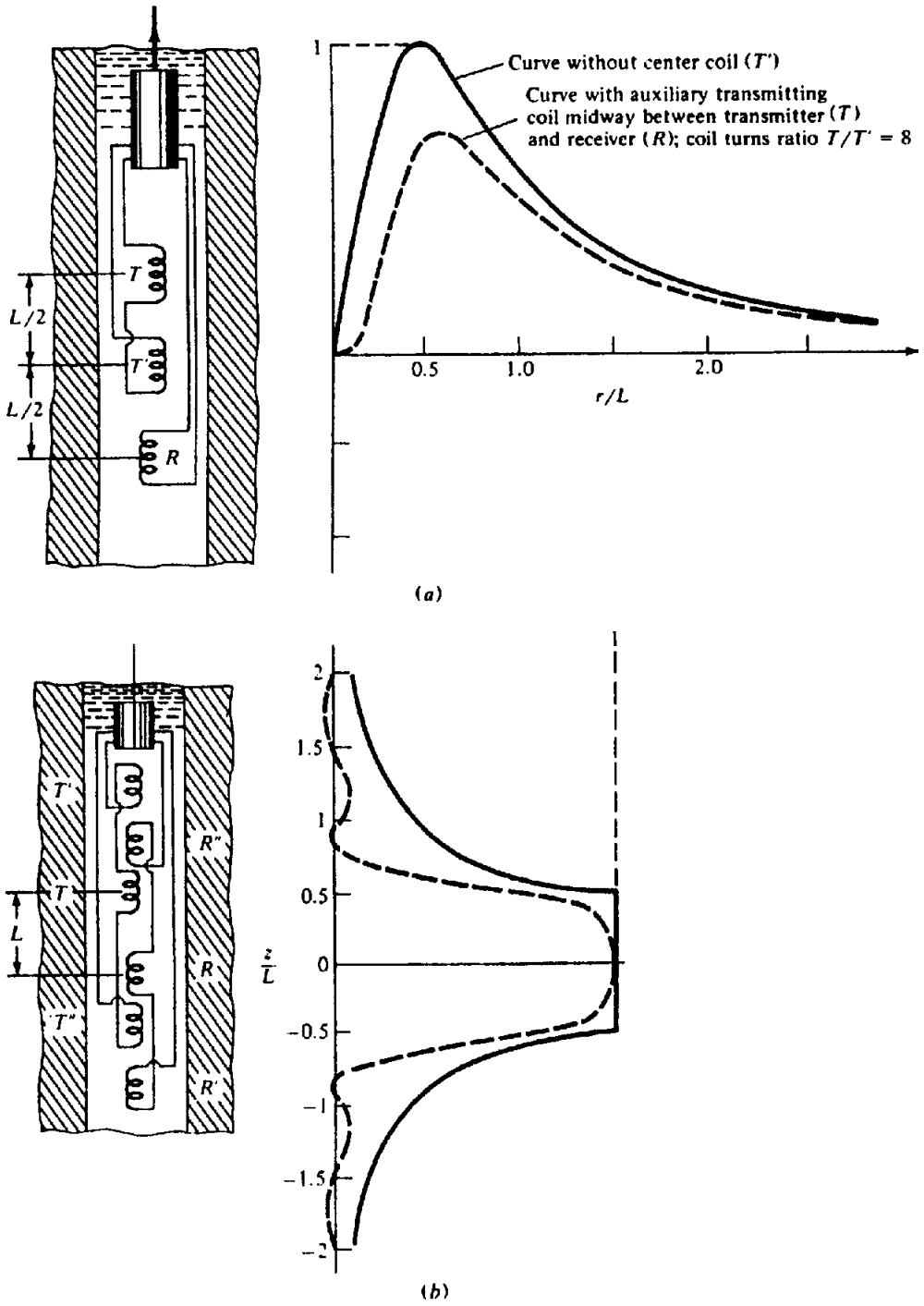

Figure 11.8. Geometric factors for induction sondes without (solid curves) and with (dashed curves) auxiliary coils (T', T'', R', R''). (After Doll, 1949.) (a) Radial factor g(r). (b) Depth factor g(z).

depth. The induction-log signal is proportional to the conductivity of the formations.

The *dual induction log* records separate responses that peak at different distances into the formation, a deep (40 in.) induction log (ILD) and an intermediate (27 in.) induction log (ILM). The induction logging tool usually also includes a shallow focused log (16 in.) so that it measures the resistivity at three distances. The three measurements with different depths of penetration can be interpreted to indicate the invasion of filtrate, implying permeability.

Ground currents generated by atmospheric effects cause no problem because of the high frequency (20 kHz) of the transmitter. Although interfaces of low-resistivity beds are sharply marked, the log is automatically corrected for adjacent bed effects and it provides an accurate measure of the conductivity for formations more than 10 cm thick. Anomalous read-

ings may result from a low-resistivity ring called an *annulus* which is sometimes produced in oil-bearing formations by the-invasion process; because of their greater mobility, hydrocarbons are displaced farther beyond the invaded zone than formation water, resulting in a high proportion of conductive formation water in a ring around the borehole. Such an annulus may move with time.

A *phasor induction log* separately measures the quadrature and in-phase signals. The additional information allows a better correction for skin effects and improves the thin-bed response. The sonde can be operated at 10, 20, and 40 kHz, which give different effective penetrations. Measurements at 10 kHz also have less skin effect [Eq. (6.17)] and those at 40 kHz give more reliable readings in high-resistivity formations. (Correction is automatically made for the skin effect with standard induction logs operating at 20 kHz.)

11.2.7. Resistivity Logging in Mineral Search

Resistivity logging has not been used extensively in mineral areas except in connection with IP logging. Because the structure in mineral areas is usually complex, the interpretation may be only qualitative. Electric logging should locate high-conductivity zones and help in identifying and correlating them. The resistivity tools, employed mainly in experimental work, are single-point resistance, normal, and pole-dipole (similar to the lateral) arrays. These have been used for estimating borehole fluid and resistivities of the host rock (Glenn and Nelson, 1979). Glenn and Nelson also used a combination of resistivity and IP logs to discriminate between disseminated and vein-type sulfide mineralization and to estimate mineral content.

Directional resistivity and *mise-à-la-masse* (sometimes called *applied potential*) configurations are illustrated in Figure 11.9 (Roy, 1984). The first is designed to locate the azimuth of conductors with respect to the borehole, whereas the second is capable of tracing interconnecting anomalies (Mansinha and Mwenifumbo, 1983) and outlining their geometry (§8.5.4d). It is necessary to calculate the geometric factor for each location of the moving electrodes.

The expression for ρ_a is given in terms of $\Delta V/I$ and a geometric factor whose general form for downhole electrodes is

$$k = 4\pi/[\{1/r_1 + 1/r_1'\} - \{1/r_2 + 1/r_2'\} - \{1/r_3 + 1/r_3'\} + \{1/r_4 + 1/r_4'\}] \quad (11.8)$$

where $r_1 = AM$, $r_2 = BM$, $r_3 = AN$, $r_4 = BN$, and

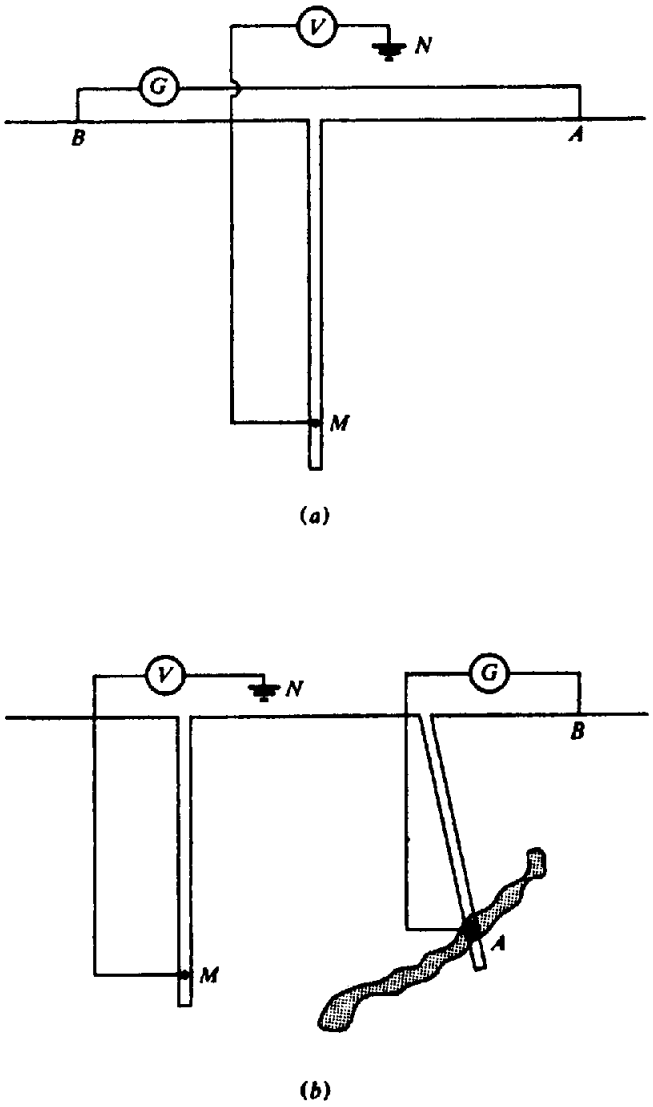

Figure 11.9. Resistivity log configurations for orebody definition. (After Roy, 1984.) (a) Directional resistivity method; the azimuthal direction of AB is changed 90° between measurements. (b) Mise-à-la-masse method with the A electrode embedded in conductive orebody and potential measured in nearby boreholes.

the r' values are the corresponding distances to the images of A, B, M, N reflected in the air–earth interface. That is, an electrode located at $+z$ below ground produces an image at $-z$ above ground (see also §8.3.3 and §8.3.4). For electrodes on the surface the r' terms are zero and k is merely twice the p factor in Equation (8.26). For downhole arrays the k factor is approximately constant.

11.3. SELF-POTENTIAL (SP) LOGGING

11.3.1. Sources of SP

The principal sources of SP (shale potential, liquid-junction potential, streaming potential, and mineralization potential) have been described in Sections 5.2.1 and 6.1.1.

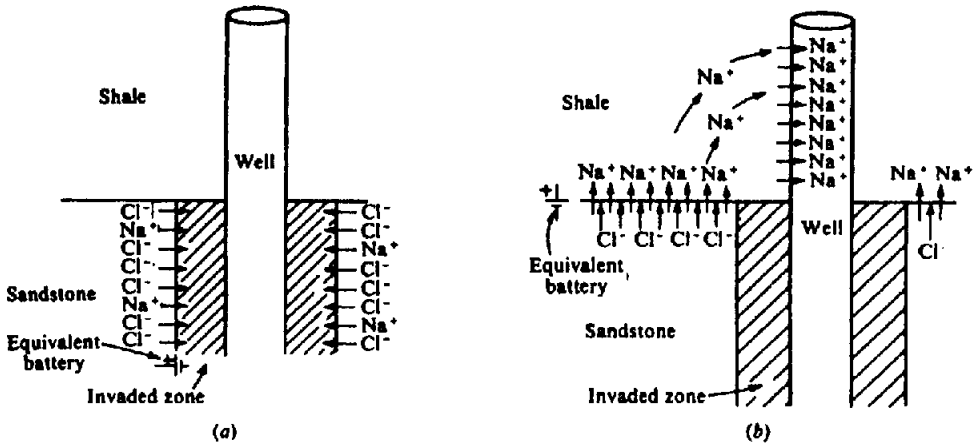

Figure 11.10. The self-potential effect in a sand–shale section. (Courtesy Schlumberger, Ltd.) (a) Liquid-junction (diffusion) potential. (b) Shale (Nerst) potential.

In oil-well logging the potentials involve principally the boundaries of the shale units, especially shale–sand interfaces, and the principal effect is the electrochemical (shale plus liquid-junction) potential, which is normally less than 75 mV. Shales are permeable to Na^+ cations but not to Cl^- anions; as a result a *shale potential* is set up when Na^+ ions pass from saline formation water in sands into adjacent shale beds, then into the fresh water of the mud. In addition, a *liquid-junction potential* develops at the interface between the fresh-mud filtrate in the invaded zone and saline formation water beyond the invaded zone; as a result of the greater mobility of Cl^- anions over Na^+ cations, there is a net flow of Cl^- into the invaded zone. These effects are illustrated in Figure 11.10.

Equation (5.4) can be modified by replacing the ratio of concentrations with the resistivity ratio to give

$$E_c = -70.7\{(T + 273)/298\}\ln(\rho_{mf}/\rho_w) \quad (11.9)$$

where E_c is in millivolts, T is the Celsius temperature, ρ_{mf} is the mud-filtrate resistivity, and ρ_w is the resistivity of the original formation water. The shale potential contributes 59.1 and the liquid-junction potential 11.6 to the factor 70.7 in Equation (11.9).

A *streaming potential* arises because of differences in pressure between fluids in the well and those in the surrounding formations. Equation (5.1) can be expressed in the form

$$E_k = 0.039\Delta P(\rho_{mc}t_{mc}f)^{1/2} \quad (11.10)$$

where E_k is in millivolts, ρ_{mc} and t_{mc} are the resistivity and thickness of the mud-cake, respectively, f is a filter-loss factor, and ΔP is the pressure difference between the borehole mud and the adjacent formation fluid.

The streaming potential usually is much smaller than the electrochemical potential, hence E_c in Equation (11.9) represents approximately the total SP anomaly in oil-well logging (Wyllie, 1949).

In mineral-zone logging a mineralization potential is usually dominant. In zones involving sulfides, graphite, and/or magnetite, the mineralization potential between the minerals and surrounding rock may be as much as 700 to 800 mV. Because this is generally much larger than the shale, liquid-junction, and streaming potentials, they can be ignored.

The principal uses of SP logs are in (1) identifying permeable zones, (2) correlation, (3) providing a measure of formation water resistivity ρ_w, and (4) providing a measure of the amount of dispersed shale in the formation pore spaces.

11.3.2. Instrumentation

Equipment for SP logging is fundamentally very simple. A recording potentiometer or dc voltmeter with high input impedance is connected across two nonpolarizable electrodes, short lead cylinders. The potential recorded is generally between a moving downhole electrode and a fixed electrode at the surface or in the borehole near the surface. In mineral logging the potential gradient between two downhole electrodes at a fixed small spacing is occasionally measured.

Errors may be caused by armor leakage, bimetalism, current leakage causing electrode polarization, or faulty design, especially when SP is run with a single-point resistance log (Keys and MacCarey, 1971; Roy, 1984). The first arises from cables with an external metal sheath in contact with the borehole fluid, which produces spurious potentials varying with cable depth. The second is the result of a voltaic cell between the probe casing (usually stainless steel) and the insulated lead electrode. Current leakage

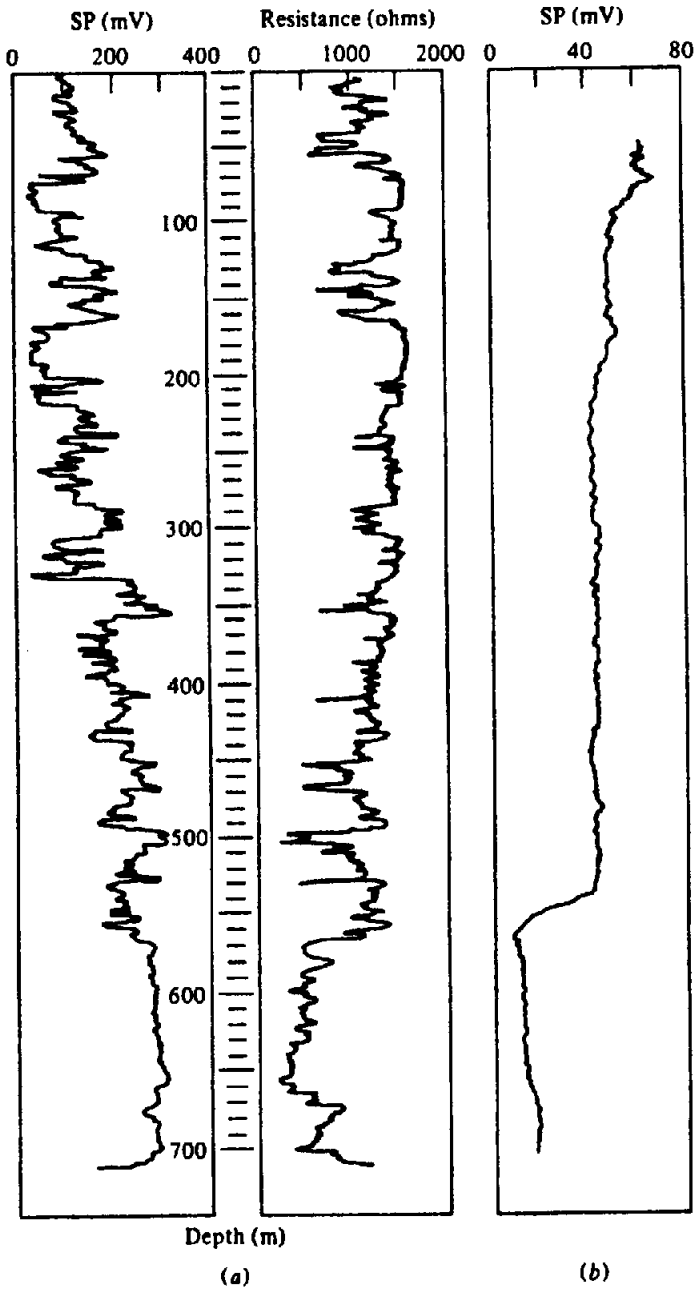

Figure 11.11. SP log comparison. (Data courtesy Atomic Energy Canada, Ltd., Chalk River, Ont.) (a) Result of a carefully designed survey. (b) Commercial log in the same borehole.

caused by large telluric transients or current injection through the SP electrode in single-point resistance logging may change the electrode polarization. Faulty instrument design usually means that the input impedance is too low. Errors tend to be more severe in mineral logging where resistivity is higher than in sediments. Errors can be reduced by using a cable with isolated external jacket, by isolating the instrument ground from the reference electrode, by insulating the SP circuit from the single-point resistance circuit, and by maintaining a high input resistance. Figure 11.11 compares an SP log produced in a carefully designed survey with a commercial log. The former shows much larger differences and more complexity, the latter is nearly a greatly smoothed mirror image of the SP log to the left with a level shift around 540 m.

11.3.3. Uses of SP Curves in Oil-Well Logging

The main uses of SP logging are locating boundaries between shales and porous beds such as sandstones, determining the cleanliness of sands, correlating between wells, and determining formation water resistivity. The shape of the SP curve is often characteristic of particular depositional conditions and

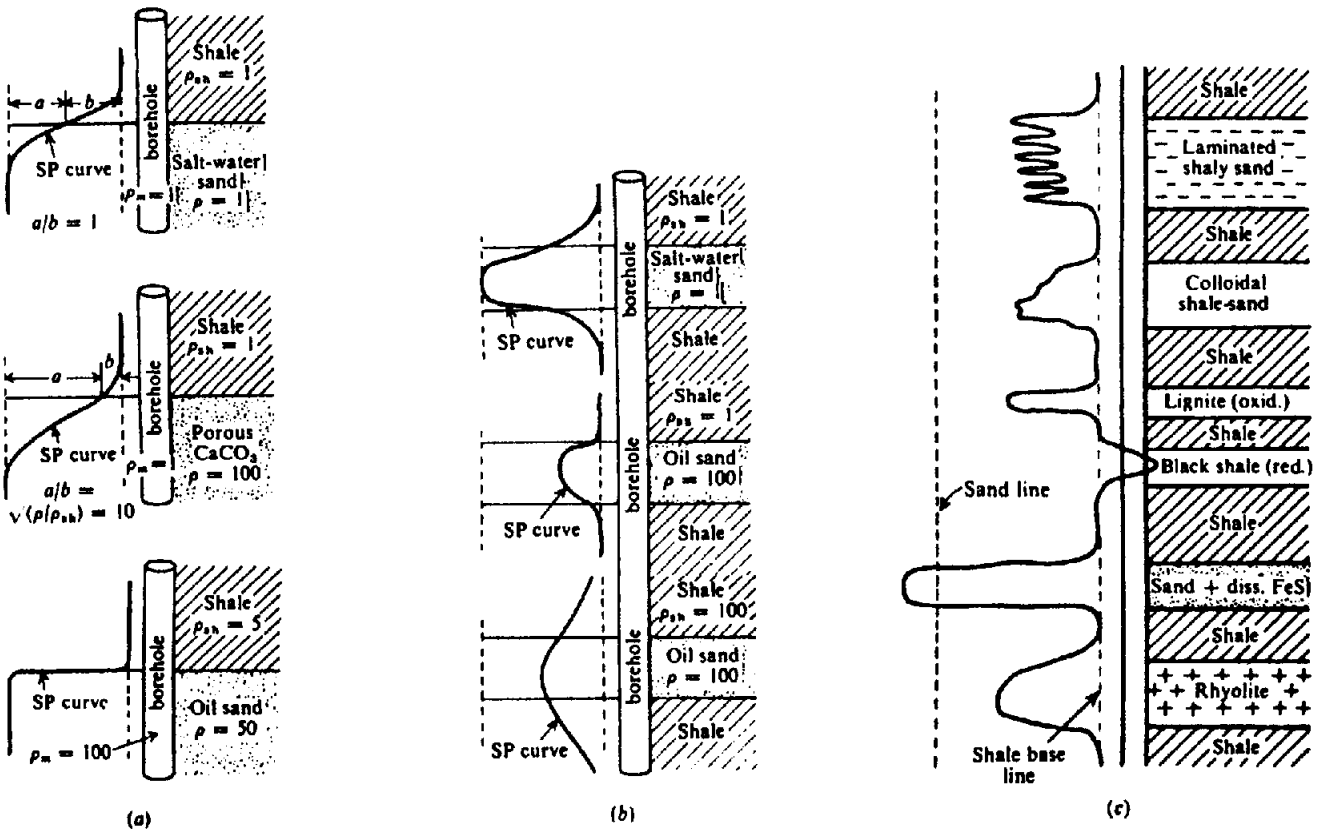

Figure 11.12. Characteristic SP curves for a sand–shale section. (After Pirson, 1970.) (a) Curves for thick beds. (b) Curves for thin beds. (c) Characteristic curves for various formations; the distance between the dashed lines is the static SP.

well-to-well correlation can be used to indicate thinning, pinching-out, and dip of formations.

Equation (11.9) is used to determine ρ_w, ρ_{mf} being found by measurements on samples of mud. Having ρ_w, we can determine F in Equation (11.1) because we can measure ρ_0 from a resistivity log. F is an important quantity in calculating water and hydrocarbon saturations.

If a thick shale is adjacent to a thick, clean, permeable sand, the maximum potential difference across the sand–shale boundary develops between two points in the well located some distance from the actual interface. The SP values at these respective points indicate the *shale-base-line value* and the *sand-line value*. The difference is called the *static SP* (SSP). The static SP depends on the difference in salinity between the mud and the formation water. If the formation water should change salinity, as might be the case between formations above and below an unconformity, the shale base line will shift. If the formation water should be fresher than the mud, the SP phenomena will be inverted and produce a *reverse SP*, sands being positive with respect to the shale base line rather than negative. When a sand is not clean but contains appreciable disseminated clay or shale, the full static SP may not develop and the SP value is called the *pseudostatic SP* (PSP).

Typical SP curves for thick beds are shown in Figure 11.12a. The interface between shales and porous beds can be located by the inflection point on the SP curve. In thin beds, as illustrated in Figure 11.12b, the maximum negative SP may be considerably less than the ideal static value.

Figure 11.12c shows an SP log through several different formations. Note the effect of the thin bedding in the laminated shale–sand, the asymmetric curves for colloidal shale–sand and rhyolite, the positive anomaly for a reducing bed, and the large anomaly associated with disseminated pyrite (FeS).

Although borehole and formation factors influence the SP curve, as with resistivity logs, most of these can be corrected. The effects of hole diameter, adjacent beds, and bed thickness can be eliminated by corrections from standard charts. The density and resistivity of the mud affect the curve greatly. Spurious effects due to streaming potentials depend on the mud density and can be removed by use of a correction chart based on Equation (11.10). The ratio of mud resistivity to formation-water resistivity, ρ_{mf}/ρ_w, is the main factor controlling the curve shape. The temperature is corrected for in Equation (11.9).

The effect of penetration of mud filtrate into porous zones is complicated. Generally the SP deflection decreases with depth of invasion, but occa-

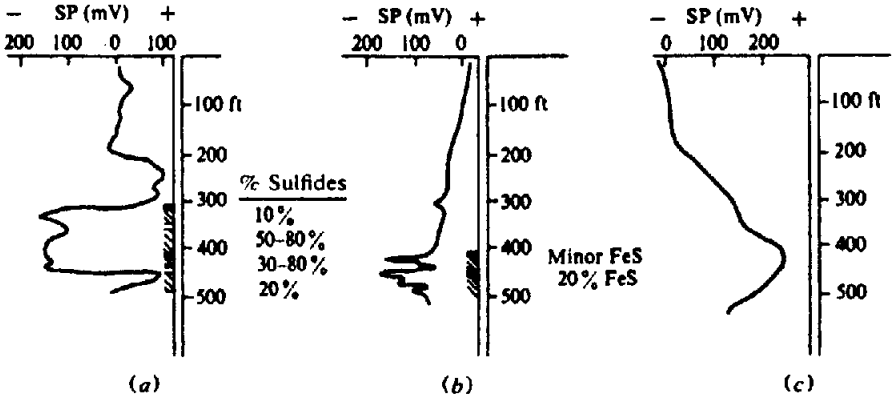

Figure 11.13. Characteristic SP curves in mineral zones. (a), (b) Logs through sulfide zones. (c) Log near a massive pyrite zone not intercepted in the borehole.

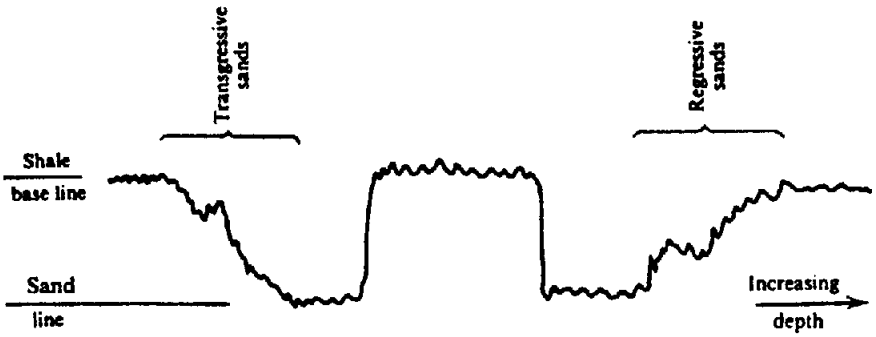

Figure 11.14. Characteristic SP curves for transgressive and regressive sands.

sionally the reverse is true. The potential may change with time as a result of invasion of zones containing water; the fact that the curve is not reproducible on successive logging runs may be diagnostic of this situation.

Polarization of electrodes, as in surface SP surveys (§6.1.2), affects SP measurement but usually the electrodes can be restored to equilibrium by leaving them in the mud for a time. Telluric currents, proximity to power lines, local electrical operations, large-scale electrolytic corrosion in the vicinity, and cathodic-protection devices affect SP readings.

11.3.4. Uses of SP Curves in Mineral Logging

Potentials may be considerably larger in the presence of sulfides (Becker and Telford, 1965) and graphite than for sedimentary beds; consequently borehole effects are insignificant as long as the hole is filled with water. Three examples of SP logs run in 2 in. diamond-drill holes are shown in Figure 11.13. From the first two curves there appears to be no correlation between the deflection and the mineral content of the anomalous zones. The largest negative potentials occur at the interface between barren rock and disseminated mineralization, but this is not too significant because "massive sulfides" are usually inhomogeneous, being composed of many thin sections of high concentration interspersed with disseminated or barren zones.

Two other effects in these logs are worth noting. In the second curve there is a base-line drift with depth, which is not due to temperature. In the third example the broad positive anomaly is caused by a massive pyrite zone near the hole but not intersected by it. The current flow in the barren host rock is from depth to surface.

By having both electrodes downhole at small fixed spacing (15 cm), one can measure the potential gradient. The resultant curve shows sharp deflections at the edges of mineral zones. Except for this feature, the regular electrode arrangement provides more information.

11.3.5. Geological Interpretation of SP

In addition to its use in identifying shales (and especially, distinguishing shales from sands in a clastic sequence) and for correlating corresponding points from well to well, other stratigraphic interpretation can sometimes be inferred from the SP curve. In a somewhat simplistic way, the SP value is read as the degree of shaliness (or the relative abundance of clay minerals) and as the inverse of the "energy" in the original depositional environment. For example,

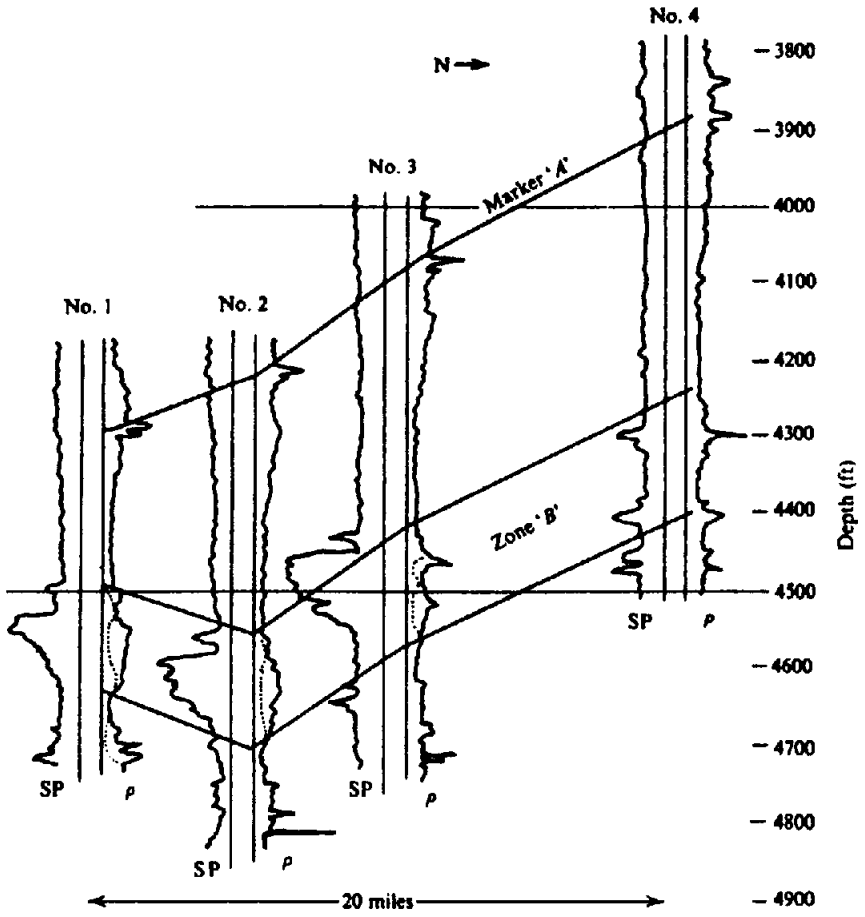

Figure 11.15. Well-log correlation. The convention for plotting well logs is to show an SP or γ-ray log to the left of the borehole and a resistivity log to the right. (After Pirson, 1970.)

proximity to a shoreline where there is wave action represents "high energy," with the consequent removal of clay minerals. Hence an SP curve that gradually increases in shaliness as we approach the surface indicates a receding shoreline and hence a transgressive sea. Conversely, increase in shaliness with depth is interpreted as a regressive sea. This concept is used to develop "theoretical" SP curve shapes such as in Figure 11.14. This concept can be expanded to many other types of sedimentation patterns (see Fig. 11.18). Correct recognition of such patterns, however, is often not very clear in practice.

Figure 11.15 shows short portions of SP and resistivity logs in four wells located approximately in a N–S line. The correlation of corresponding points on these curves is clear despite minor differences. The resistivity curve in the vicinity of the point *A* is characteristic of a marker bed that can be correlated over a fairly wide region. Obviously the formations dip south about 400 ft in 20 miles; this is a gentle slope of $\frac{1}{4}°$. The SP curve deflection to the left in region *B* indicates sand in a predominantly shale environment. The shortened distance between marker *A* and the top of this sand in well no. 1 indicates missing section – a normal fault with about 150 ft of throw. The lower portion of sand *B* indicates a regressive pattern as far as well no. 3. Sand *B* is not seen in well no. 4; correlations of points below the sand compared with those above indicate that the sand has not merely been faulted out but rather that shale was being deposited at the location of well no. 4 while sand was being deposited in the other three wells. Hence a sand–shale facies boundary must lie between wells no. 3 and no. 4. Such a pinchout, of course, represents a potential oil field.

11.4. THE DIPMETER

In some cases formation dip can be estimated by correlation between holes where no structure intervenes, but often the determination is difficult or impossible. Early dipmeters employed EM response and later SP.

The modern dipmeter (Fig. 11.16a) employs four microresistivity pads in the same plane, pressed against the borehole wall at 90° intervals. The upper

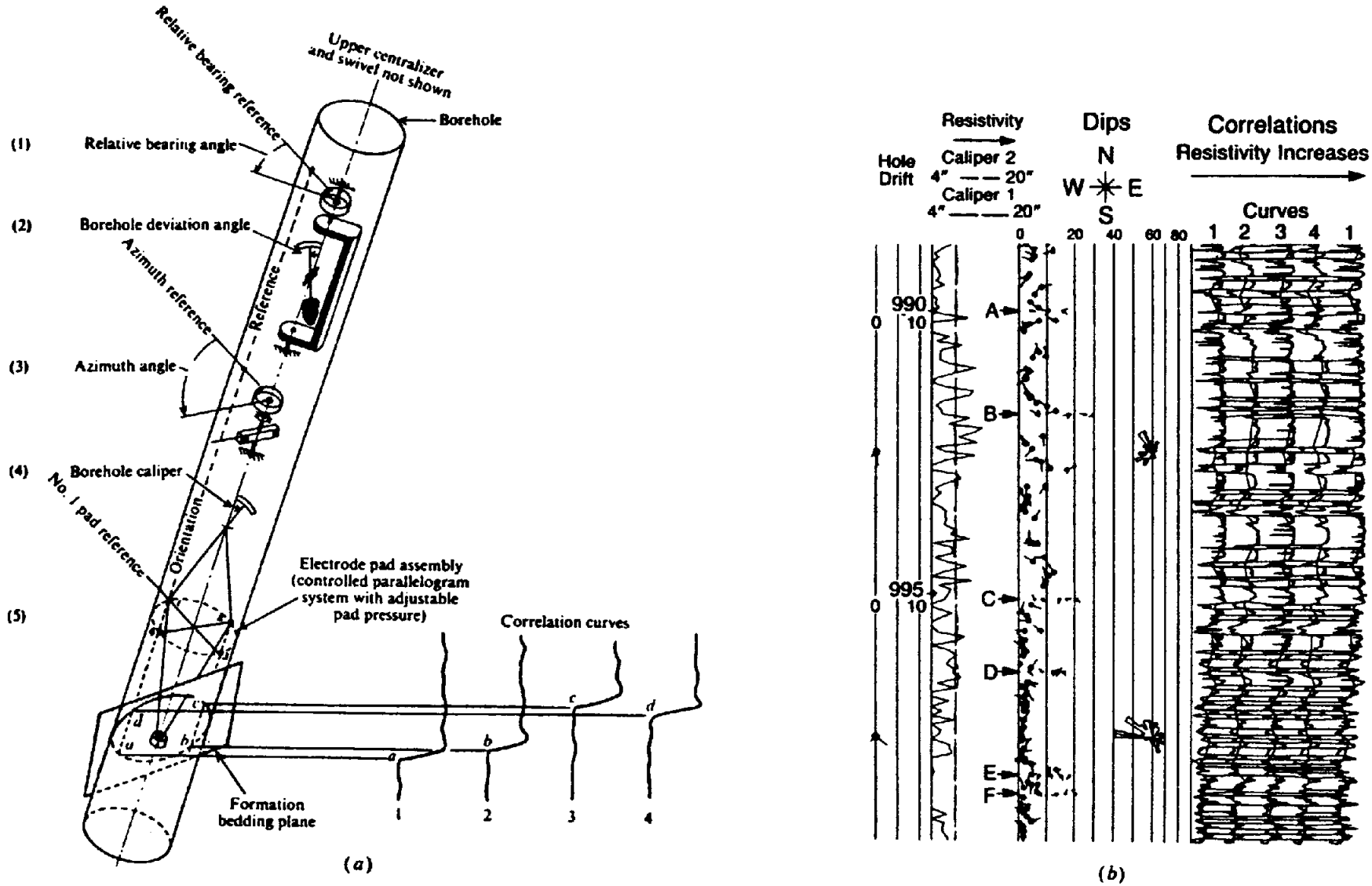

Figure 11.16. The dipmeter. (a) Schematic of diplog tool. (Courtesy Dresser Industries.) (b) Portion of a four-arm processed dipmeter log showing deviation of the hole, caliper log, smoothed resistivity, tadpole plot of dips, rosettes (each showing directions of all dips within a 10 ft. interval), and output of the four microresistivity pads with computer-drawn correlations. (Courtesy Schlumberger Ltd.)

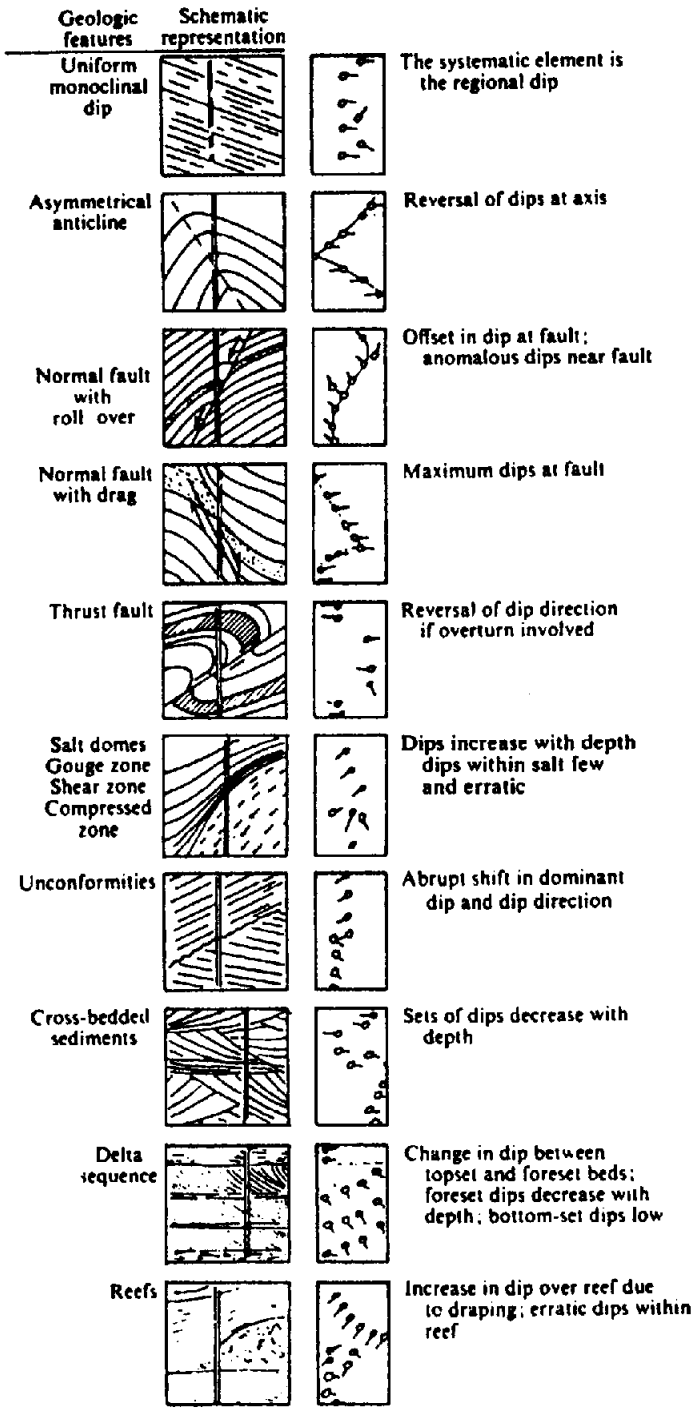

Figure 11.17. Idealized dipmeter patterns indicating structural and stratigraphic features. (After Pirson, 1970.)

part of the 16 ft (4.9 m) long sonde contains an inclinometer to record the drill-hole drift angle and bearing and a magnetometer to determine the azimuth of the reference pad. Two hole-caliper logs at right angles are also recorded. The log recorded in the field shows the azimuth of the no. 1 electrode, the relative bearing of hole drift, the deviation of the hole from the vertical, the resistivity curves from the four pads, and the caliper logs. A portion of such a log is shown in Figure 11.16b.

Formation boundaries are defined by the microresistivity curves and the dip and strike are determined from the slight differences in depth of the boundaries and the orientation data. Rough interpretation based on major features of the raw plots can be made fairly easily. The correlation of many closely spaced points, however, requires processing. The result is usually a "tadpole plot" such as shown in Figure 11.16b where the result of each correlation is shown as a small circle indicating the dip angle, with a short ray

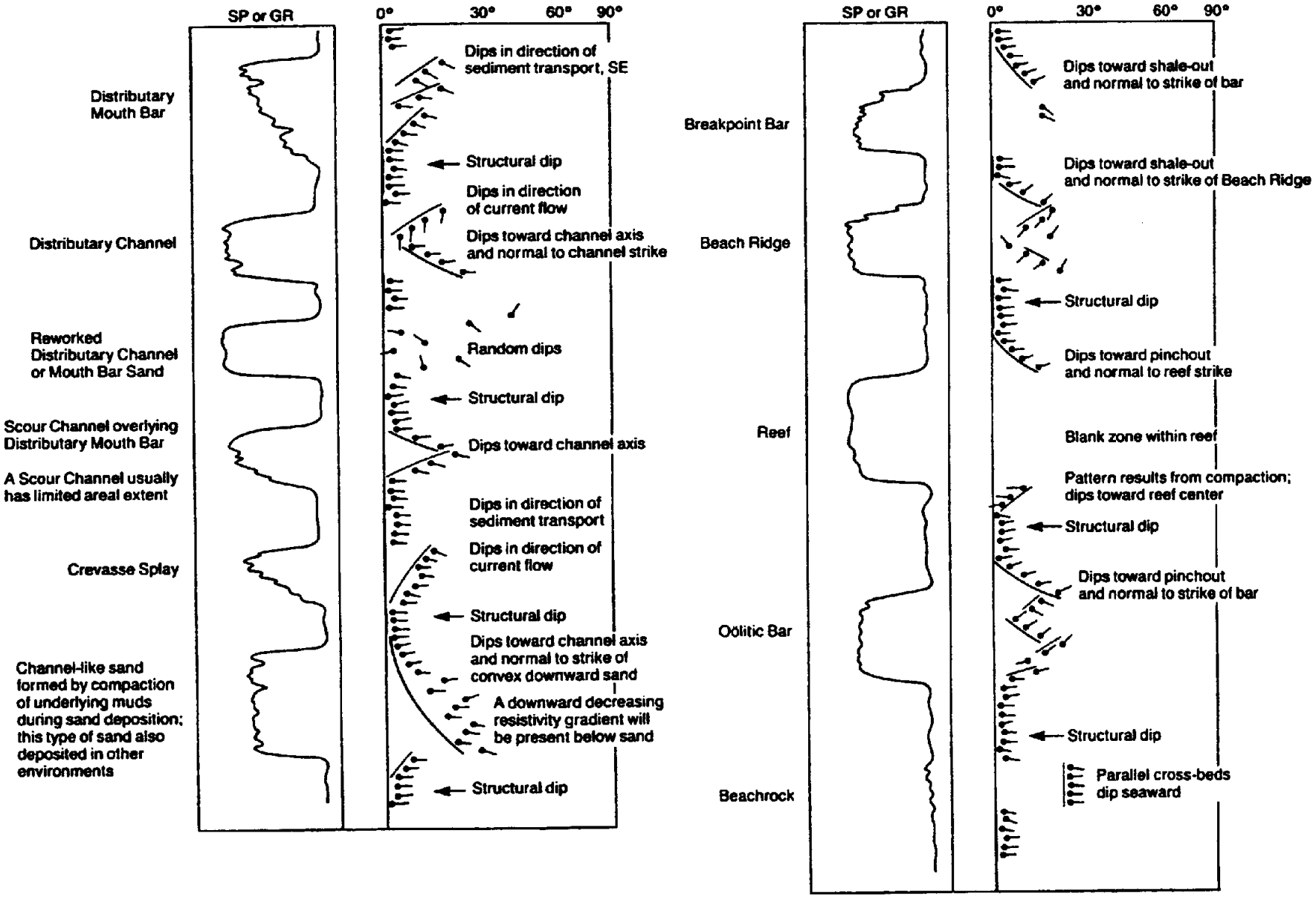

Figure 11.18. Stratigraphic patterns in SP (or γ-ray) and dipmeter data. (From Gilreath, 1987.)

emerging from the circle indicating the down-dip direction, north being upward, east to the right, and so forth.

The variation of dip with depth often indicates geological structure, as shown in Figure 11.17. The dip distortions resulting from fault movement may not extend very far from the fault plane. Various types of sedimentation patterns sometimes may be distinguished when many detailed correlations exist (Fig. 11.18).

11.5. ELECTROMAGNETIC WAVE PROPAGATION METHOD

Although the induction log discussed in Section 11.2.6 is an electromagnetic method, this term is usually reserved for other devices.

The phase velocity of an electromagnetic wave at gigahertz frequency V is given by (Freedman and Vogiatzis, 1979; Pascal, 1983)

$$V = 1/\left\{\mu\varepsilon + (\alpha/2\pi f)^2\right\}^{1/2} = 1/\tau \quad (11.11)$$

where μ is the magnetic permeability, ε is the dielectric permittivity, α is the absorption coefficient, f is the frequency, and τ is the time to travel a unit distance equal to *interval transit time*. Both the attenuation and the interval transit time can be measured. Because the dielectric permittivity of water is much larger than that of oil or rock (by a factor of 10 to 40), water dominates measurements with an electromagnetic log. The large contrast between the dielectric permittivity of water-saturated sediments and rock salt makes it possible to map a salt dome from a borehole in the dome.

Nickel et al. (1983) report a survey of this type using a pulse system operating at 20 and 40 MHz in a salt-dome borehole. With closely spaced Tx and Rx antennas they obtained good reflections from zones of anhydrite, clay, and basalt embedded in the highly resistive salt at distances of several hundred meters. They also measured absorption in these structures by moving the receiver to a second borehole. The results were compared with sonic log data from the same location.

By analogy with the time-average equation [Eq. (11.14b)] used in sonic log interpretation, we write for the porosity seen by the electromagnetic waves ϕ_{EM},

$$\phi_{EM} = ((\tau - \tau_m)/(\tau_w - \tau_m) \quad (11.12)$$

where τ_m and τ_w are the interval transit times for the rock matrix and for the water in the pore spaces. Because the total porosity ϕ can be obtained from neutron and density logs, we can solve for the water saturation S_w:

$$S_w = \phi_{EM}/\phi \quad (11.13)$$

The electromagnetic propagation log at 1.1 GHz defines interfaces sharply but has limited penetration and thus yields mainly the water saturation of the invaded zone. In conjunction with density and neutron logs, it also locates hydrocarbons, identifies the hydrocarbon type, indicates mobile oil, and provides residual oil values. The EM propagation log at 10 to 50 MHz ordinarily has a penetration of about 1 m and is useful where the salinity is small.

Modifications of EM surface-prospecting units (§7.4.2 and §7.4.3) have been employed to a minor extent in mineral-hole logging. Usually the aim is to locate mineralized (high-conductivity) zones nearby, rather than to evaluate the formations intersected by the drill hole (Worthington, Kuckes, and Oristaglio, 1981). An example is shown schematically in Figure 11.19a. The transmitting coil is a conventional vertical loop, set up near the hole and pointing toward it; connected in series with this loop is a small vertical vernier coil, which can be rotated about its vertical axis. The sonde lowered into the hole consists of a small receiver coil wound on a high-permeability core, amplifier, and battery. The received signal can be nulled by rotating the vernier transmitting coil and the azimuth angle is plotted against sonde depth. The measurement is repeated during the uphole passage, this time with the transmitter coil and vernier rotated 90°. The maximum azimuth angles of the two curves, when plotted as vector components parallel to the planes of the transmitter coils produce a resultant vector that points toward the conductor; the depth can be obtained from the curves. The amplitudes of the maximum azimuth angles are roughly indicative of the horizontal distance and/or the conductivity of the zone, and the distance between null points of the curve gives an indication of the vertical extent. The range of investigation is about 100 m.

A somewhat different drillhole EM log is illustrated in Figure 11.19b. The transmitter loop is a large square of one to four turns laid out on the surface. The vertical depth of penetration desired and the type of objective determine the required loop size; loop sides are usually 125 m or longer. A receiver coil with preamplifier is lowered into the hole, the gain being adjusted to maintain constant meter reading; gain is then plotted against depth. Alternately, two coils 15 m apart are connected in opposition to produce a difference signal, as with the Turam method. The transmitter square with the hole

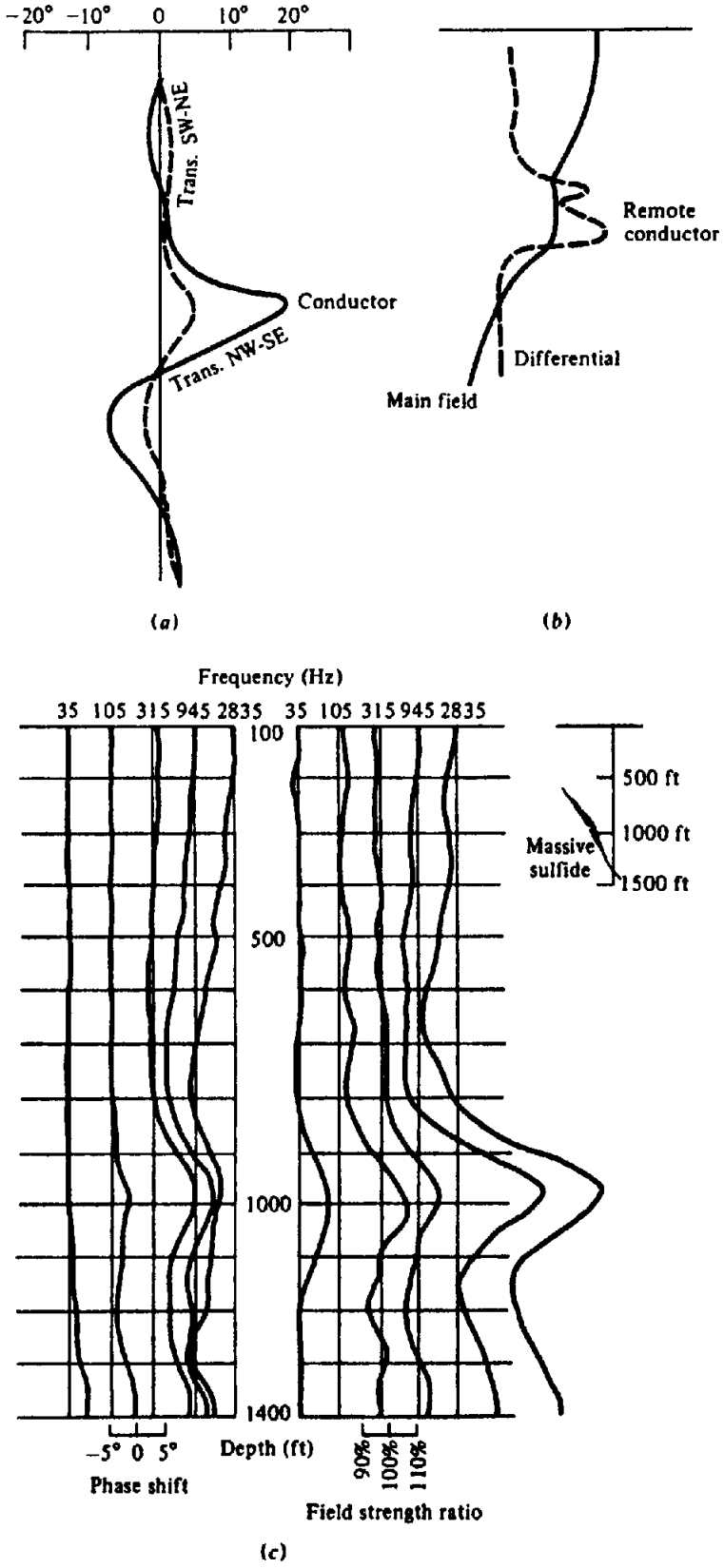

Figure 11.19. EM logging. (a) Logs for two orthogonal directions of the vertical transmitter loop. (b) Logs for a horizontal transmitter loop and one (solid line) or two (dashed line) receivers in the hole. (c) Multifrequency logs. (After Seigel, 1979.)

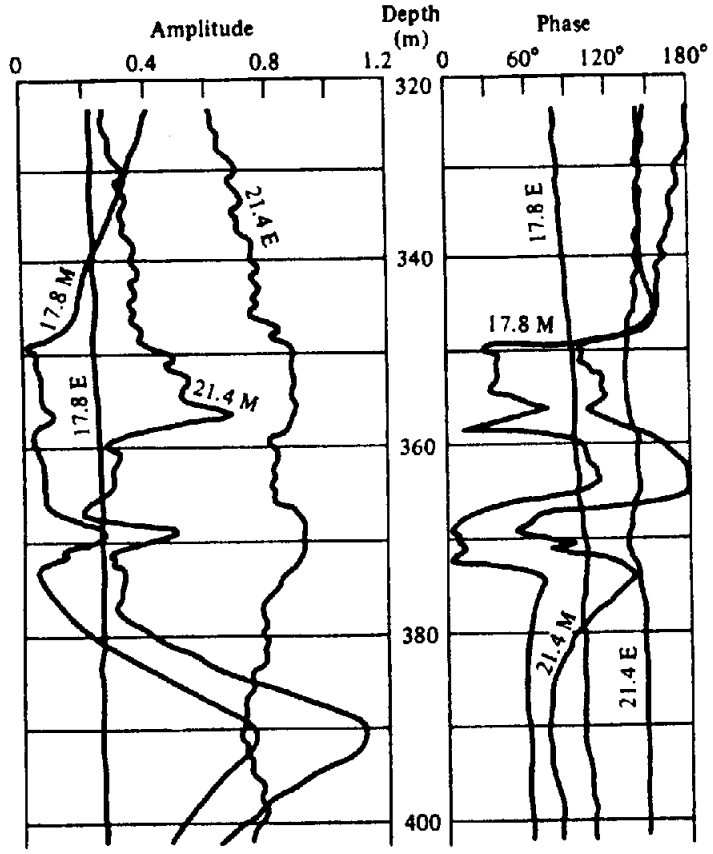

Figure 11.20. Amplitude and phase plots of VLF log past a conductor. E is the electric and M is the magnetic reading, each at 17.8 and 21.4 kHz.

located at one corner is rotated 90° for a successive logging run so that a rough estimate of conductor azimuth can be made. The interpretation is qualitative.

A recently developed EM log uses a large transmitter loop laid out on the ground to one side of the borehole. A moving detector coil coaxial with the hole compares the axial *H*-field amplitude and phase at five frequencies with those obtained from a similar near-surface coil. Logs from a drill hole near the Gertrude sulfide deposit west of Sudbury, Ontario, are displayed in Figure 11.19c.

The EM16 VLF receiver (§7.4.2f) has been adapted for borehole logging (Roy, 1984). The downhole unit has magnetic and electrical sensors that detect in-phase and quadrature components of the axial magnetic field and electrical potential. A surface reference magnetic sensor is oriented for maximum coupling with the distant VLF transmitter and provides reference data for the downhole magnetic readings; the downhole potentials are measured with respect to surface potentials nearby (analogous to SP – see §11.3.2). The log (Fig. 11.20) shows the amplitudes and phases of the VLF magnetic and electrical vectors measured with respect to the surface values. Both vectors are determined at two frequencies: 17.8 and 24.1 kHz. The effects of two conductors are quite clearly seen.

11.6. INDUCED POLARIZATION LOGGING

IP can be measured simultaneously with resistivity, either in the frequency or time domain, to determine the frequency effect, phase shift, chargeability, and complex resistivity (Wagg and Seigel, 1963). The Kennecott IP-resistivity logging tool gives continuous measurement of IP amplitude and phase as well as resistivity to depths of 1,500 m. Glenn and Nelson (1979) suggest a relation between IP and sulfide percentages. For disseminated porphyry-type mineralization, the resistivity is independent of sulfide concentration whereas the phase shift is proportional to the sulfide surface area exposed to pore fluid. In vein-type mineralization, the phase is independent of sulfide content and the resistivity decreases inversely as the square of the sulfide percentage.

11.7. ELASTIC-WAVE (ACOUSTIC) METHODS

11.7.1. Elastic Waves in Boreholes

Elastic (seismic) wave travel was discussed in Chapter 4. The sonic log transmitter generates several wave modes (Paillet and White, 1982; Schmitt and Bouchon, 1985), which are subsequently picked up

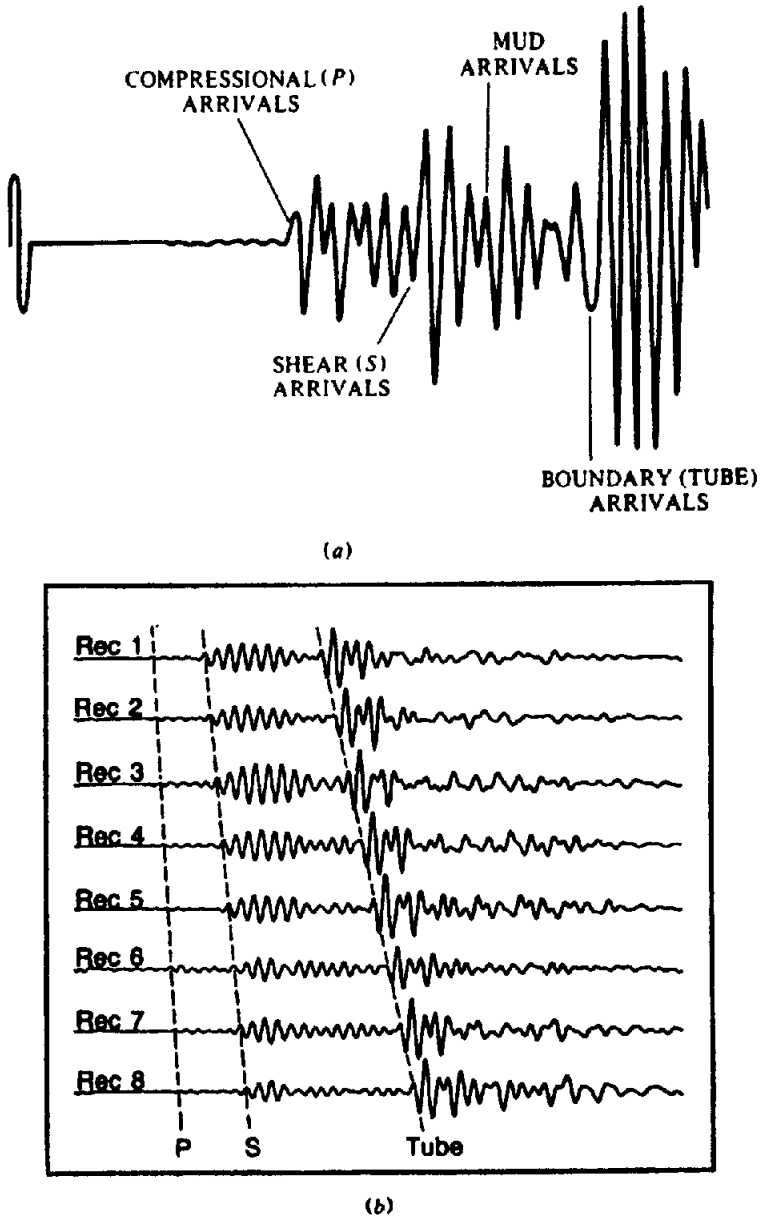

Figure 11.21. Waveforms recorded in a borehole. (a) Waveform showing formation arrivals (P and S waves), mud arrivals, and boundary (tube-wave) arrivals. (Courtesy Schlumberger.) (b) Waveforms from eight broad-band receivers spaced at intervals of 6 in. (15 cm). (After Morris, Little, and Letton, 1984.)

by the receivers (Fig. 11.21). The first energy to arrive is almost always a refracted P wave (headwave mode) in the rock wall. It has impinged on the borehole wall at the critical angle $\theta_p = \sin^{-1}(V_f/V_p)$, where V_f is the seismic (acoustic) velocity of a P wave in the borehole fluid and V_p that in the formation (Fig. 11.22). The sonic log records the transit time (reciprocal of velocity) of this wave. Some of the headwave energy "peels off" at various places along its travelpath, reflects at the sonde or opposite borehole wall, and rejoins the headwave; this adds tail to the headwave, which thus develops a "ringy" appearance.

The acoustic wave striking the borehole wall at the angle $\theta_S = \sin^{-1}(V_f/V_S)$, where V_S is the S-wave velocity in the formation, generates a converted S wave (also a headwave mode) whenever V_S is larger than V_f. The S-headwave develops a ringy character by the same mechanism as the P-headwave. It is usually the second arrival and stronger than the P-headwave.

Much of the energy reflects at the borehole walls to reverberate in the borehole fluid. Energy striking the borehole walls at angles larger than θ_S is totally reflected and bounces back and forth in the borehole as a trapped dispersive wave (*guided wave*; see §4.11.3). This energy constitutes a *mud wave* (whose onset may not be recognizable). Most of the reverberatory energy striking the borehole walls at angles between θ_p and θ_S is also reflected, except for small

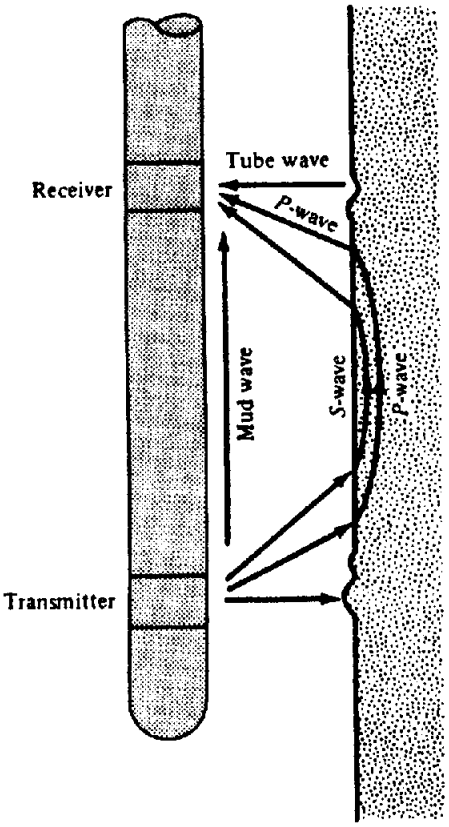

Figure 11.22. Propagation paths for P, S, mud, and tube waves. (From Labo, 1987.)

portions which are lost by being converted to refracted *S* waves; this *leaky-mode* transmission is also part of the reverberatory trapped wave. The trapped mode is often the strongest in terms of energy density and sometimes obscures the *S*-wave arrival, especially in soft formations.

A tube wave, also called a *Stoneley wave*, travels as a surface wave on the borehole wall (see Sheriff and Geldart, 1982, pp. 51–52). This wave is only mildly dispersive and thus shows as a reasonably sharp arrival. The shear modulus can be calculated from the Stoneley-wave velocity. The Stoneley wave is often very strong and of relatively low frequency content.

All of the waves travel as *P* waves in the borehole fluid, and hence the terms *acoustic* and *sonic*; however, the major interest is usually in the seismic wave in the adjacent rock formations. Although it was introduced to determine seismic velocity as an aid in seismic prospecting, determining porosity, which correlates with seismic velocity, soon became the major application of this log. Sonic logs continue to be used for seismic velocity measurement and reflection (synthetic seismogram; see §4.10.2) analysis. Seismic detectors located in boreholes are also used for determining surface-to-depth traveltimes for velocity surveys (§4.5.5) and for vertical seismic profiling (VSP) studies (§4.11.4).

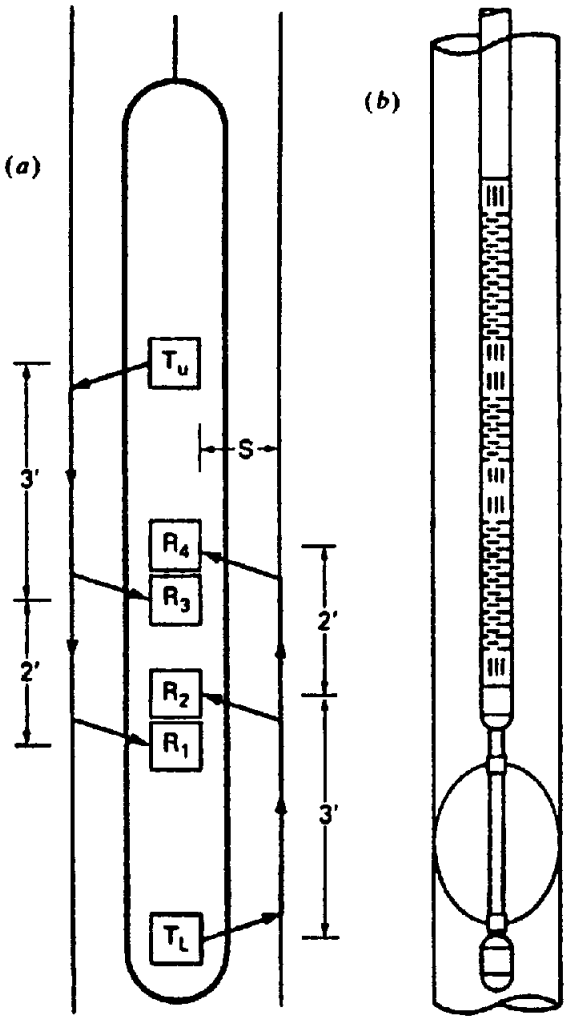

Figure 11.23. Sonic logging sonde. (a) Borehole-compensated sonde. (b) The sonde in a borehole. Vertical slits are openings to transmitters and receivers; horizontal slits prevent signal travel in the sonde itself.

11.7.2. Sonic Log

Early continuous velocity loggers consisted of a single receiver a few meters away from a transmitter that emitted pulses of acoustic energy. The traveltime of the first arrival was measured to determine the *P*-wave velocity in the adjacent rock. The design of the logging sonde prevents energy travel through the sonde from transmitter to receiver. The traveltime is determined by the time when the receiver output exceeds a threshold that is set higher than the noise but lower than the first cycle of energy. If the threshold should be too high, triggering may not occur until a later cycle, producing an error in measurement, called *cycle skip*. Cycle skipping is more likely when the signal has been attenuated by unconsolidated formations, fractures, gas in the pore spaces, aerated mud, or caved sections. Errors of this kind can usually be recognized and eliminated. However, with single transmitter-receiver sondes, errors also resulted when the axis of the sonde was not

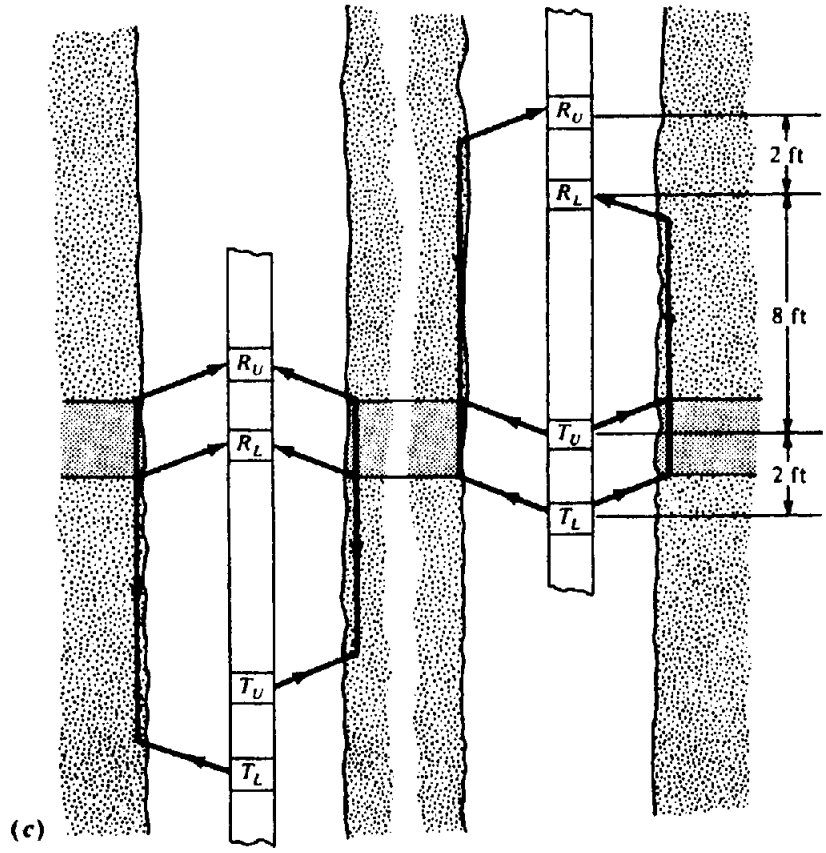

Figure 11.23. (Continued) (c) Long-spaced sonde in the two positions for borehole compensation.

Table 11.1. *Fluid and matrix velocities.*

Material	*P* waves		*S* waves	
	V_f or V_m (m/s)	Δt (μs/m)	V_f or V_m (m/s)	Δt (μs/m)
Water (20% salt to pure)	1,400 – 1,600	714 – 625	[870][a]	[1,150][a]
Salt	4,570	219		
Shale	4,875	205		
Iron casing	5,334	187		
Unconsolidated sands	5,180	193		
Sandstone	5,490 – 5,940	182 – 168	3,550	282
Anhydrite	6,100	164	3,030	330
Limestone	6,400 – 7,010	156 – 143	3,400	294
Dolomite	7,010 – 7,925	143 – 126	4,000	250

[a]Although water does not carry *S* waves, use of this value in the time-average equations yields good results.

parallel to the borehole wall, from enlarged borehole, from mud buildup, and from inadequate penetration beyond the altered invaded zone.

Errors in transit-time measurements occur because of hole-size changes (caving) or tilt of the sonde in the borehole. These effects opposite the transmitter are largely eliminated by measuring the difference in the traveltimes to two receivers at different distances. Likewise, the use of two transmitters allows eliminating variable effects opposite the receivers. The borehole-compensated sonic-logging sonde, illustrated in Figure 11.23a, employs two transmitters (which emit short 20 kHz pulses alternately about every 50 ms) and four receivers. About five measurements are averaged for each value recorded and the sonde is usually moved at about 15 cm/s, so that it moves about 3 cm during a measurement cycle. Centralizers keep the sonde in the center of the borehole.

The borehole-compensated sonde just described does not always correctly measure the velocity in the formation. Penetration may not extend beyond the

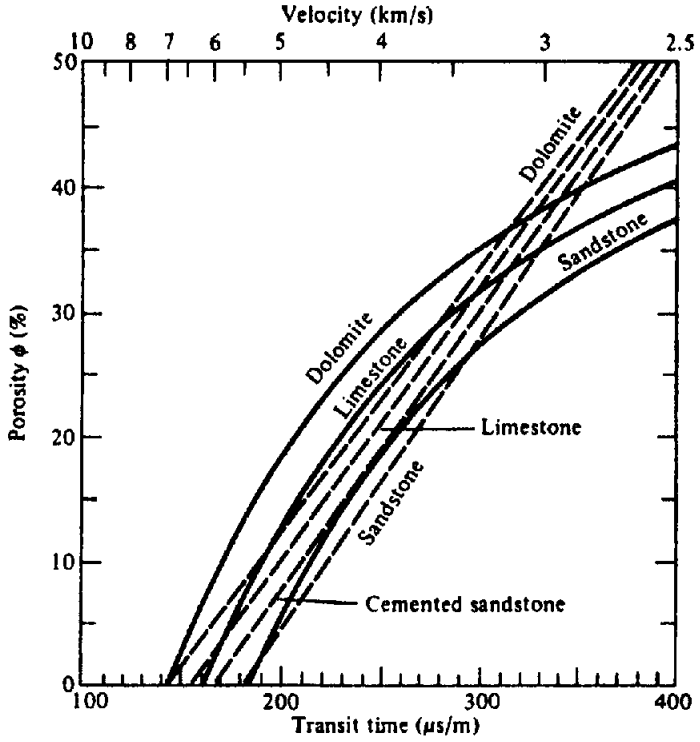

Figure 11.24. Porosity versus interval transit time. The curved lines are empirical, the straight lines give values from the time-average equation. (After Schlumberger, 1986.)

invaded zone, and shales at the borehole wall may have been altered so as to have lower velocity than those farther away from the borehole wall. Use of a long-spaced sonde, shown in Figure 11.23c, remedies these defects. Because the sonde moves, the transmitters are subsequently opposite the portion of the borehole that the receivers previously occupied (Fig. 11.23c); this permits averaging appropriate values to compensate for changes in borehole diameter and other abnormalities.

The sonic log displays the time interval for the sonic wave to travel one foot, usually expressed in microseconds per foot. Porosity usually is determined from the empirical *time-average equation* developed by Wyllie, Gregory, and Gardner (1958):

$$\Delta t = 1/V_p = (\phi/V_f) + (1 - \phi)/V_m \quad (11.14a)$$

or

$$\phi = (\Delta t - \Delta t_m)/(\Delta t_f - \Delta t_m) \quad (11.14b)$$

where Δt is the formation transit time (or *slowness*), V_p is the formation velocity, $V_f = 1/\Delta t_f$ is the velocity in the fluid which fills the pore spaces, $V_m = 1/\Delta t_m$ is the velocity in the rock matrix, and ϕ is the porosity. Velocities used in this calculation, given in Table 11.1, involve ranges from which the velocity that gives the best porosity values is selected. Figure 11.24 indicates the dependence of matrix velocity on porosity and provides a way of getting better porosity values from Equation (11.14).

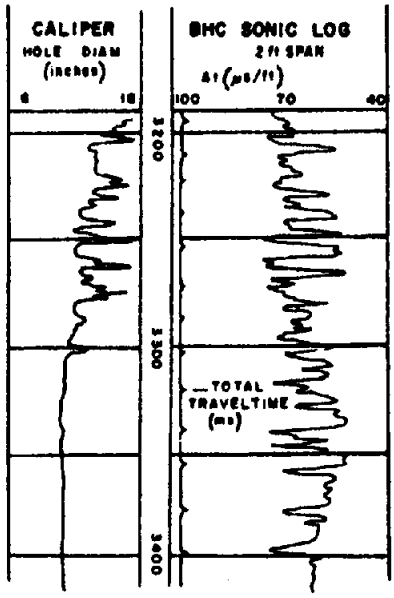

Figure 11.25. Portion of a sonic log. (From Schlumberger, 1987.)

For many formations, especially consolidated sandstones, the interval time in sands does not depend markedly on whether mud filtrate, formation water, or silt fills the pore spaces. Consequently the porosity calculated for shaly sands is too large. Where a sand is filled with oil or gas, especially with high porosity sandstones, the actual porosity is often 70 to 90% of the calculated porosity. In unconsolidated sands, porosities are sometimes corrected by dividing by 1/100th of the transit times (in microseconds per

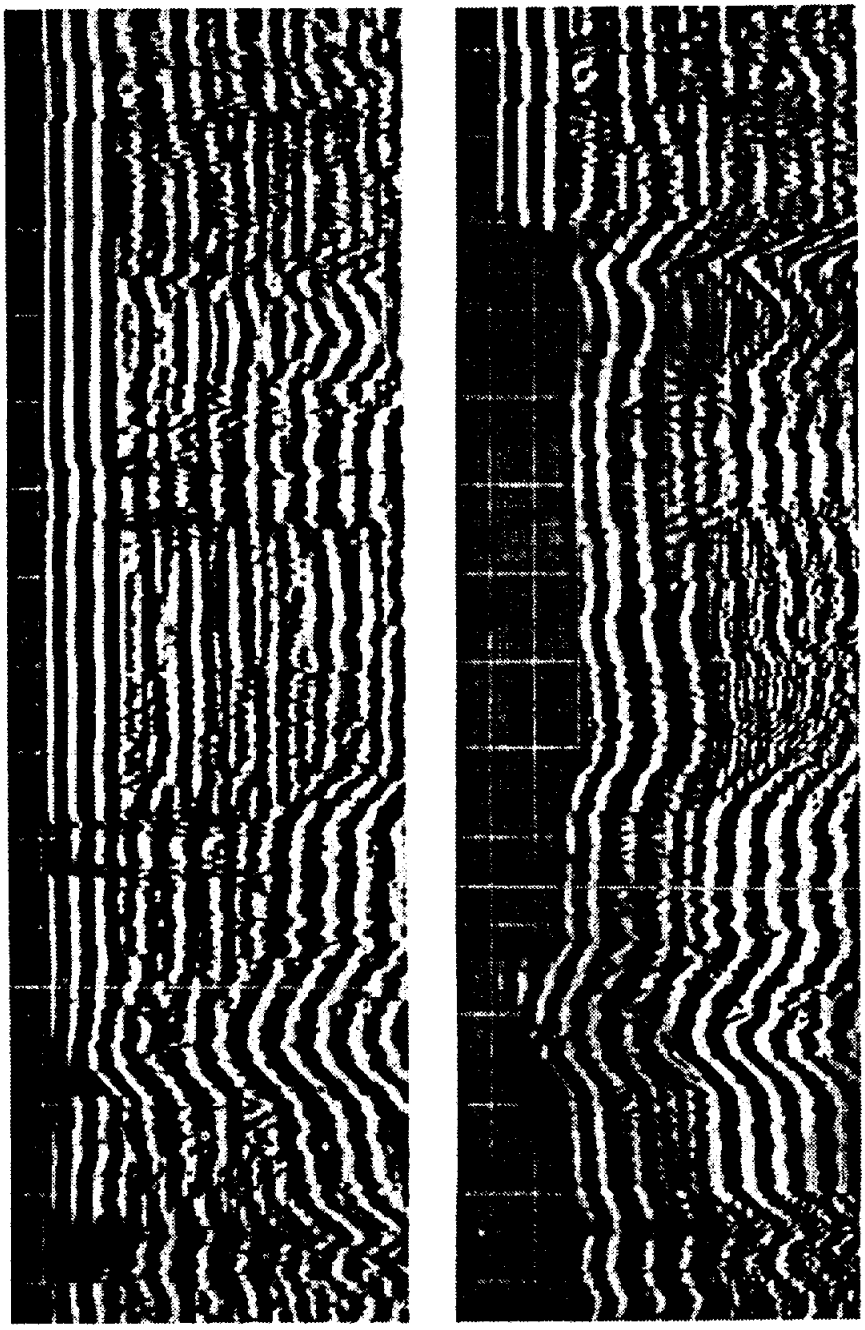

Figure 11.26. Microseismogram log used to indicate cement bonding. (Courtesy Welex.) (a) The first arrival is a strong signal transmitted through the casing before cementing. (b) After bonding the casing to the formation with cement, the first arrival is energy which travels through the formation.

foot) of adjacent shales (when the shale transit time > 100 μs/ft). The transit-time of shale normally increases rather steadily with depth, except where the shale is overpressured (§4.2.8a); a break in the shale transit-time curve provides an indication of an abnormal pressure situation. In carbonates the velocity is mainly determined by the primary porosity and vugular and fracture secondary porosity has relatively little effect. Correction is also accomplished from cross-plots with values determined from density and/or neutron logs (§11.10.2) and in other ways.

The sonic log is automatically integrated to give the total traveltime; this is shown on logs as ticks at intervals of 1 ms (track 2 in Fig. 11.25). However, small systematic errors tend to accumulate in integration. Traveltimes from check shots (from a source at the surface to a geophone in the well) can be used to remove accumulated errors.

11.7.3. Amplitude and Full-Waveform Logs

Whereas the sonic log measures only the traveltime of the first arrival *P* wave, the amplitudes and

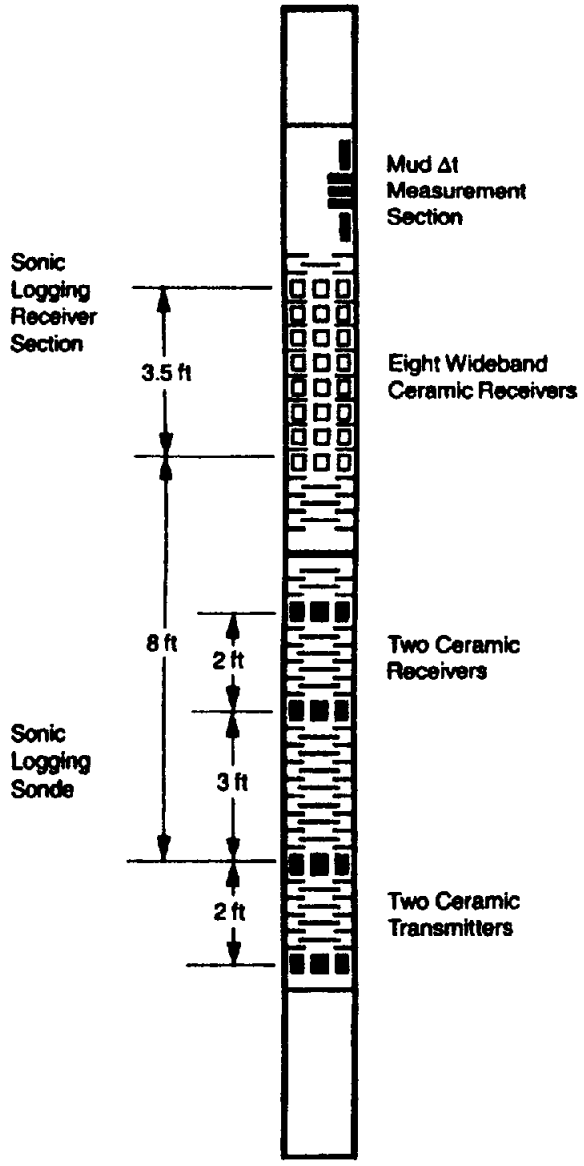

Figure 11.27. Array sonic sonde with two transmitters and 10 receivers. An example of the output of the upper 8 receivers is shown in Figure 11.21. (From Schlumberger, 1987.)

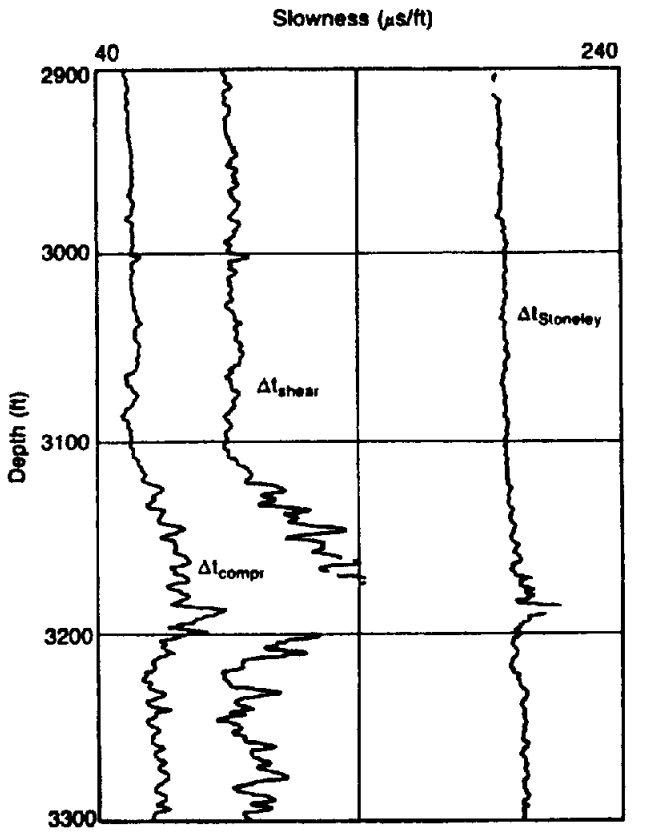

Figure 11.28. Log of P-, S-, and Stoneley-wave transit times. (From Schlumberger, 1987.)

traveltimes of the various arrivals also convey information. The amplitude of arrivals is plotted in an acoustic amplitude log. The entire acoustic wavetrain is recorded on the microseismogram and variable density logs. Such a log is shown in Figure 11.26. These logs may use only a single transmitter and receiver separated by a greater distance than for sonic logging. Logs of this type are also made of the *S*-wave arrival.

An *array sonde* (shown in Figure 11.27) multiplexes (§4.5.3f) and transmits to the surface for computer analysis the measurements from a number of receivers. It yields the same measurements as the borehole-compensated and long-spaced sondes, plus additional ones. It determines the traveltime slopes, and hence the transit times, by searching for semblance maxima (§4.7.13) of *P*-, *S*-, and Stoneley-wave arrivals among the full-waveform signals recorded by eight wideband receivers (Fig. 11.21b). These are displayed as shown in Figure 11.28. The mud transit time is also measured on fluid drawn through the upper part of the sonde. The *S*-wave transit time plotted against *P*-wave transit time helps identify lithologies, as discussed in Section 4.11.5. *S*-wave arrivals have appreciably higher amplitude than *P*-wave arrivals, so *S*-wave transit times can also be detected by setting the picking threshold high enough that the *S*-wave triggers the time counting. However, where the *S*-wave velocity is low, mud- and Stoneley-wave arrivals may override the *S*-wave arrivals.

Amplitudes are especially useful in determining the quality of the cement-to-casing and cement-to-formation bonding. Where the casing is not well cemented to the formation, the first-arrival headwave in the casing is especially strong, but when it is well cemented, the energy passes on through into the formation. Figure 11.26 shows a *cement-bond log*, a microseismogram log used to indicate the quality of cementing. High-velocity formations ($\Delta t < 57\ \mu s/ft$) can be logged behind casing when they are well cemented to the casing.

Sonic logs are used for fracture detection. Fractures cause a decrease in seismic amplitude, often by

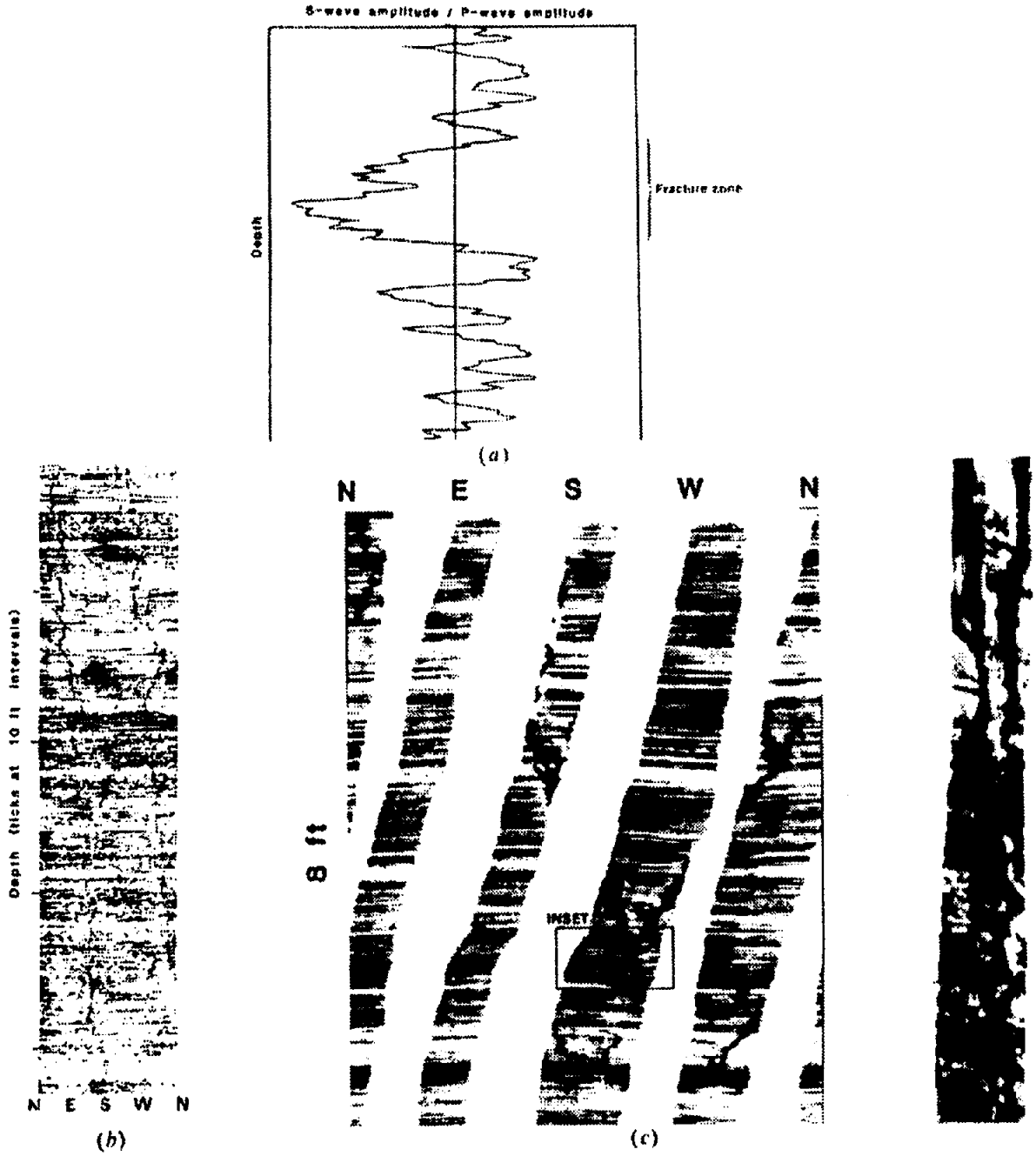

Figure 11.29. Fracture detection. (a) Fracture finder log showing low S-wave/P-wave amplitudes in a fractured zone. (After Labo, 1987.) (b) Fracture seen by a borehole televiewer. (Courtesy Gearhart Industries.) (c) Formation microscanner showing fractures. The microscanner uses a number of electrodes on each of four pads pressed against the borehole walls to give four swaths of closely spaced electric log responses. The sonde was twisting somewhat during this log run. (Courtesy Schlumberger.)

a factor of 10. However, thin beds, thin shale streaks, and healed fractures often give much the same response. Fractures dipping up to 70° also may cause a 20 to 30% lowering of *P*-wave amplitude and a 60 to 80% lowering of *S*-wave amplitude (Labo, 1987). The fracture-finder log measures the peak amplitude within a gate that includes both *P*- and *S*-wave arrivals (Fig. 11.29a). Fractures also tend to show on full-waveform logs. Off-centering of the sonde in the borehole may also reduce amplitude due to waves from different azimuths not arriving simultaneously. An amplitude decrease where Δt is constant may indicate fracturing.

11.7.4. Borehole Televiewer

An ultrasonic transmitter–receiver is rotated in the borehole as the sonde is raised. The ultrasonic beam, which does not penetrate into the formation, traces a helix on the borehole wall. The receiver records the amplitude of the reflection from the borehole wall (Fig. 11.30). The display is as if the borehole wall

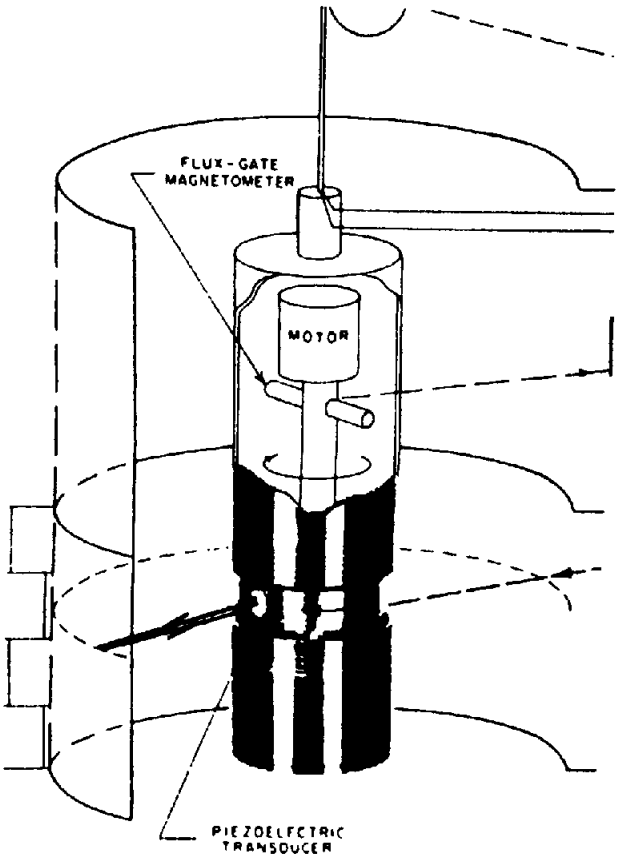

Figure 11.30. The borehole televiewer. (From Zemanek et al., 1970.) (a) Schematic view of the sonde; the magnetometer gives the sonde orientation.

were cut longitudinally and then laid out flat (Zemanek et al., 1970). The result is used to study fractures (see Fig. 11.29b).

11.8. NUCLEAR METHODS

11.8.1. Nuclear Processes

(a) Introduction. As discussed in Chapter 10, some atomic nuclei emit natural radiations and others can be induced to do so by bombardment. The nuclear radiations are in the form of α, β, or γ rays. Natural and induced γ radiation and neutrons possess appreciable penetrating power and are used in radioactivity logging.

Well-logging instruments that measure radioactivity of nearby formations may be considered under three headings: (i) those that detect γ radiation resulting from natural radioactivity, (ii) those that employ artificial γ rays, and (iii) those that use neutron sources to induce nuclear processes. Instruments employing γ-ray detectors are calibrated by measuring the detector response at various distances from a standard γ-ray source. Slow-neutron devices are calibrated by surrounding them with a standard volume of hydrogen-bearing material.

(b) Natural radioactivity. Natural radioactivity results from the presence of small amounts of U, Th, and ^{40}K; it is usually lowest in basic igneous rocks, intermediate in metamorphic rocks, and highest in some sedimentary rocks, especially shales. Although the γ radiation from either the U or Th series is much higher intensity than that of ^{40}K (see Table 10.3, §10.2.4), ^{40}K is far more common and the total background radiation is attributable more-or-less equally to the three elements.

Gamma-ray emissions of U, Th, and K are shown in Figure 11.31. The energy spectra of U and Th are broad and relatively complex, with characteristic γ rays: 1.76 MeV from U (^{214}Bi) and 2.62 MeV from Th (^{208}Tl). The γ ray from ^{40}K is monoenergetic at 1.46 MeV. Radiation of different energies can be distinguished by using a γ-ray spectrometer (§10.3.4) sensitive only to narrow bands.

(c) Interaction of γ rays. An energetic γ ray may interact with the surrounding material by three distinct processes (see also §10.3.3b): (i) it may transfer its entire energy to a single atomic electron (*photoelectric conversion*), (ii) it may lose a fraction at a time to several electrons in successive collisions

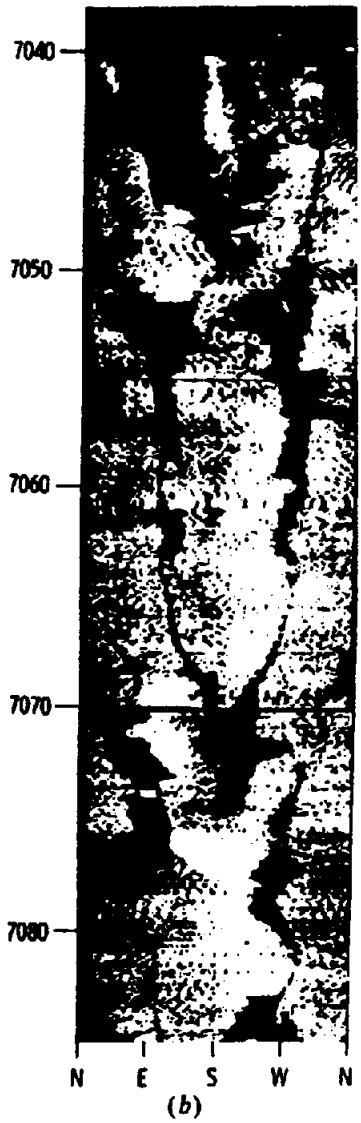

Figure 11.30. (Continued) (b) Portion of a log showing fractures.

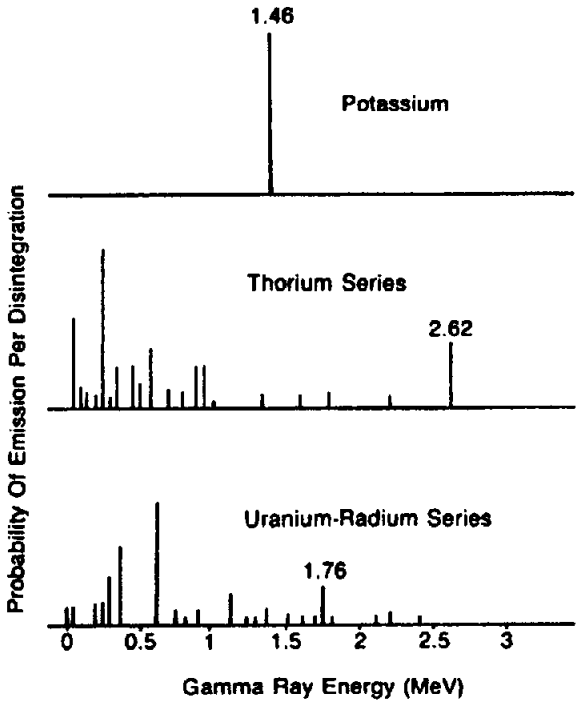

Figure 11.31. Gamma-ray spectra of potassium and the thorium and uranium series. (From Schlumberger, 1987.)

Table 11.2. *Absorption of γ rays in various materials.*

Energy (MeV)	Half-value layer (cm)			
	Water	Sandstone, $CaCO_3$	Iron	Lead
0.2	5	2	0.7	0.1
1.0	10	5	1.5	1.0
5.0	23	10	3.0	1.5

(*Compton scattering*), or (iii) the γ ray may disappear in the creation of an electron–positron pair (*pair production*). The probability of each process occurring depends on the energy of the photon. The photoelectric effect occurs mainly at low energies (< 0.2 MeV), whereas pair production can take place only if the γ-ray energy is sufficient to create two particles of 0.51 MeV each (that is, > 1.02 MeV). The three processes are all related to the density of electrons in the medium, that is, to the atomic number Z. Photoconversion is proportional to Z^6, Compton scattering to Z, and pair production to Z^2. The attenuation of a γ ray is thus determined by the material through which it passes. Most logging sources do not emit γ rays of sufficient energy to cause pair production.

Table 11.2 shows the penetrating power of γ rays in various media. The attenuation is measured in terms of the material thickness, which reduces the intensity to some fraction of the original. The relation is exponential, as for electromagnetic waves generally:

$$I = I_0 e^{-\mu x} \qquad (11.15)$$

where μ is the absorption coefficient. When $I/I_0 = 1/2$, the thickness of the half-value layer is $x_{1/2} = (1/\mu)\ln 2 = 0.69/\mu$. The average energy of natural γ rays is about 1 MeV and their range in sediments is roughly 30 cm. About half the γ rays detected in a borehole originate within 15 cm of the borehole walls. Casing reduces the intensity by about 30%.

(d) Interaction of neutrons. The interaction of neutrons with surrounding matter is also diagnostic of the medium. Fast neutrons (kinetic energy > 0.1 MeV) are slowed down by elastic and inelastic collisions with nuclei. Inelastic collisions result in the nucleus (in addition to acquiring kinetic energy) being left in an excited state; it subsequently emits a characteristic γ ray. Elastic collisions result in a

Table 11.3. *Neutron-capture and inelastic-scattering cross sections with characteristic γ rays emitted.*

Element	Cross section (barns)		Characteristic γ rays (MeV)
	Inelast. scatt.[a]	Capture	
Hydrogen		0.33	2.2
Beryllium	0.4	0.01	6.8
Boron		755	
Carbon	0.25	0.003	1.3, 4.9
Oxygen		0.0002	
Sodium	0.5	0.53	3.6, 3.9
Magnesium	0.7	0.27	2.8, 3.9
Aluminum	0.7	0.23	2.8, 7.7
Silicon	0.7	0.16	2.7, 4.9
Sulfur	0.8	0.52	3.0, 5.4
Chlorine	0.8	34	2.0, 6.1, 6.6
Potassium	1.0	2.1	4.4, 7.7
Calcium	1.0	0.43	1.9, 6.4
Manganese		13.3	1.8, 5.3, 7.2
Iron	1.2	2.6	5.5, 6.2
Cobalt	1.4	3.7	
Nickel	1.4	4.6	8.5
Copper	1.5	3.8	7.9
Zinc	1.5	1.1	
Molybdenum	2.0	2.7	
Silver	2.0	6.3	
Cadmium	1.9	2,500	1.0 – 7.0
Tin	1.6	0.63	
Tungsten	2.5	19	4.8
Gold	2.5	99	4.0 – 7.0
Mercury	2.5	360	3.8
Lead	1.8	0.7	6.7, 7.4
Uranium		7.7	1.0, 3.0

[a]Average value over the energy range 1 to 14 MeV.

partition of energy and the rate at which a neutron loses energy varies inversely with the mass of the target nucleus. When a neutron has been slowed to a velocity compatible with the temperature of the environment (kinetic energy < 0.025 eV), it is called a *thermal neutron* and can be captured by a nearby nucleus, which then emits a characteristic γ ray. The probability of neutron capture depends on the *capture cross section*, a quantity that is measured in barns (1 b = 10^{-24} cm^2). Table 11.3 gives neutron capture cross sections and some of the characteristic γ rays emitted on capture.

11.8.2. Gamma-ray Logging

(a) The gamma-ray log. The γ-ray sonde consists of a detector and an amplifier. Early γ-ray logging used either an ionization chamber or a Geiger counter, but these have been replaced by the more efficient scintillation counter. The last two detectors are described in Section 10.3. A scintillation counter is only ~ 20 cm in length so that resolution is good. Several measurement units have been employed, such as microroentgens per hour (μR/hr), counts per minute, and micrograms of Ra-equivalent per ton (μg of Ra-eq/ton), but γ-ray logs are now calibrated in API units (American Petroleum Institute units, which are different from API neutron units; §11.8.4b). The difference between the high- and low-radioactivity sections of cement in the API calibration pit at the University of Houston is defined as 200 API units. Average shales have values around 100 API units.

In sediments the γ-ray log (Wahl, 1983) reflects mainly shale content because the radioactive elements tend to concentrate in clays and shales. Volcanic ash, granite wash, formation waters that contain radioactive salts, potash, and uranium ores may cause γ-ray anomalies. The γ-ray log responding to shale and clay is generally correlatable with the SP log. It now often replaces the SP log in general logging, especially where the SP is not diagnostic, as in very resistive formations where there is little difference between the salinities of the mud and formation water, or with oil-based muds, in empty holes, and in cased holes.

Figure 11.32 shows a schematic γ-ray log. Statistical variations, significant at low counting rates, are

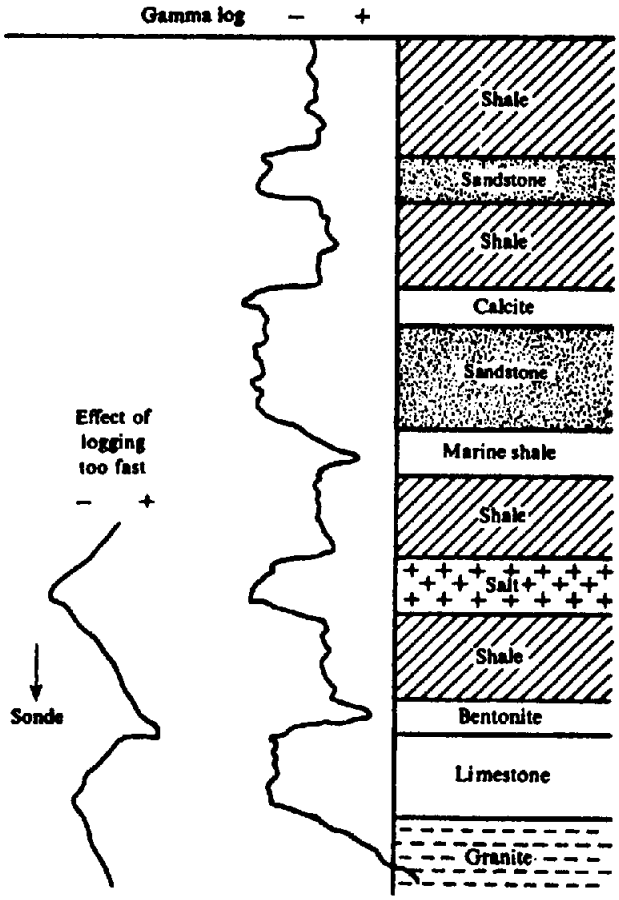

Figure 11.32. A γ-ray log.

smoothed out by integration over a time interval of several seconds. If the hole is logged too quickly, the smoothing effect causes barren zones to be apparently shifted in the direction of the logging, as illustrated in Figure 11.32, and thin beds to be missed. The logging speed is determined by the measurement time interval selected. It generally defines beds thicker than 1 m.

The interface between adjacent barren and radioactive beds is located fairly accurately at half the maximum deflection when the beds are thicker than 1 m. For thinner beds the bed center is taken as the peak deflection. Because the γ-ray log generally defines formation interfaces sharply in both open and cased holes, it is often run with other logs and production tools so that one can correlate the cased and open-hole logs and relate other logs to specific formations with greater certainty. The γ-ray log is used quantitatively to indicate shale percentage and to grade uranium deposits. It is the only logging tool used routinely in the mineral industry.

(b) Natural gamma-ray spectroscopy. The natural gamma-ray spectroscopy tool (§10.3.4) measures the energy level of γ-rays and permits determining the concentrations of K, U, and Th in rocks. The NaI scintillation detector is held against the borehole wall as with the γ-ray log. The spectra of potassium, uranium, and thorium are smeared out (as shown in Fig. 11.33). Measurements in four or five windows permit solving for concentrations of K, U, and Th. A portion of a γ-ray spectrometer log is shown in Figure 11.34. This log is used to identify and evaluate radioactive minerals. It can also be used to identify clay types.

11.8.3. Density Log

(a) Density log. The *density log*, or *gamma-gamma log*, is used to determine porosity. Figure 11.35 is a schematic diagram of a density-logging sonde; the sonde is pressed against the borehole wall. The bottom of the sonde usually contains ^{137}Cs, a concentrated source of 0.662 MeV γ rays; early sondes used a ^{60}Co source. A scintillation meter is ~ 60 cm above the source. Both source and detector are surrounded by lead shielding except for windows facing the wall, so that only γ rays that have traveled through the adjacent formation reach the detector. The spring force that presses the sonde against the borehole wall is considerable and the skid has a plow-shaped leading edge so that it cuts through soft mud cakes. The sonde occasionally sticks and then jerks free. The γ rays from the source interact with the elements in the rock mainly by Compton scattering, to a lesser extent by photoconversion (the sonde design excludes the portion of the spectrum affected by photoelectric absorption). The detected γ-ray intensity is an exponential function of the rock density. The maximum depth of investigation is about 15 cm, with most of the signal coming from the first 8 cm. Modern devices measure separately the Compton scattering and photoelectric absorption effects, the former depending mainly on formation density, the latter on lithology.

The instrument is calibrated for source intensity and detector sensitivity by clamping an aluminum, manganese, or sulfur block to it. Corrections for borehole size are small for hole diameters under 10 in. (25 cm) but amount to ~ 0.03 g/cm^3 for large holes. It may be used in empty holes as well as those filled with mud. Logging through casing is generally poor (accuracy ≈ ±0.05 g/cm^3). A hole caliper log is an auxiliary output. Because the tool is short, adjacent beds or thin beds have little distorting effects. The logging speed must be adjusted in relation to the instrument time constant to avoid distortion of the curves and loss of sensitivity. Because count rate is high, fairly fast logging (2,000 m/hr) is permitted.

The compensated density-logging sonde employs two detectors at different distances from the source. The shorter spacing is more affected by mud buildup

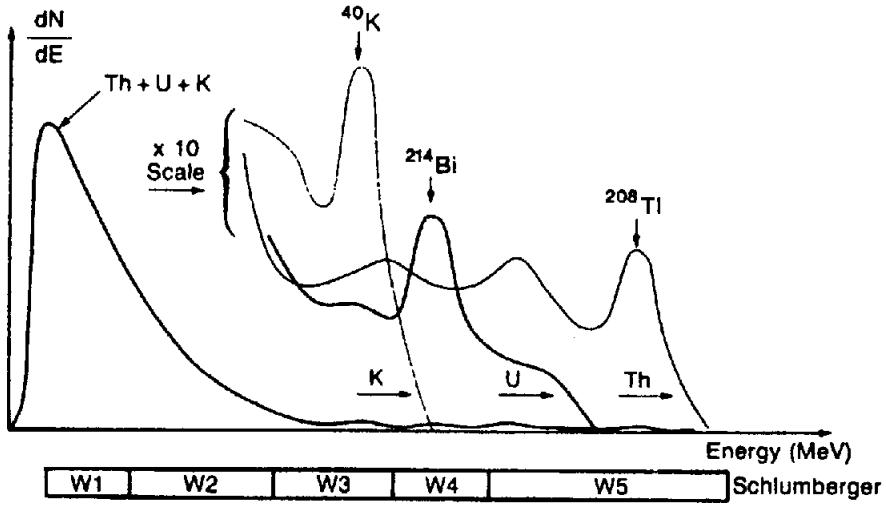

Figure 11.33. Gamma-ray spectra using a NaI crystal detector and energy windows for examining portions of the spectra. (From Schlumberger, 1987.)

and the difference between the readings from the two detectors is used to correct for the thickness and density of the mud cake.

Compton scattering cross sections per electron are nearly independent of the atom containing the electrons, and so the density log responds to the density of electrons (Table 11.4). Most atoms have nearly two electrons per atomic-weight unit; hydrogen is an exception and a few other elements also depart slightly from this ratio. The density log is usually calibrated for fresh-water saturated limestone, but it also gives quite accurately the bulk density in sandstone and dolomite. Corrections are needed to give the bulk density in salt, gypsum, anhydrite, coal, and gas, for which the ratio of electron density to atomic weight departs from that for limestone ($Z/A = 0.5$).

Porosity ϕ can be determined from the bulk density ρ_b by the exact relation

$$\phi = (\rho_{ma} - \rho_b)/(\rho_{ma} - \rho_f) \qquad (11.16)$$

where ρ_f and ρ_{ma} are the densities of the formation fluid and the rock matrix. Density values are too low (up to 0.08 g/cm^3) for formations that contain gas (because the pore fluid is assumed to be brine). The matrix density of most clay minerals is close enough to that of quartz that no difficulty is encountered in calculating the porosity of shaly sands. Disseminated shale often has a lower density than interbedded shale. Density logs are used to predict overpressure (Fig. 11.36) because shale density begins to decrease 100 m or so above high-pressure sands. The bulk porosity determined with this log includes secondary porosity and porosity that is not interconnected. If interpreted with other porosity-sensitive logs (§11.10.2), some of these complicating factors can be sorted out.

(b) Lithodensity log. The lithodensity logging sonde employs a beryllium window that passes low-energy γ rays. By comparing counts at very low energies with those at higher energies (Fig. 11.37), this log measures a *photoelectric absorption index* (Tittman, 1986, pp. 33–6) which is related to lithology of the formation.

11.8.4. Neutron Logging

(a) Neutron reactions, sources, and detectors. High-energy neutrons from a source in the sonde bombard the formations and lose energy mainly in elastic collisions with nuclei. The energy loss per collision is greater when the neutron and the nucleus with which it collides have comparable masses. Hence, the rate of energy loss (*moderation*) for fast neutrons is almost proportional to the density of protons (which have nearly the same mass as neutrons). Consequently, the response is primarily to hydrogen content, and neutron logs locate porous zones and determine the amount of liquid-filled porosity. The amount of hydrogen per unit volume is called the *hydrogen index*. After neutrons have been slowed to thermal energies, they may gain or lose energy in collisions because their energy is comparable to that of the colliding particle. Eventually they are captured by nuclei, which then emit capture γ rays. Where thermal neutrons or capture γ rays are measured, the nature and abundance of the capturing nucleus have a perturbing effect.

Several neutron sources have been used for the neutron log. These include combinations of beryllium with an α-particle source such as radium, polonium, plutonium, or americium. Most logs today use

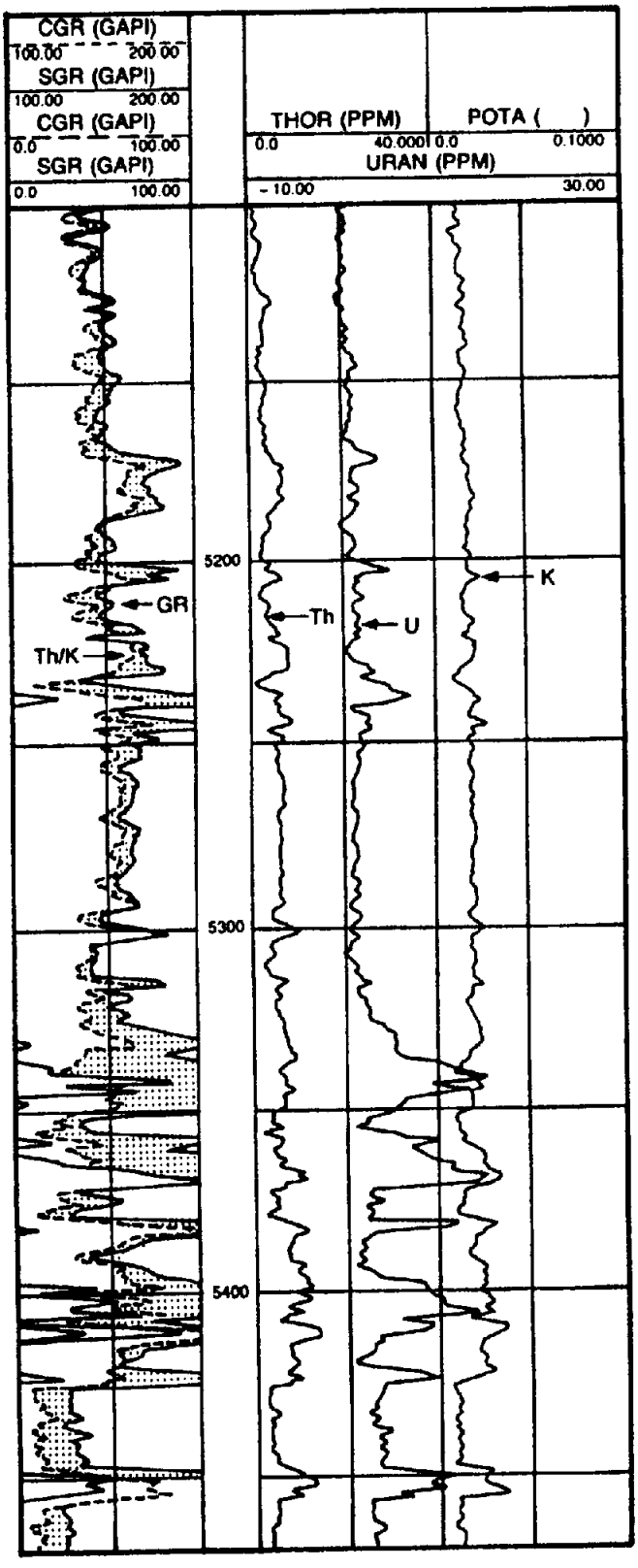

Figure 11.34. A natural γ-ray spectrometry log. (From Schlumberger, 1987.)

an americium–beryllium source with a 460 yr half-life. The reaction is

$$ {}_2He^4 + {}_4Be^9 \rightarrow {}_6C^{12} + {}_0n^1 \qquad (11.17) $$

A 16 curie source produces about 4×10^7 neutrons/s. Charged-particle accelerators have also been used to produce neutrons by the reactions

$$ \left.\begin{aligned} {}_1H^2 + {}_1H^2 &\rightarrow {}_2He^3 + {}_0n^1 \\ {}_1H^2 + {}_1H^3 &\rightarrow {}_2He^4 + {}_0n^1 \end{aligned}\right\} \qquad (11.18) $$

The first reaction produces 2.3 MeV neutrons, the second 14.3 MeV neutrons. These neutron sources are monoenergetic and the source can be shut off.

Either the capture γ rays or the neutrons themselves may be counted. In porous formations saturated with water or oil, the neutrons lose energy rapidly so that the counting flux is high and most of the response is within 20 cm or so of the borehole. In low-porosity formations the neutrons penetrate farther, producing low counting flux, and the response range is of the order of 60 cm.

Several types of detectors are used. Some use a proportional counter shielded by a sheet of cadmium that absorbs thermal neutrons, so that only neutrons with energy above some threshold are detected.

(b) Neutron log (hydrogen index log). The neutron log indicates porosity by determining the amount of hydrogen and hence the amount of fluid filling the pore spaces. The first neutron logs were nondirectional and their detectors responded to both thermal neutrons and high-energy γ rays resulting from the neutron capture; however, these logs needed correction for salinity, mudcake, hole size, and casing. Best resolution was obtained when the hole was small, so that fewer neutrons were lost in the mud column. Sometimes the source–detector spacing was increased for operation in large diameter holes.

The *sidewall neutron log* is a sidewall device (like the density logging sonde); it was used in empty (but not cased) holes, but it is now obsolete. It employed a proportional counter so shielded that it measured only epithermal neutrons (energy ≈ 0.4 eV), whose energy is greater than that of the thermal neutrons involved with capture. Hence it was not perturbed by neutron absorbers, such as chlorine and boron, and was not sensitive to hole size. However, the count rate of epithermal neutrons was small so the detectors had to be close to the source and consequently depth of penetration was small and invasion effects large.

The *compensated neutron log* measures thermal neutrons. It employs two detectors spaced at different distances from the source, which makes it possible to correct for the effects of mud cake and hole roughness (*rugosity*). It has greater depth of penetration than the sidewall tool and can be run in either cased or uncased holes but not in empty holes. It is sensitive to shales, which often contain small amounts of boron and other elements with high capture cross section.

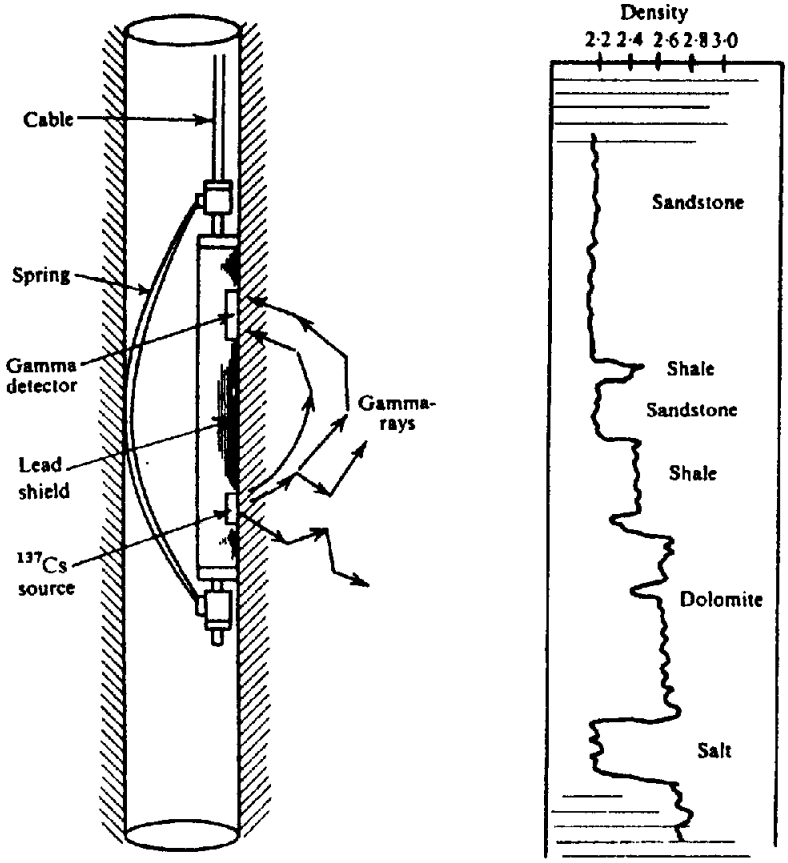

Figure 11.35. Density log schematic and typical log.

Table 11.4. *Common elements encountered in hydrocarbon exploration.*

	Z	A	Z/A
H	1	1.007	0.9921
C	6	12.011	0.4995
N	7	14.006	0.4998
O	8	15.999	0.5000
Na	11	22.989	0.4785
Mg	12	24.312	0.4934
Al	13	26.981	0.4818
Si	14	28.085	0.4984
Cl	17	35.453	0.4794
K	19	39.098	0.4859
Ca	20	40.08	0.4990

The *dual porosity neutron log* employs two detectors to measure thermal neutrons and two detectors to measure epithermal neutrons, neutrons of both energy classes being measured at different distances from the source (Fig. 11.38). The additional measurements permit corrections for shale content and salinity, and also yield improved gas detection in shaly reservoirs.

Neutron logs are usually plotted either in API neutron units or in "limestone porosity," which assumes that the matrix is limestone. API neutron units are based on measurement in a standard neutron pit where 19%-porosity water-filled limestone is defined as 1,000 API neutron units. Correction is made for mud weight, temperature, hole-size variations, and salinity. The salinity is usually taken as that of the formation water except for invaded zones, where it is assumed to be that of the mud. A plot of a portion of a dual-porosity neutron log is shown in Figure 11.39.

Neutron logs are affected by all protons, including those in bound water associated with shales or water of crystallization, such as contained in gypsum. Consequently, shales and gypsum have distorting effects. Because neutron logs are affected by lithology, the best porosity values are obtained from the combined interpretation of neutron logs with other porosity-sensitive logs, especially with density logs (§11.10.2); this is particularly useful with a density log to indicate gas in the pore spaces.

(c) Pulsed-neutron logging. Pulsed-neutron logs, which include the *thermal-decay-time-log* and *neutron-lifetime log*, record the rate of decay of thermal neutrons. Chlorine, the most common element with high capture cross section (Table 11.3), is found in most formations and is the principal absorber of thermal neutrons. Consequently pulsed-neutron logs mainly determine the amount of chlorine, that is, the amount of saline water present. They thus accom-

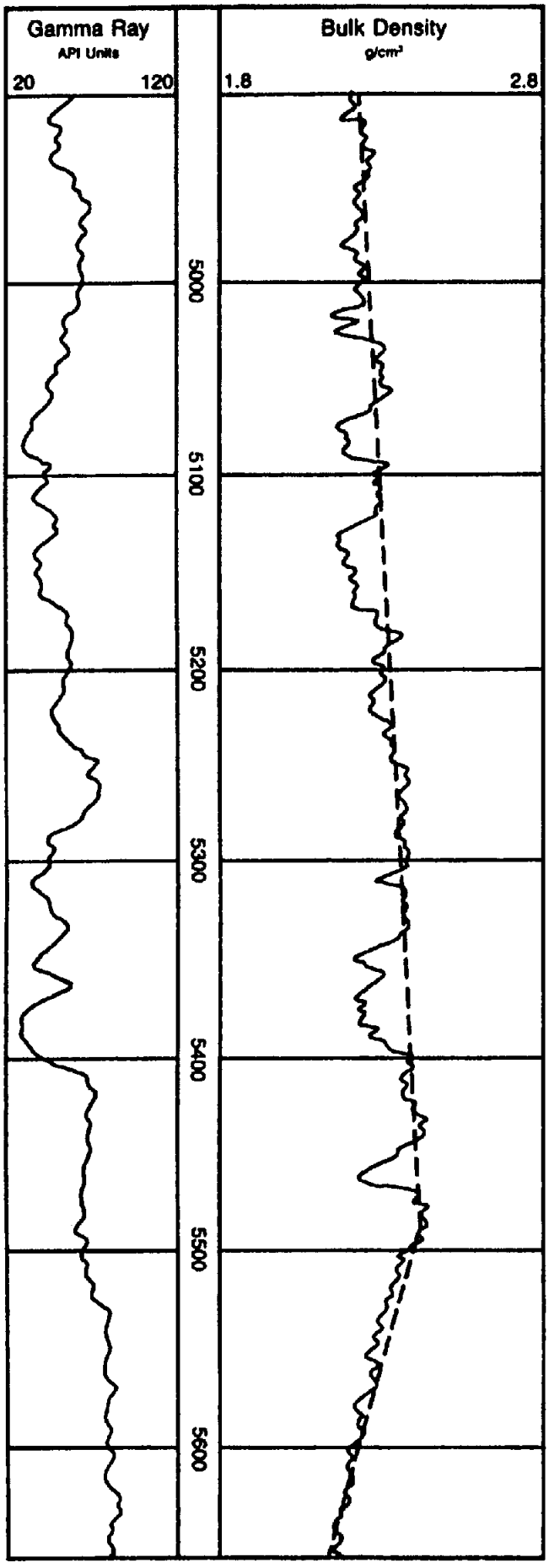

Figure 11.36. Density log, with overpressured shale below 5,490 ft. (From Schlumberger, 1987.)

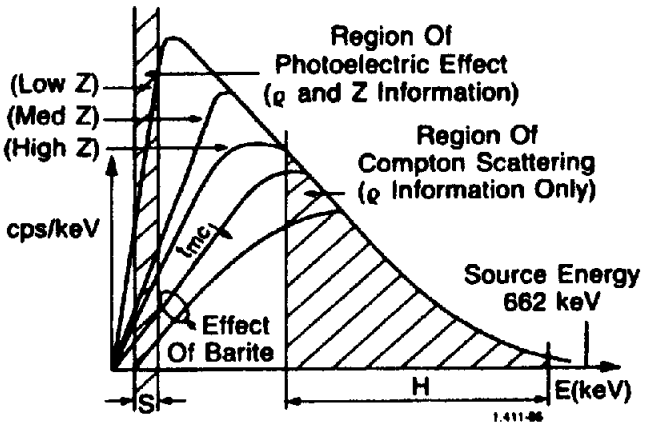

Figure 11.37. Gamma-ray energy spectrum showing the two windows in which measurements are made. The counts in the high-energy window H depend on density only, whereas those in the low-energy windows depend on both density and atomic number Z of the capturing atom. (From Snyder and Fleming, 1985.)

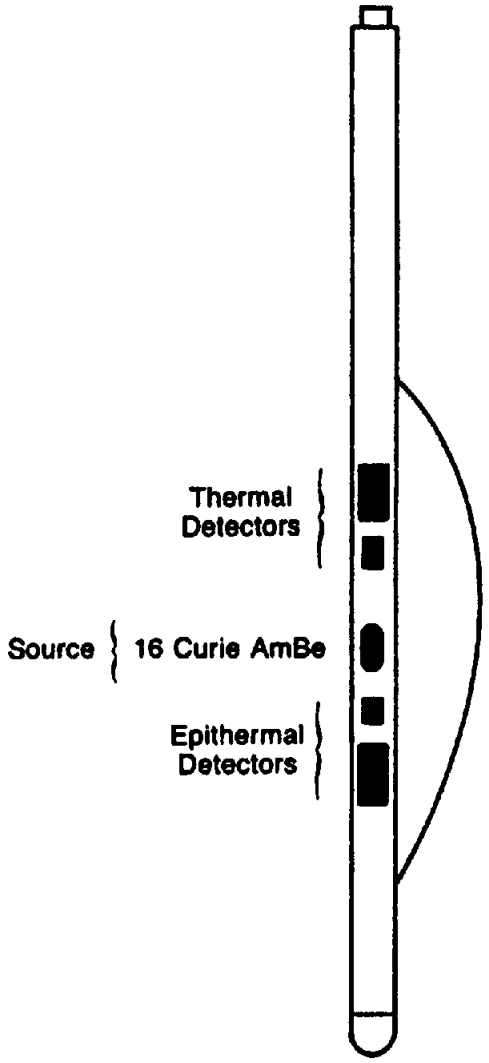

Figure 11.38. Schematic of dual-porosity neutron-logging sonde. (From Schlumberger, 1987.)

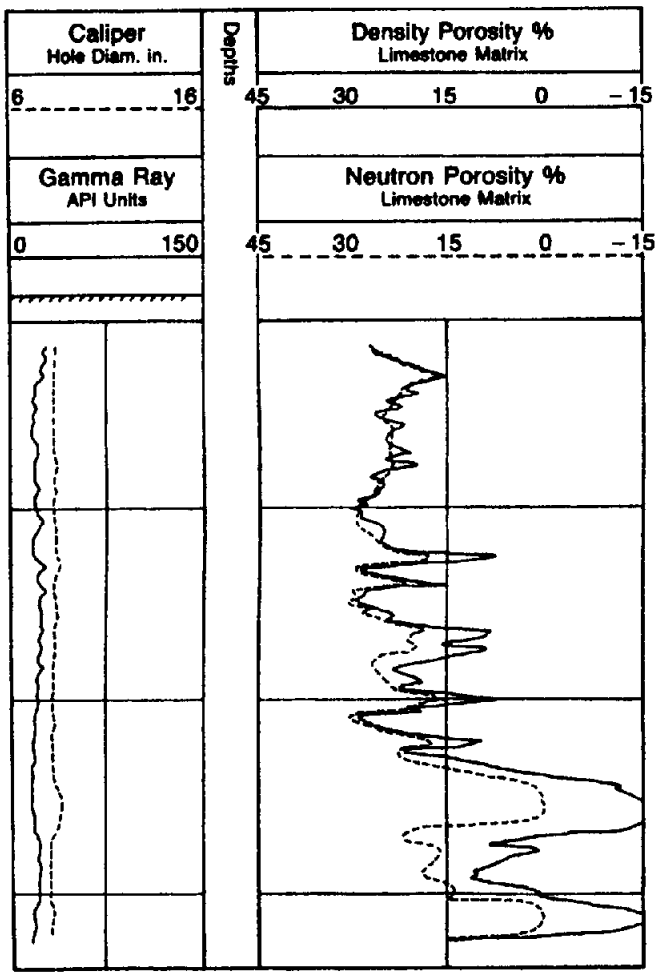

Figure 11.39. Portion of a dual-porosity neutron log. (From Schlumberger, 1987.)

plish essentially the same purpose as resistivity logs and can generally be correlated with them. Their advantage over resistivity logs is that they can be used in cased holes.

A neutron generator emits a burst of high-energy neutrons, as in Equation (11.18). These are rapidly slowed to thermal energies and captured, whereupon capture γ rays are emitted. The γ rays arriving during a fixed time interval after the burst are detected a short distance away from the source. Measurements are made over two or more time intervals (Fig. 11.40) to determine the *die-away* time; this permits correcting for background effects and determining the rate of thermal-neutron capture. Absorption by the borehole fluid and casing primarily affects readings made soon after the burst; absorption effects can be largely eliminated by delaying the first measuring interval.

The *gamma-ray spectrometry log* involves a 256-channel spectral analysis of either elastic scattering or capture γ rays in two modes of operation. It gives water saturation independent of salinity and provides the data for determining the ratios of various elements, such as C/O and Si/Ca, by measuring their capture γ rays. This tool can also be used in analysis for coal, Cu, Fe, and U.

11.9. GRAVITY, MAGNETIC, AND THERMAL METHODS

11.9.1. Gravity and Magnetic Field Logging

Borehole gravity measurements were discussed in Section 2.3.4b. Borehole magnetic measurements (Silva and Hohmann, 1981) can be made with fluxgate or proton-precession instruments (§3.4.2 and §3.4.3). Vertical-gradient measurements can also be made in boreholes.

11.9.2. Susceptibility Log

Borehole instrumentation is similar to the field susceptibility meter (§3.3.8a). The solenoid is wound on

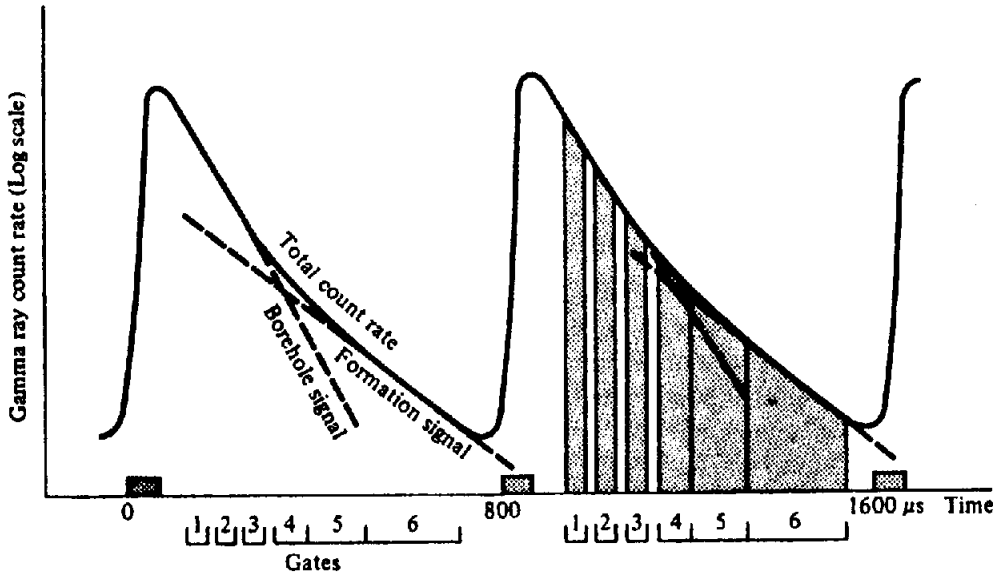

Figure 11.40. Pulsing and gating parameters for pulsed neutron log. A burst of neutrons occurs every 800 μs. (From Snyder and Fleming, 1985.)

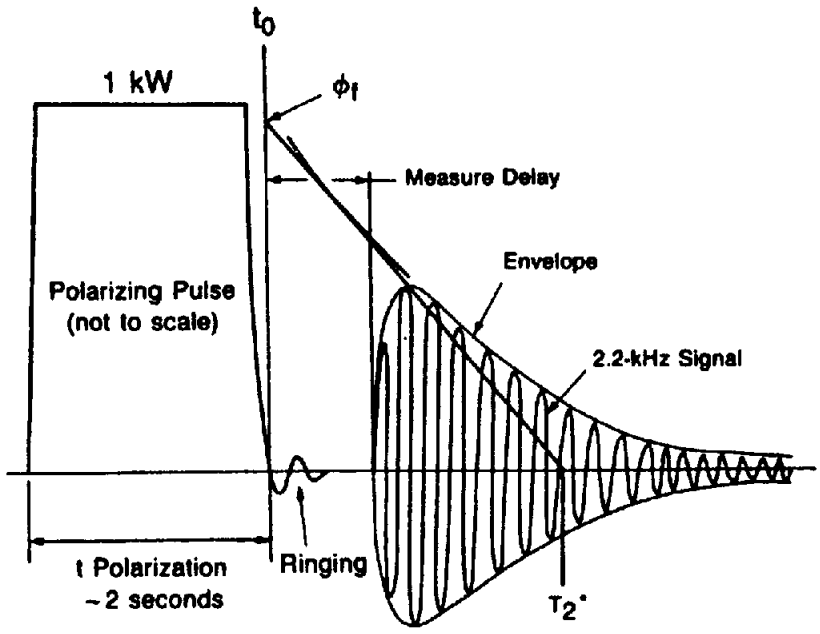

Figure 11.41. Nuclear-magnetic-resonance signal decay. Signals from resonances other than those of the free fluid decay before measurement begins. The signal decay is exponential so that the free-fluid index (ϕ_f) can be found by extrapolating the log of the decay back to zero time. (After Pinnington, 1981.)

a core of low-reluctance material and connected to one arm of a Wheatstone bridge. If the bridge is balanced in a barren environment, the presence of formations of anomalous susceptibility or conductivity unbalances it, because the susceptibility effect changes the reactance and produces a quadrature voltage whereas the conductivity produces an in-phase voltage. The effects can be separated by phase detectors and logs of susceptibility and conductivity displayed separately. The susceptibility log is not affected by mud resistivity and can be run in dry holes. The conductivity log compares favorably with resistivity logs for $\rho_a > 2$ Ωm. Depth of penetration is about equal to the coil length.

Anomalous susceptibility may indicate the presence of magnetic materials, such as magnetite, ilmenite, and pyrrhotite. Good correspondence between SP and susceptibility logs indicate that porous zones have been enriched by ground-water deposition of magnetic minerals.

11.9.3. Nuclear Magnetic-Resonance Log

The proton-precession magnetometer was discussed in Section 3.4.3 as a device to determine the magnetic field strength, which is proportional to the measured Larmor frequency. [Eq. (3.30a)]. When, in the measurement cycle, the impressed field is removed, the protons with aligned spins gradually get misaligned (and the proton signal decays) as the protons are affected by somewhat random local magnetic fields. The time required for the proton resonance signal to decay following the removal of an impressed field is a measure of the environment of the protons. The nuclear magnetic-resonance log measures the decay rate to determine this environment.

An impressed field at a large angle to the Earth's field is applied for about 2 s to orient the proton spins, and then the impressed field is cut off. The signal due to the residual oriented spins (Fig. 11.41) precessing about the Earth's field is measured beginning ~ 25 ms later (to allow transients to die out). The signal decay is affected by the protons in the borehole fluid, protons in moveable formation fluids, and protons bound to the lattice. The borehole fluid signal decays very rapidly because the drilling mud contains finely divided magnetite and the contribution of the borehole fluid is over before the measurement period begins. Protons in solids or bound to surfaces also have very short decay times. Thus the only significant contribution during the measurement period is that due to the protons in fluids that are free to move in the rock's pore spaces. The amplitude of the decaying signal is thus a measure of the amount of fluid (hydrogen) that is free to move. The measurement yields a *free-fluid index* (FFI), a measure of the porosity occupied by free fluids ϕ_f. The rate of signal decay further indicates the type of fluid (water or hydrocarbons). Combining these measurements with data from other logs permits estimates of the *irreducible water saturation* (trapped water which is not free to flow), the permeability, and the *residual oil saturation* (the oil that can not be

flushed out by invading fluids) in the invaded zone (Tittman, 1986).

11.9.4. Thermal Logging

Measurement of temperature has been employed mainly to determine large-scale terrestrial heat flow, but it can also be used to locate thermal anomalies caused by fluid flow, abnormal radioactivity, and oxidation regions. Various types of thermometers have been used, including resistance thermometers and thermisters.

11.10. WELL-LOG INTERPRETATION

11.10.1. General

Interpretation of well logs for mineral objectives is usually qualitative, that is, locating and correlating anomalous zones. Interpretation for oil objectives, on the other hand, is highly developed. A variety of methods is employed and an enormous amount of data is accumulated. Oddly enough, geophysicists play a minor role in oil well-log interpretation. The logging contractor usually carries out routine interpretation, whereas detailed assessment is left to a specially trained oil-company geologist who has all the pertinent data (including classified data) at his disposal. Detailed log interpretation for the evaluation of porous and permeable formations for potential production is beyond the scope of this book.

Inspection of conventional electric logs (SP, normal, lateral, microlog, induction) often can locate, correlate, and identify formations of interest. When this information is combined with data obtained from additional logs (caliper, acoustic, radioactivity), the interpretation begins to be diagnostic and quantitative. Finally, in favorable situations, quantitative estimates of porosity, fluid content, water : oil ratio, and so on can be made. The results are controlled by the combination of logs available and borehole and drilling factors.

11.10.2. Combining Measurements from Several Logs

Each log is affected by a number of parameters (Hoyle, 1986) of the rocks and borehole conditions, and different kinds of logs depend on the same parameters. By using combinations of logs, the interpreter hopes to separate these effects.

As an example, consider the measurement of porosity. Resistivity, sonic, density, and neutron log measurements all depend on both the porosity and the lithology, but in different ways. *Cross-plots* involve plotting results from different kinds of measurements against each other. Figure 11.42 shows plots of the porosity calculated from density and from neutron logs. These calculations, in limestone porosity units, presumably give correct porosity values if the lithology is limestone (the limestone curve on this graph is linear with 45° slope). However, if the lithology is not limestone, the porosity is in error, but by different amounts depending on the nature of the lithology; thus the location of a plotted point on this graph gives both the lithology and the correct porosity. For mixed lithologies, interpolation be-

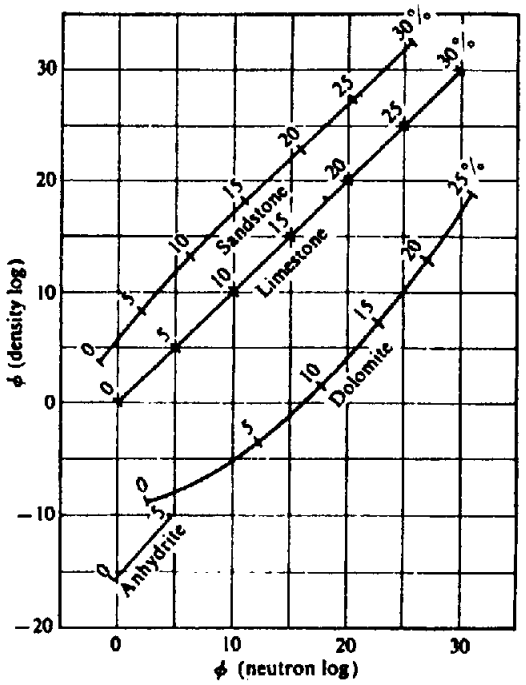

Figure 11.42. Porosity cross-plot. (Courtesy Schlumberger Ltd.)

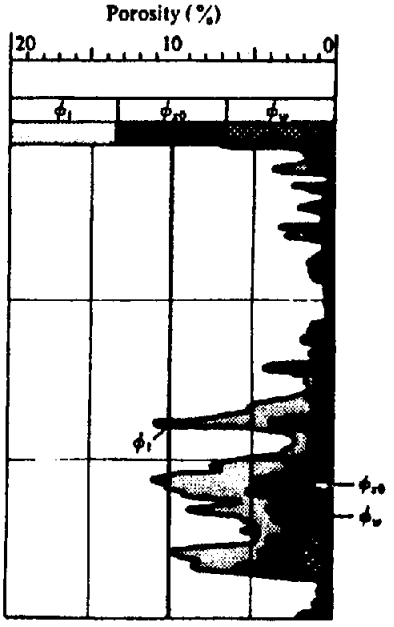

Figure 11.43. Moveable oil plot. (Courtesy Schlumberger Ltd.)

tween the curves gives the porosity and the average lithology, although the latter usually involves some ambiguity. Hopefully this can be further reduced by cross-plotting different log combinations.

The fact that the porosity determined from different logs is different is used in a moveable-oil plot (Fig. 11.43). Total porosity (ϕ_t) is calculated from a sonic log (§11.7.2), apparent water-filled porosity (ϕ_w) from a deep-investigation resistivity log such as a laterolog (§11.2.3), and flushed zone porosity (ϕ_{xo}) from a shallow resistivity log such as a microlaterolog (§11.2.5). The difference between the latter two curves is interpreted as "moveable hydrocarbons" and the difference between the first two as "residual hydrocarbons."

The concept of cross-plotting two sets of measurements to separate the effects of two factors can be generalized to separate more than two factors. Extended analysis generally requires a computer with lookup tables of empirical relationships. Several analysis programs are now available. The Saraband* sand–shale program utilizes five cross-plots and the Coriband* complex lithology program utilizes many more. The "wild-card" in most analyses is clay content. Ions in the layer of water surrounding clay minerals contribute to the rock conductivity, requiring modification of relations, such as the Archie equations, which assume that the formation water is the only conductor present. A dual-water model allows for both the bound water and the formation water. It forms the basis for several computer-analysis programs (Volan*, Cyberlook*, and Global*).

11.11. FIELD EXAMPLES

Although the detailed interpretation of well-log data is beyond the scope of this book, a few simple examples may indicate the possibilities. These are taken mainly from Pickett (1970). The variety of minerals encountered in these examples illustrates the versatility of logging techniques, especially combinations of logs.

11.11.1. Analysis of an Oil Sand

Figure 11.44 shows SP, resistivity, and acoustic-velocity logs for a Miocene sand section containing gas and oil. The SP log has a distinct break of 100 mV from positive to negative at 9,270 ft, indicating shale above and sand below this (compare with Fig. 11.12). Having found the mud filtrate resistivity by other means, we can use Equation (11.9) to get ρ_w; it is about 0.06 Ωm. Using a combination of the lateral and normal curves with departure charts to correct for borehole, invasion, and thin-bed effects, we obtain the formation resistivity ρ_t. It is about 30 Ωm from 9,272 to 9,308 ft and 0.6 Ωm between 9,308 and 9,350 ft. Finally, by means of Equation (11.3), the water saturation S_w is found to be about 15% between 9,272 and 9,308 ft and 100% below 9,308 ft.

Significant qualitative information may also be derived from these logs. Separation of the two microlog curves (note that the electrode spacing is different) indicates sections that are more permeable. The resistivity logs suggest which of these contain gas and oil (because of the resultant high resistivity).

In this rather simple example using only four logs, we can estimate a possible 15 ft of gas-bearing sand and 15 ft of oil-bearing sand, both having an average porosity of 30% [calculated from the sonic log and Eq. (11.14b)] and a water saturation of about 15%.

11.11.2. Analysis of Carbonate Section

The section in Figure 11.45 consists of dolomitic sands, evaporites, carbonates, and shaly carbonates. Gamma-ray, sonic, SP, and induction logs are shown at the left. The break in the SP curve is less definite than in the previous example so that an estimate of ρ_w would be unreliable. The induction log gives a reasonable value for ρ_t in the sands, but not for the higher-resistivity carbonates. The porosity estimate from the acoustic log was questionable because the values of V_f and V_m for Equation (11.14) were not well established. Thus an evaluation of the carbonates was not possible with this log combination.

Neutron and focused resistivity logs were added to aid in determining ϕ and ρ_t in the carbonates. In both these devices the relative response between different zones was reliable but the absolute calibration was not. Sand porosities obtained from the acoustic log were used to calibrate the neutron-log response and the carbonate porosities were then determined. A similar calibration of the Laterolog-7, using the induction-log response in sands, permitted estimates of ρ_t in the carbonates. Values of ρ_w were obtained by measurements on cores. This interpretation does not seem as satisfactory as in the previous example; more logs would be required for a more reliable evaluation.

11.11.3. Coal Identification

Coal may be identified by high resistivity, low density, and low acoustic velocity. Electric logs were used as early as 1931 for this purpose. Figure 11.46 shows a section containing bituminous coal beds from a well in Colorado. The logging program included density, sonic, induction, 16 in. normal, γ-ray

Tradename of Schlumberger, Ltd.

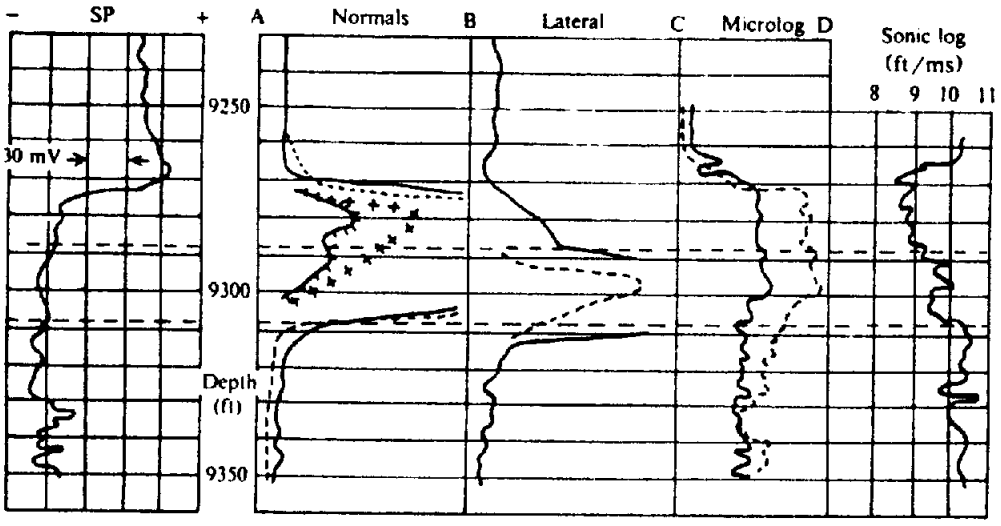

Figure 11.44. Log suite in Miocene sand section containing oil and gas. Full scale for the 16 in. normal (solid curve) is 10 Ωm, for the amplified 16 in. normal (solid hachured) is 100 Ωm, for the 64 in. normal (dashed) is 10 Ωm, for the amplified 64 in. normal (crosses) is 1,000 Ωm, for the 18 ft 8 in. lateral (solid) is 10 Ωm, for the amplified 18 ft 8 in. lateral (dashed) is 100 Ωm, and for the microlog inverse (solid) and for the micronormal (dashed) is 10 Ωm.

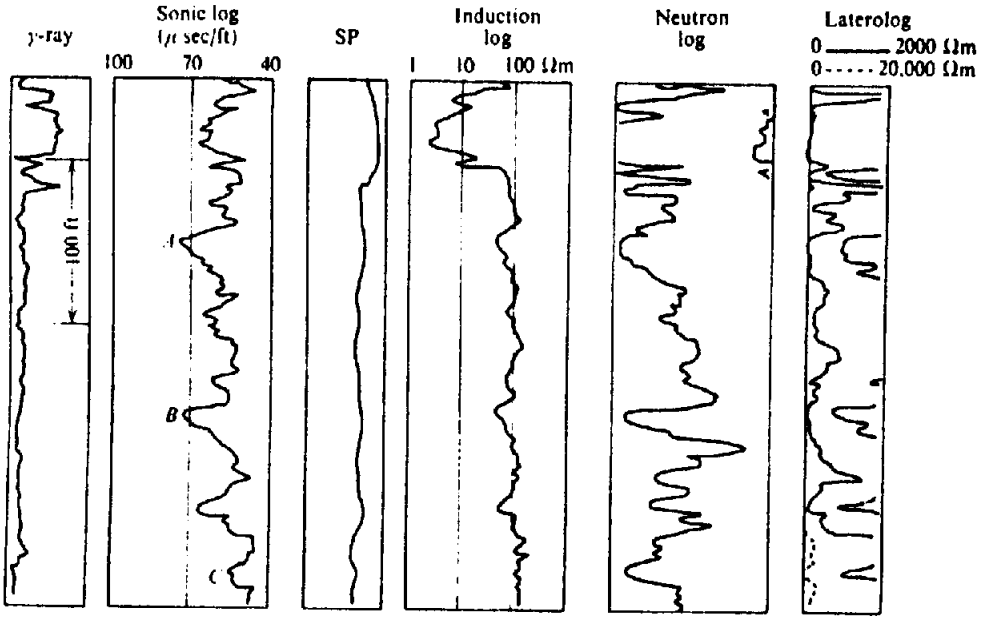

Figure 11.45. Log suite in Minnelusa oil-bearing sand section. Zones A, B, and C contain oil.

(not shown), and SP logs. The first three correlate particularly well with coal seams.

Generally the Δt values from the sonic log are larger for coal than in the adjacent shale beds, although the contrast depends on the coal grade and depth, both of which affect the compaction. For example, lignite produces a larger Δt excursion than anthracite, but increasing depth of burial will reduce the variation. The same factors affect the resistivity log, because higher grade coal and deeper beds contain less moisture and consequently have higher resistivity. The density log is probably the most reliable, because coal density is considerably lower than that of the adjacent beds, ranging from a maximum of 1.8 for anthracite to less than 1.0 g/cm^3 for lignite. The SP curve occasionally is anomalous opposite a coal seam.

11.11.4. Evaporites

Caliper, γ-ray, and density curves through a section of interbedded shale, halite, and anhydrite are displayed in Figure 11.47. Halite and anhydrite are nonradioactive evaporites. The γ-ray log would be

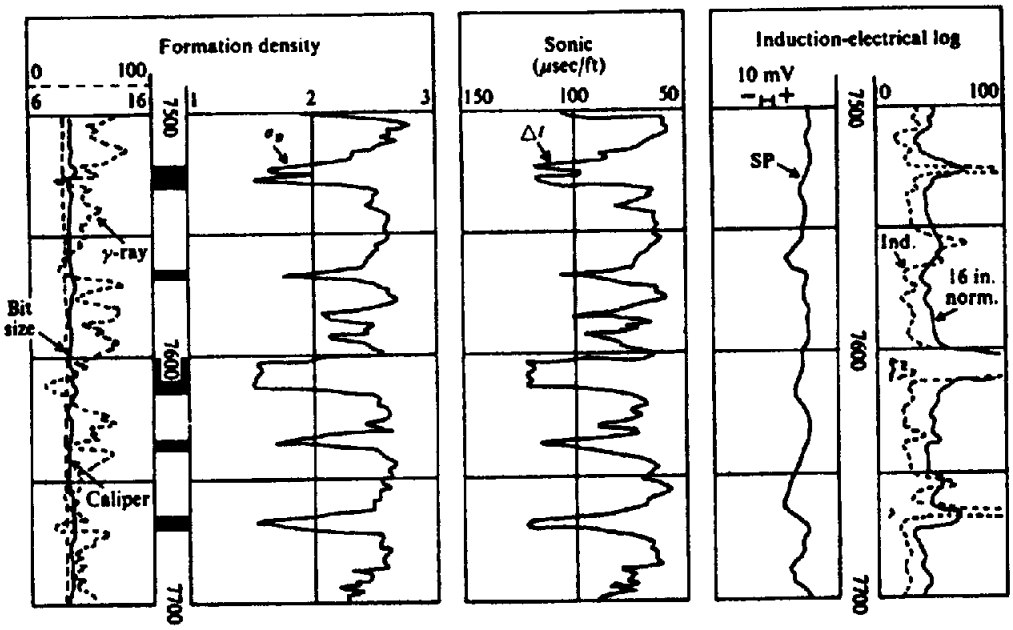

Figure 11.46. Identification of coal beds by density, sonic, and resistivity logs. (From Tixier and Alger, 1970.)

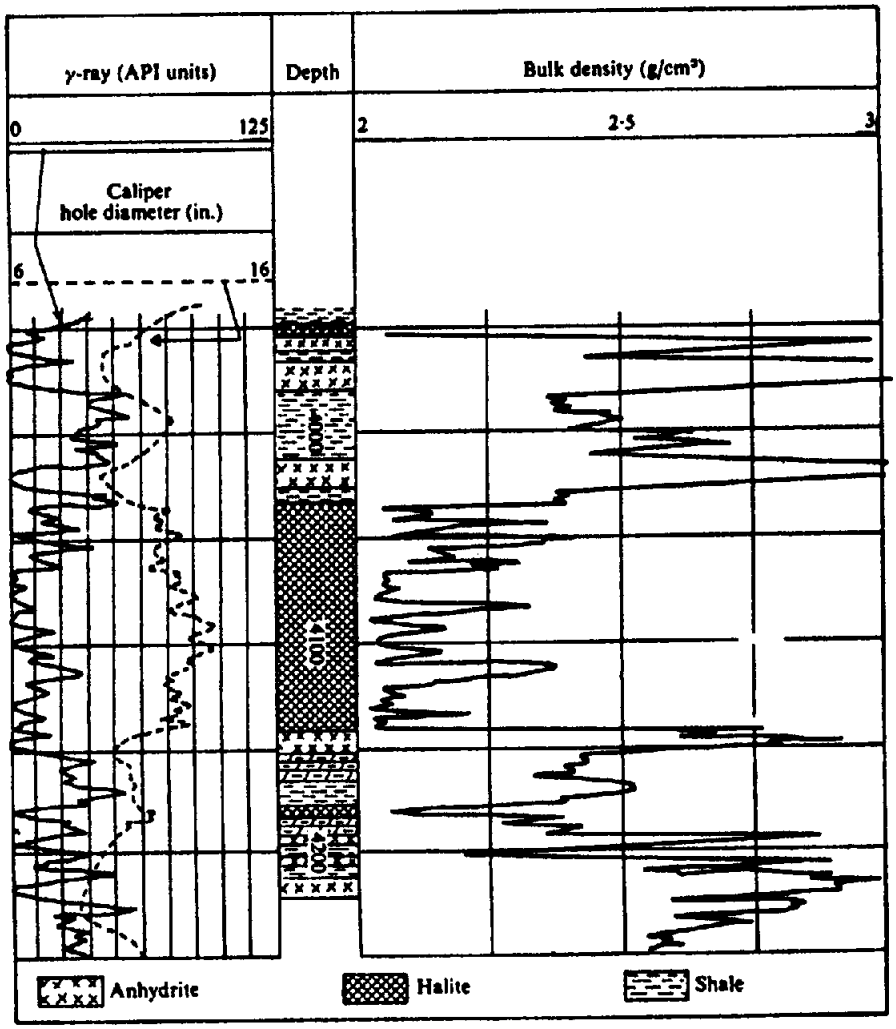

Figure 11.47. Identification of evaporites by density, γ-ray, and caliper logs. (From Tixier and Alger, 1970.)

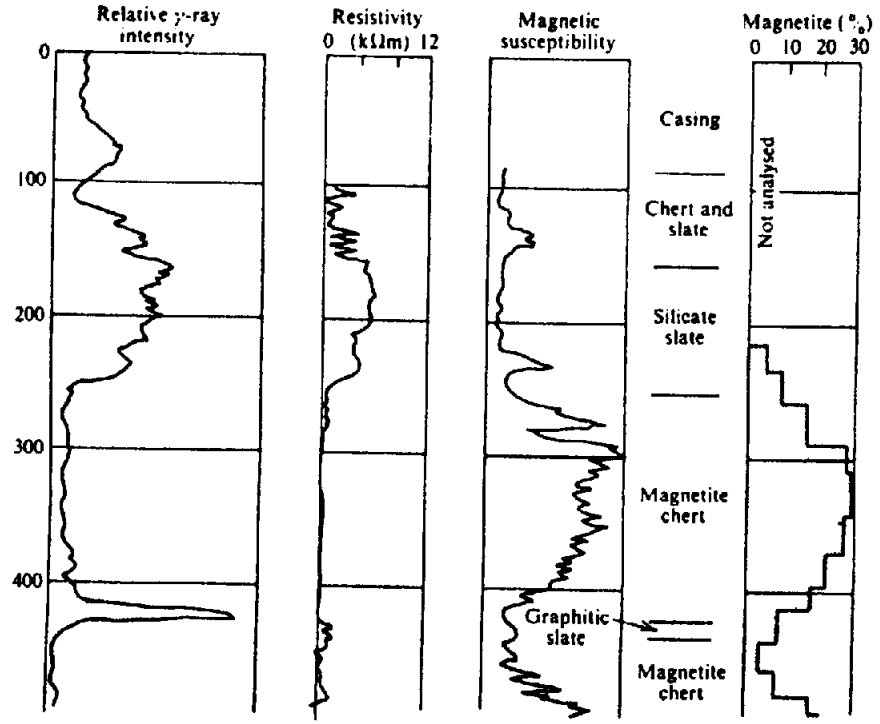

Figure 11.48. Gamma-ray, susceptibility, and resistivity logs in chert and slate beds.

more useful for potash, sylvite, and similar varieties containing potassium. The γ-ray log identifies the shale beds because of their higher radioactivity. The caliper log shows hole enlargement in the salt and shale zones. Anhydrite, with a density of nearly 3 g/cm^3, is clearly identified by the density log, whereas the intercalated shale is indicated by coincident highs and lows in the γ-ray and density curves.

11.11.5. Sulfur

Sulfur, which occurs mainly in limestone, may be identified by the density or acoustic log because of its low density and low velocity (large Δt). The neutron log is also useful in sulfur detection. Occasionally the neutron log is replaced by a resistivity device for porosity determination.

In formations containing only limestone, sulfur, and water, two of these logs may suffice to provide a quantitative evaluation as well as identification. Where other rock minerals are also present, it may be necessary to employ all three logs.

11.11.6. Slate and Chert

Figure 11.48 shows resistivity, γ-ray, and magnetic-susceptibility logs through a section of slate and chert beds. The γ-ray log clearly shows the slate because of its K content and the susceptibility curves show the chert because it is enriched with magnetite.

11.11.7. Mineral Exploration

The Lac Dufault orebody northwest of Noranda, Quebec, is a classic example of the use of geophysical well logging in mining exploration where no other technique is feasible. Massive sulfides, pyrite, pyrrhotite, chalcopyrite, and sphalerite are found in gently dipping contacts between rhyolite and andesite at depths greater than 1,000 ft. Although the lateral extent of these ore zones is small, the high grade of chalcopyrite and sphalerite makes an attractive mining operation, provided they can be located. However, a deep-hole diamond drilling program on 200 ft centers is extremely costly.

Salt (1966) described a logging study that was carried out in 1962 using vertical-loop EM, horizontal-loop EM (large Turam-type transmitter loop), induced-polarization, and resistivity methods. The problem was to establish the existence of a nearby mineralized zone by logging a hole that missed it. It was found that any one of these methods would detect an orebody roughly 400 × 400 ft in horizontal extent and 150 ft thick using a vertical drill hole within 125 ft of the edge of the orebody. However, it was difficult to determine the direction of the orebody with respect to the hole and to distinguish between massive sulfides and other conductors of unknown character. A plan of the orebody and diamond-drill-hole (DDH) locations can be seen in Figure 11.49a.

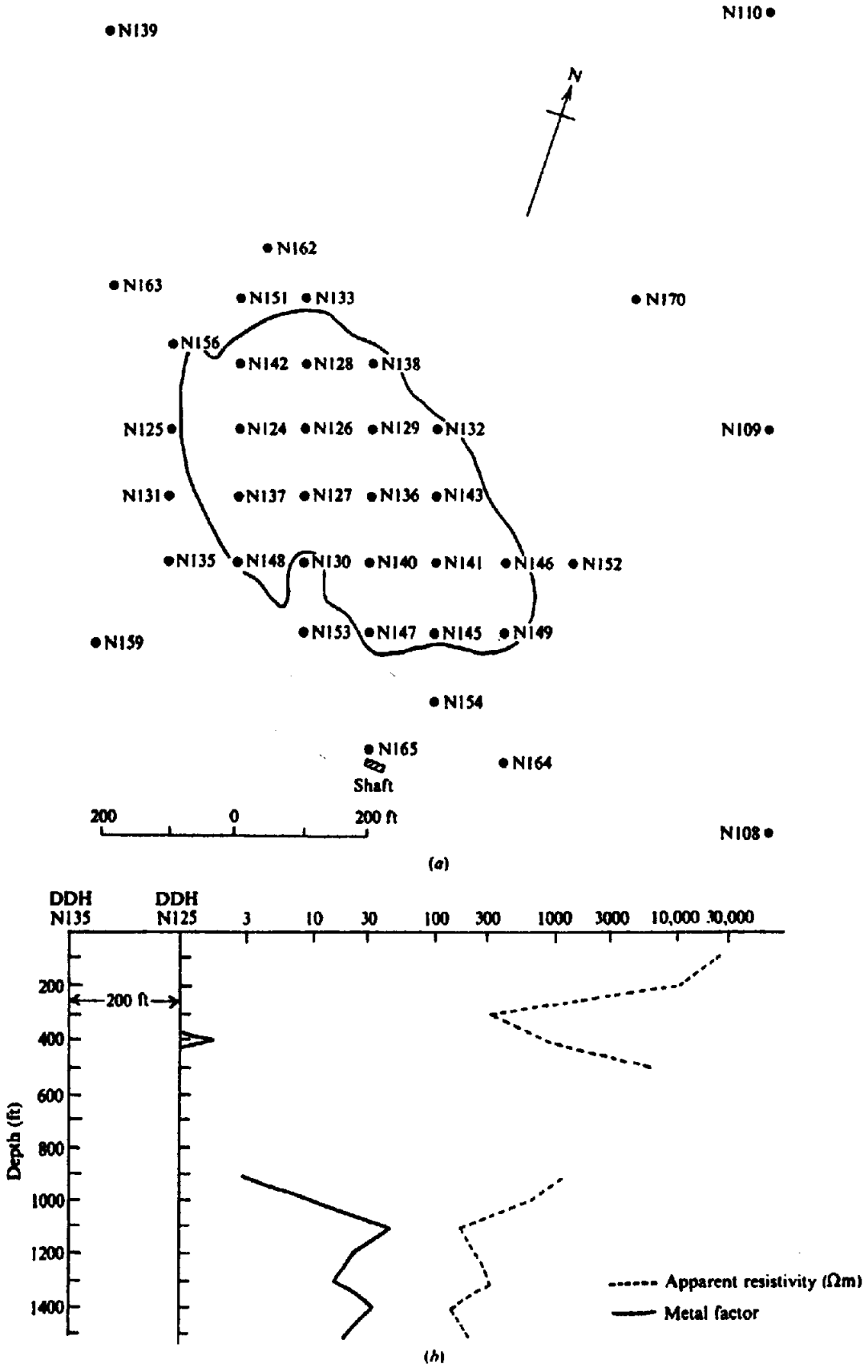

Figure 11.49. Combined IP– electrical survey to locate orebody at depth, Lac Dufault, Quebec. (From Salt, 1966.) (a) Plan of orebody and diamond-drill holes. (b) IP logs in DDH N125 and N135.

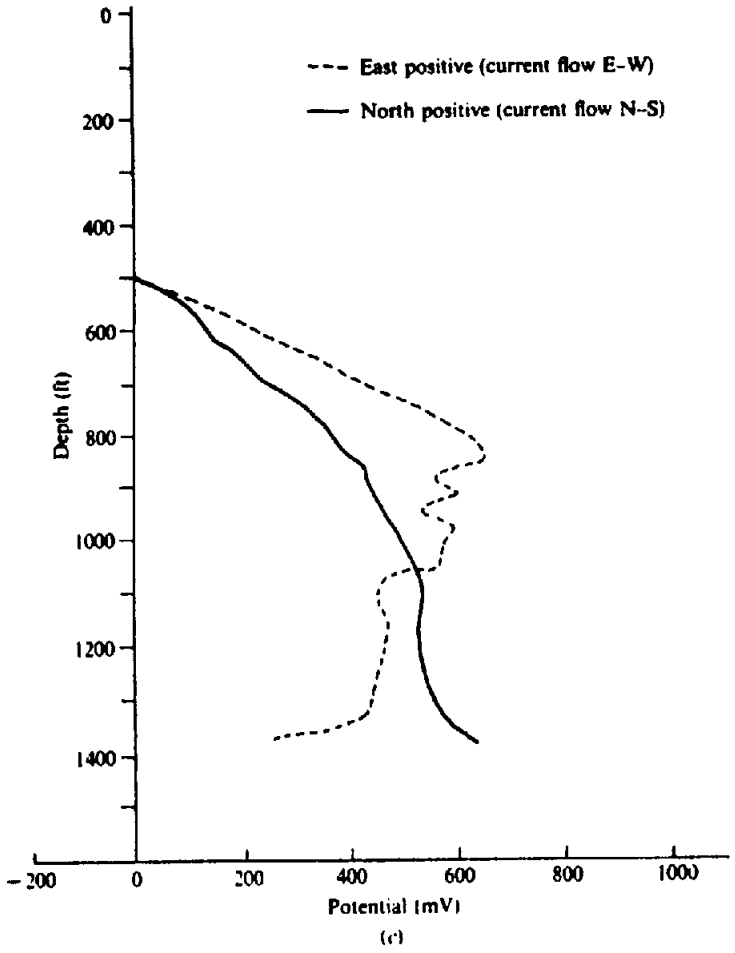

Figure 11.49. (Continued) (c) Log of potential in DDH N135.

Two logs from this study are shown in Figure 11.49b and c. Figure 11.49b shows metal factor and apparent resistivity measured with a frequency-domain IP unit. Large cable-coupling effects made it necessary to place the current and potential electrodes in separate drill holes (N125 and N135); with one current electrode at a distant point on the surface, a second current electrode was lowered down one hole and the two potential electrodes down the other at the same time. In Figure 11.49b the anomaly around 400 ft is not explained, but a definite peak at 1,100 ft corresponds to the massive sulfides east of the electrodes. Both the MF and ρ_a peaks decrease slowly to 1,300 ft, indicating that the sulfides lie mainly below 1,100 ft. The response at 1,400 ft is caused by disseminated sulfides below the main ore zone.

The second log, Figure 11.49c, is essentially the vertical potential distribution produced by current flow from two orthogonal pairs of current electrodes (connected alternately) at the surface. One potential electrode is fixed near the top of DDH N135 and the other is lowered in the hole, while direct current flows from north to south between surface electrodes 2,000 ft apart straddling the hole. Then the moveable potential electrode is raised, with current flow E-W between similarly spaced current electrodes. In both curves the potential increases steadily downhole to about 850 ft. The E-W potential curve remains relatively constant between 850 and 1,050 ft and then falls off at greater depths. This effect is not apparent in the N-S curve, although the positive gradient is not so pronounced below 850 ft. From the differences between the two curves and the direction of current flow, one concludes that a conductor is located east of drill hole N135 and has a depth extent no greater than 200 ft.

Neither log is conclusive by itself, nor were the other techniques used in the survey. However, the reduction of drilling costs by allowing increased hole spacing would be significant and the possible control of future drilling programs by immediate logging is attractive.

11.11.8. Borehole Methods in the USSR

Borehole geophysics apparently is essentially routine in the USSR (Zietz et al., 1976; Buselli, 1980). Well logging is carried out during detailed surveys with all types of mineralization; this is said to reduce by 50%

Table 11.5. *Well-logging techniques used in USSR.*

Borehole logging method	Purposes for which used
Various nuclear logs	Qualitative, quantitative mineral valuation
Gamma, gamma-spectroscopy	Locate U, Th, K, evaluate formations
Gamma-gamma	Determine density, porosity, clay content
Three-component magnetics and magnetic susceptibility	Dip, strike measurements, evaluate formations, locate and trace missed beds
IP, resistivity	Structure, continuity, sulfide evaluation
Three-component EM	Outline structures, locate missed conductors
SP	Determine depth extent of sulfide bodies

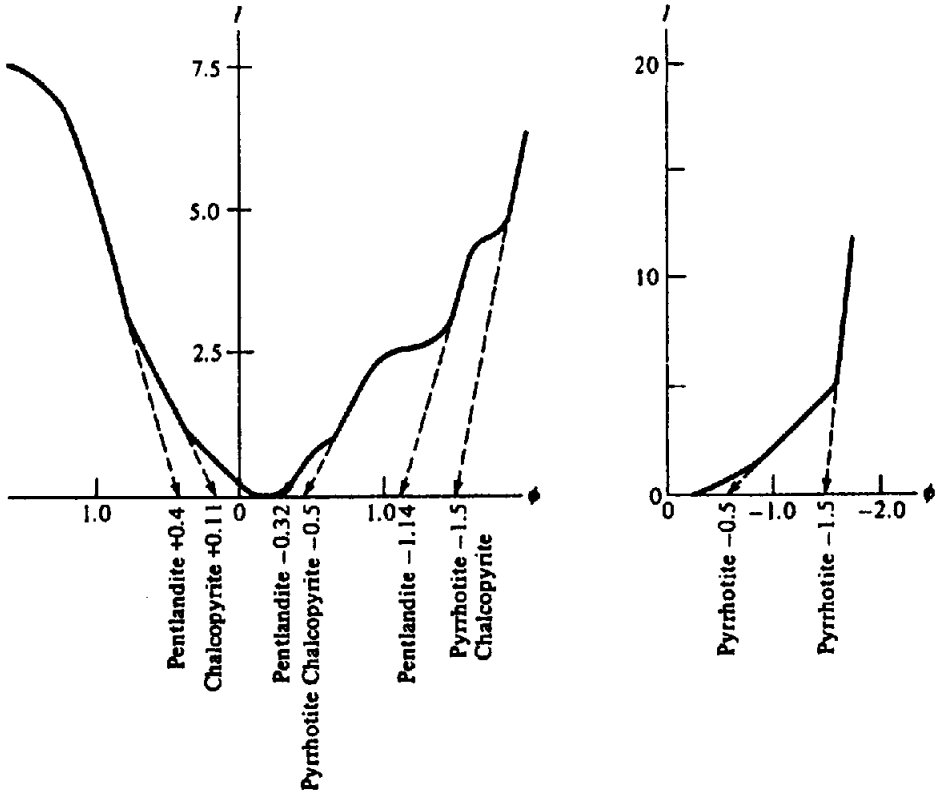

Figure 11.50. Polarization curves for a copper–nickel and pyrrhotite ore bodies. Current I is in amperes and contact potential ϕ is in volts.

the drilling required to evaluate an orebody. Table 11.5 lists methods and applications; the last four methods in this table are used between holes and for *mise-à-la-masse* applications as well as in single holes.

An *acoustic shadow* technique uses an exploding wire source in one hole and receivers in another a few hundred meters distant. It is designed to outline faults, fractures, and anomalous beds. A radiowave shadow technique using frequencies in the range 150 kHz to 40 MHz is used to locate conductors in hole-to-hole measurements.

A piezeoelectric method detects seismic and electric signals from a small explosive charge; it is used to trace quartz veins, sphalerite, and cassiterite mineralization between adjacent holes up to 120 m apart.

A contact method of polarization (somewhat analogous to *mise-à-la-masse*, see §8.5.4d) uses one current electrode downhole in contact with mineralization and the other on the surface; voltage measurements are made on a surface grid as current is increased from 0 to ~ 250 A. The breaks in a curve (Fig. 11.50) represent diagnostic contact potentials of various minerals; these are identified by extending the linear segments back to the ϕ axis. The maximum current required to produce complete polarization curves indicates whether the mineralization is economic.

11.12. PROBLEMS

1. In the example in Section 11.11.7, is it possible to conclude from the IP log that the conductor is

definitely located east of drill holes N125 and N135 or merely that it is either east or west?

A direct-current source was used with the surface electrodes for the resistivity log in hole N135. By sketching the current lines and equipotentials, attempt to reproduce the curves in Figure 11.49c. How would you change either curve if the electrode polarization were reversed? Sketch the E–W potential curve if the drill holes were east of the orebody. What difference would it make if ac were used?

2. The IP log shown in Figure 11.51 was obtained in a base-metal survey in northwestern Quebec. The mineralization consists of pyrite (up to 20%) and chalcopyrite (maximum 2.6% Cu) in a host rock of tuffs and agglomerates. One current and one potential electrode were lowered in the hole with

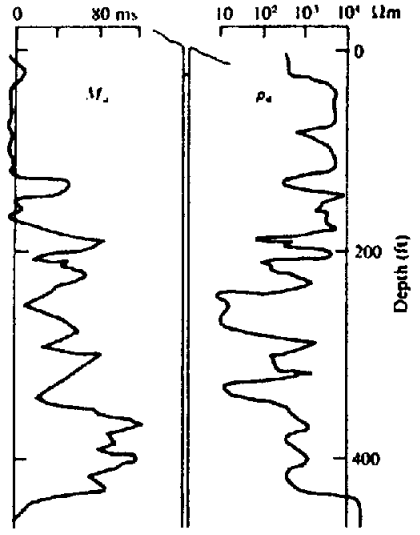

Figure 11.51. IP log in northwest Quebec.

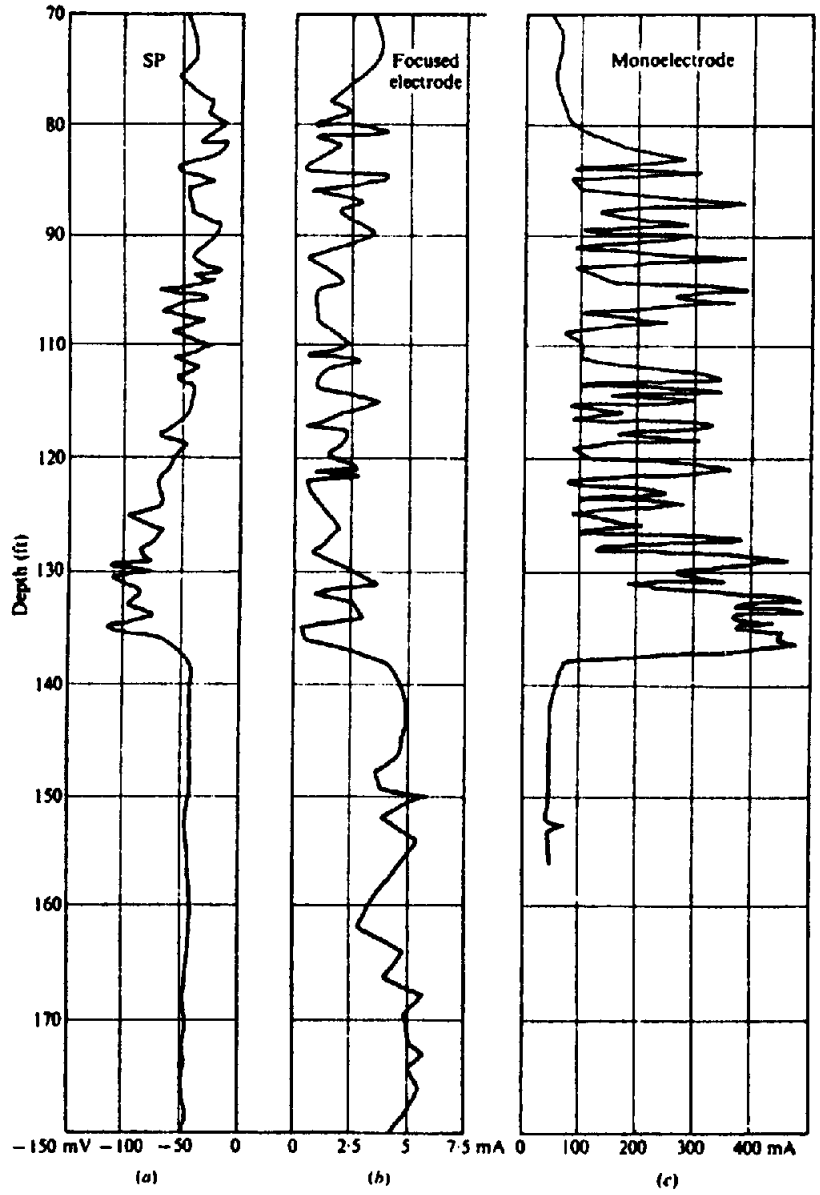

Figure 11.52. Experimental logs in base-metal area. (a) SP log. (b) Focused electrode sonde. (c) Monoelectrode survey using current-return electrode 80 to 110 ft deep in adjacent hole.

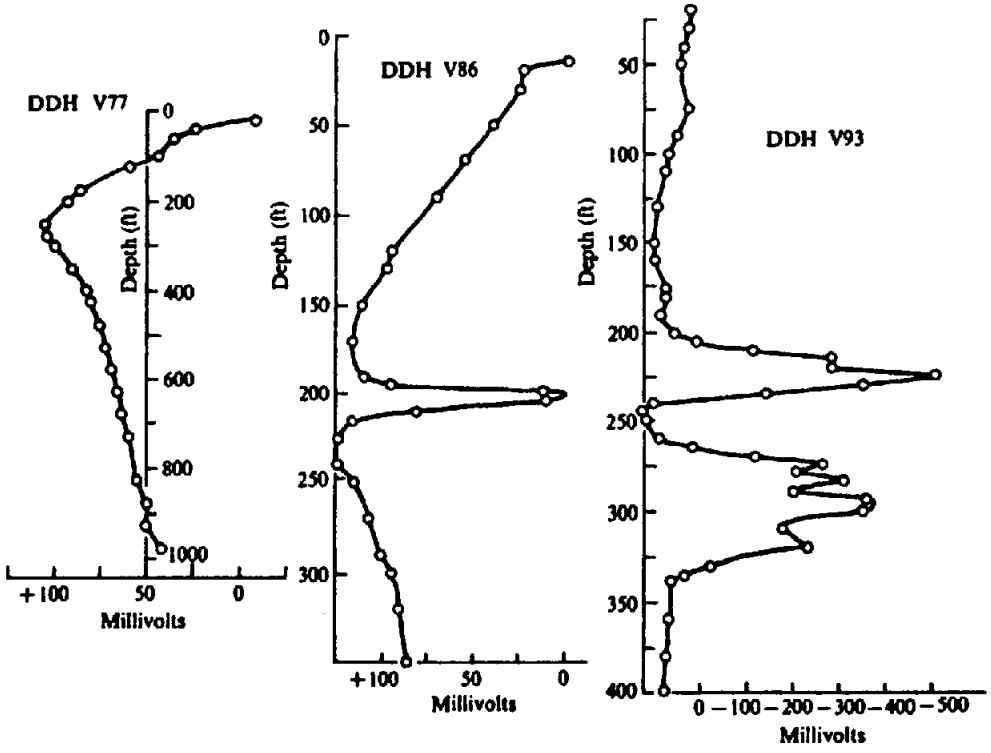

Figure 11.53. SP-logs in base-metal zones.

a fixed separation of 2 ft; the second current and potential electrodes were located on the surface at a considerable distance from the drill collar. Identify the mineral zones and if possible distinguish between chalcopyrite and pyrite sections.

3. Some results from an experimental logging study in base-metal areas are shown in Figure 11.52. The mineralization here occurs in two steeply dipping zones, one containing pyrite and chalcopyrite, the other mainly pyrite. The diamond-drill hole from which the logs were obtained was inclined approximately 60°.

   The SP log is conventional with one fixed electrode in the hole just below the water level (and below the casing). The focused-electrode sonde, similar to Figure 11.6a, was made from 1 in. diameter lead–antimony pipe with PVC spacers, with 2 ft guard electrodes, 3 in. measuring electrode, and 2.5 in. spacers. Current return was through the uphole fixed SP electrode. The current source was a small 60 Hz motor generator.

   The *monoelectrode* curve in Figure 11.52 measured the current between the focused-electrode system and a second hole (previously logged and found to be essentially barren) in an attempt to establish mineralization continuity. The electrode in the second hole (an aluminum rod) was long enough to straddle the main mineral intersections; specifically, it extended from 80 to 110 ft. The two holes were about 100 ft apart. Identify the mineralization zone or zones. Is there any indication of lateral extent? Calculate the effective resistivity at a few points on the focused resistivity curve from the formula of Dakhnov (1962),

$$\rho_e = 2\pi\left(\frac{L_m}{L_r}\right)\left(\frac{V}{I}\right)\frac{(L_r^2-1)^{1/2}}{\log(L_r^2-1)}$$

   where L_m is the length of the focused electrode, L_r is the ratio of length to diameter of the electrode assembly, V is the potential of the focused electrode (110 V), and I is the current in the focused electrode.

4. SP logs at a base-metal property in northwestern Quebec are shown in Figure 11.53. The host rocks are andesites, diorites, and rhyolites, the overburden is sand and clay. The mineralization consists of pyrite, pyrrhotite, sphalerite, chalcopyrite, and, in places, bands of magnetite. An earlier surface SP survey showed no anomaly. What is your explanation for the barren surface SP? Given the additional information that massive sulfides were found from 25 to 31 ft and from 65 to 89 ft in a fourth hole nearby, would you change your explanation? Can you account for the pronounced positive excursion in holes V77 and V86 between surface and 200 ft? Make as complete as interpretation as you can.
5. Use of airborne and ground radiometrics for gold exploration has been reported in Soviet journals since 1970; these indicate a strong association

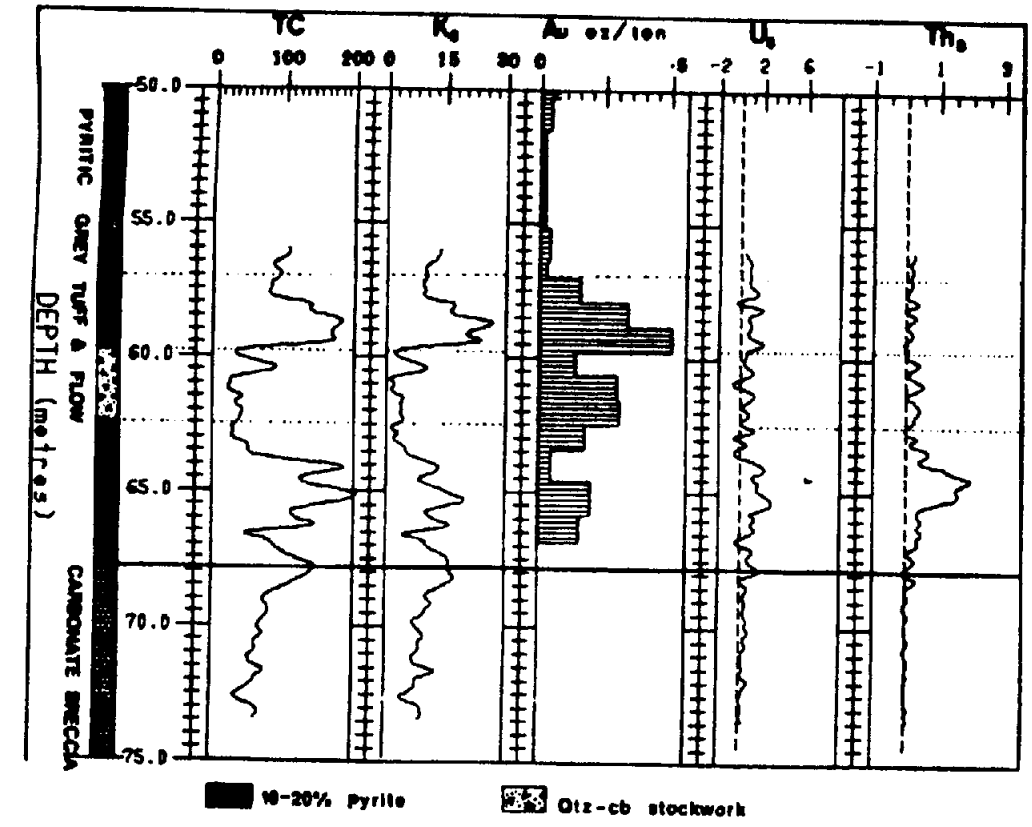

(a)

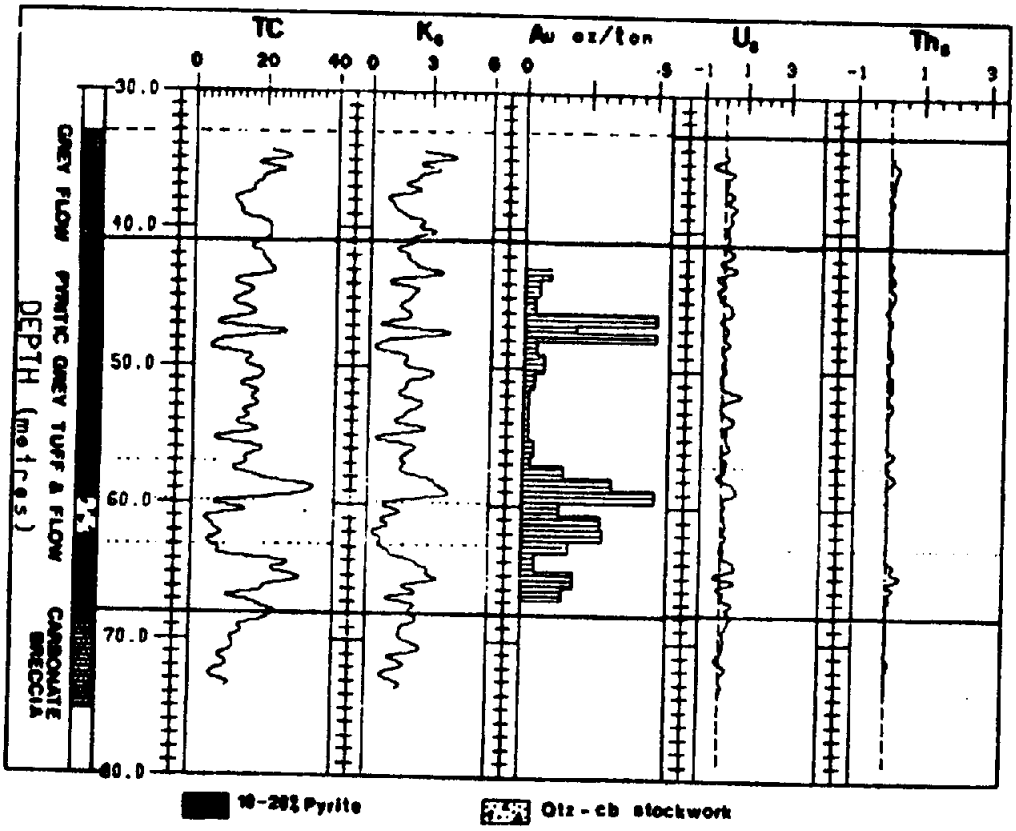

(b)

Figure 11.54. Gamma-ray spectral logs in four boreholes in the Larder Lake gold camp, northern Ontario. (a) Logs in boreholes BL-80-25, (b) BL-80-40.

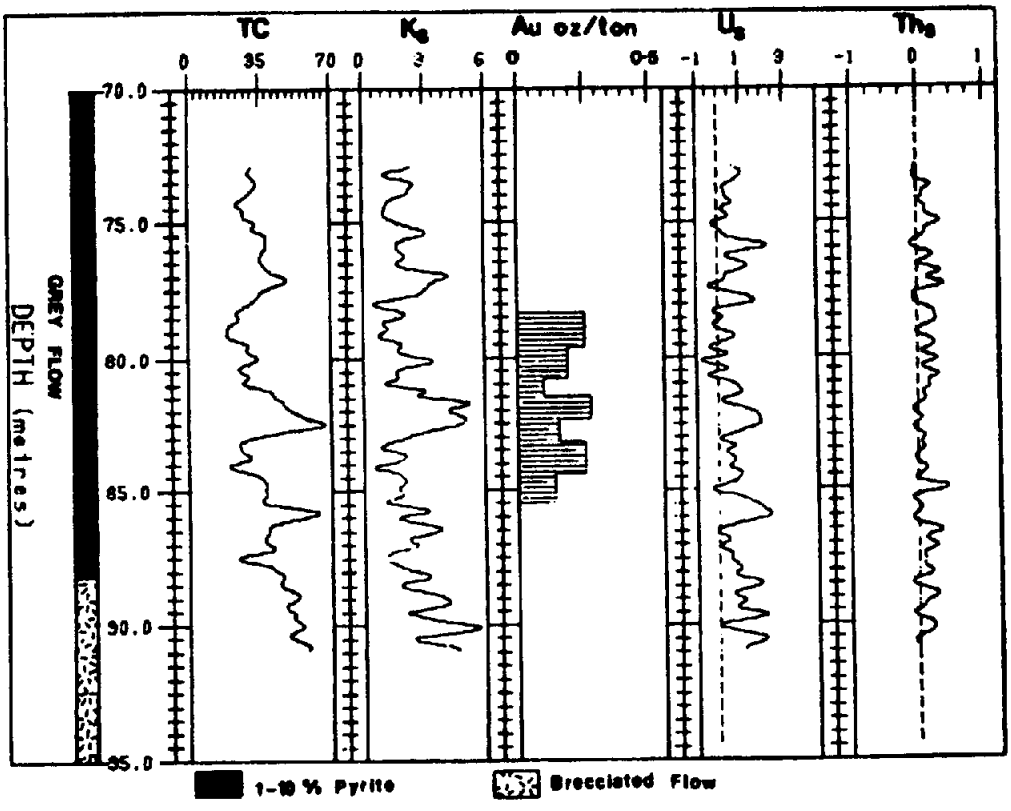

(c)

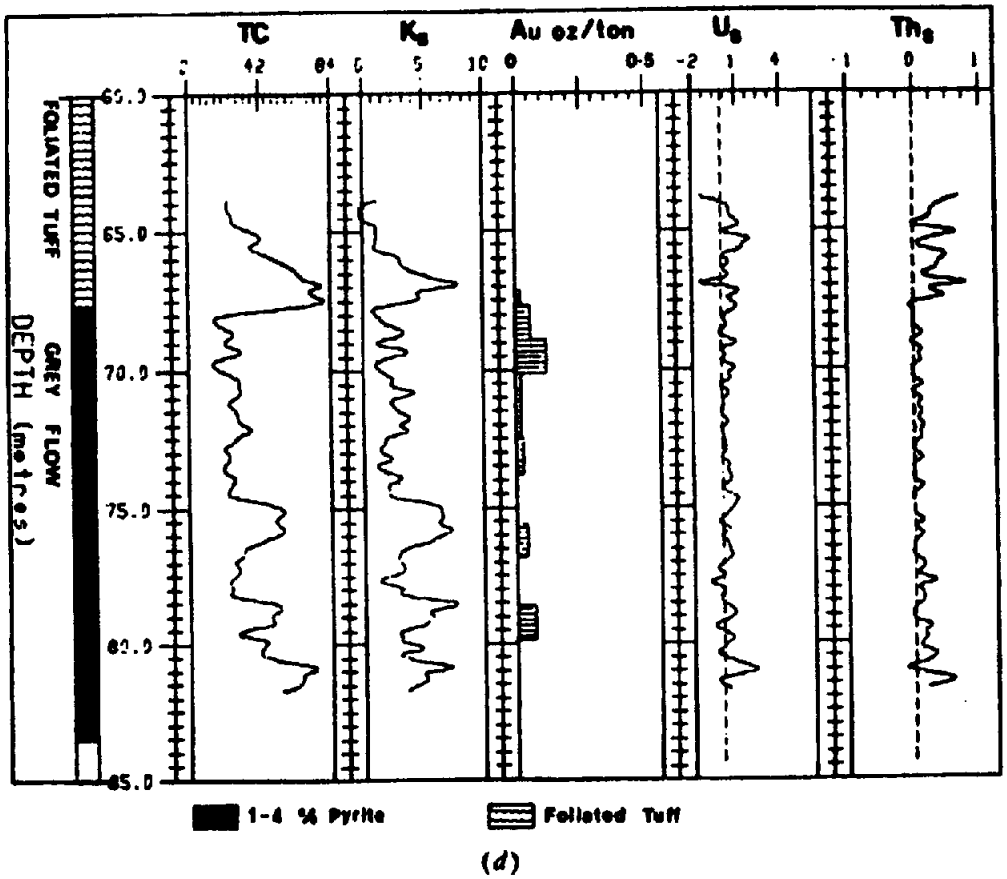

(d)

Figure 11.54. (Continued) (c) BL-80-31. (d) BL-80-30. (From Mwenifumbo, Urbancic, and Killeen, 1983.)

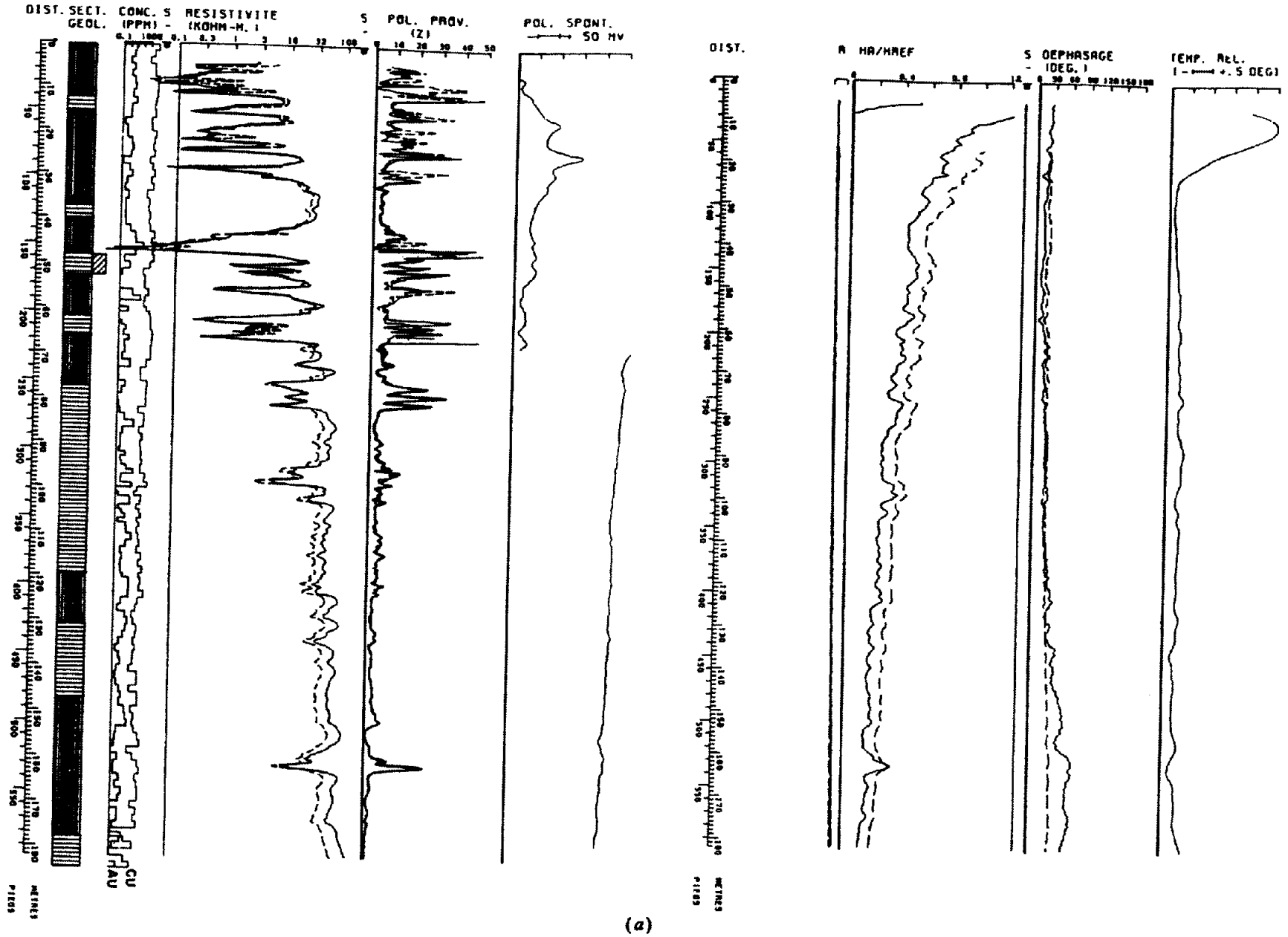

Figure 11.55. Logs from three holes in the Pascalis gold area near Val d'Or in northern Quebec. For the first hole, gold and copper assays are shown; for the second hole, gold assays are shown. (a) Logs in boreholes 83 – 22.

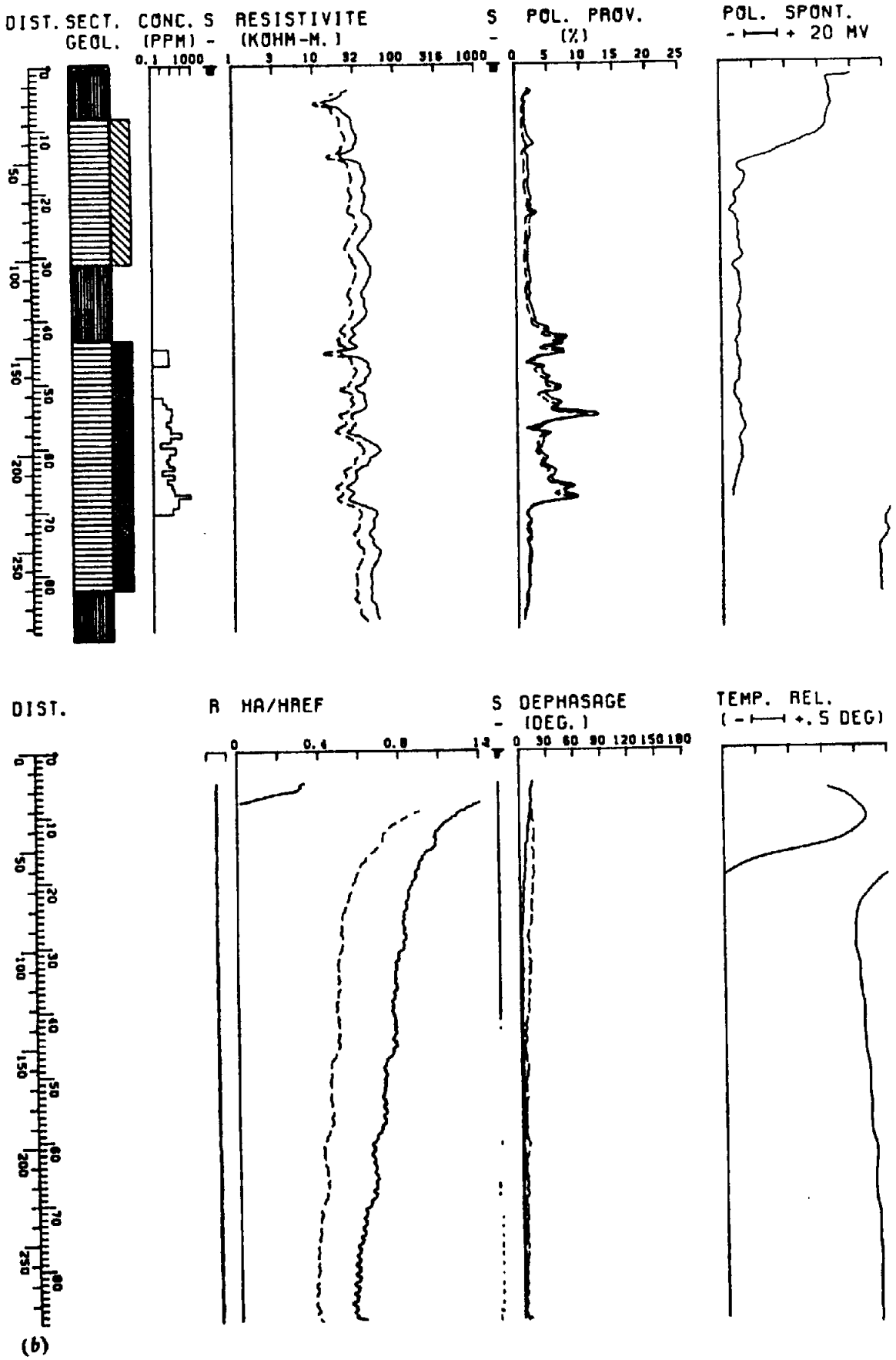

Figure 11.55. (Continued) (b) 83– 102.

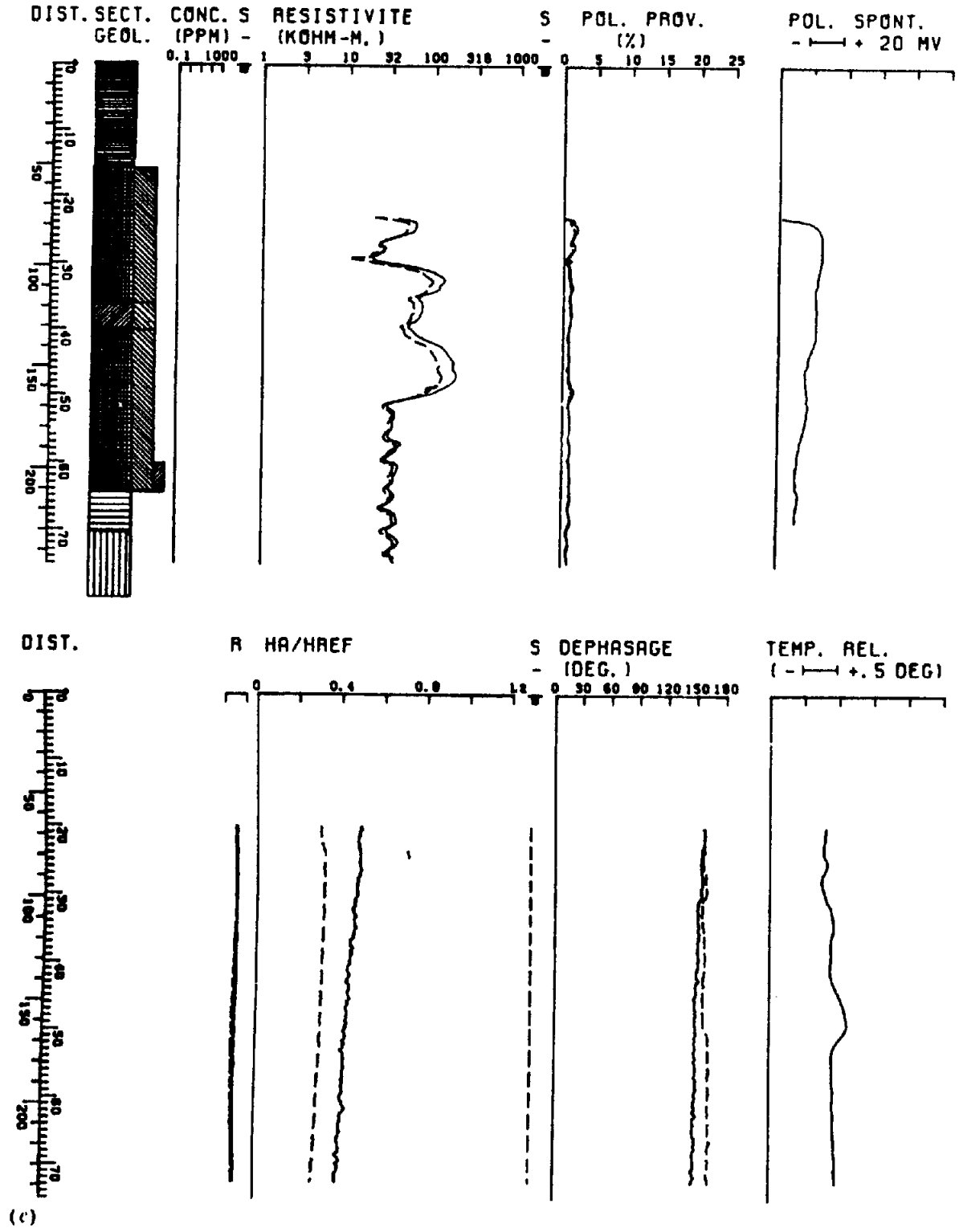

Figure 11.55. (Continued) (c) 83 – 116.

between gold mineralization and potassium alteration zones. Mwenifumbo, Urbancic, and Killeen (1983) applied γ-ray spectral logging in the Larder Lake gold camp in northern Ontario. They used a Geological Survey of Canada logging unit described in Conaway, Bristow, and Killeen (1980). Results from four boreholes are displayed in Figure 11.54 which include total count (TC), stripped K, U, and Th (K_s, U_s, and Th_s) (§10.7, problem 4), gold assay (Au), and core logs showing pyrite mineralization. The geology consists of flow-type pyritized and silicified zones lying in altered volcanic flows and tuffs. Gold correlation with pyrite mineralization is very good. What can you say about gold association with ^{40}K? The ratios Th/K, U/K, and U/Th are used as halo indicators around mineral deposits; do they correlate with gold? What logging techniques are suited for detecting the pyrite zones? Some elementary statistical analysis should be useful.

6. Pyrite, after quartz, is the most abundant mineral associated with gold; a more general statement would link gold occurrences with a variety of sulfide mineralization. Examples are shown in Figure 11.55 from the Pascalis gold deposit near Val d'Or in northern Quebec (Roy, 1984). Three drill holes were logged with SP, IP, resistivity, and VLF EM tools. The SP is conventional with one electrode downhole, the other at surface. IP and resistivity, measured simultaneously, are identical either in the normal or pole-dipole configuration. Two spacings are available for each; for the normal, $AM = 0.4$ or 0.8 m, $MN = 7.5$ or 2.2 m, respectively, whereas for the pole-dipole, $AM = MN = 7.5$ or 15 m. The VLF log measures two phase components of the downhole signal, with a maximum-coupled magnetic sensor at the surface for phase and amplitude reference. The VLF frequencies used were 17.8 kHz (NAA Cutler) and 21.4 kHz (NSS Annapolis). Figure 11.55 shows an uninteresting SP log, strong IP, and resistivity response at the two normal spacings, much less so for the pole-dipole. Figure 11.55a also shows gold and copper assays over the 180 m depth extent of DDH 83-22 and Figure 11.55b shows only gold. The VLF amplitude and phase variations have been normalized. Correlate these logs with gold and copper as completely as possible.

REFERENCES

Archie, G. E. 1942. The electrical resistivity log as an aid in determining some reservoir characteristics. *Trans. A.I.M.E.* 146, 54–64.

Becker, A., and Telford, W. M. 1965. Spontaneous polarization studies. *Geophys. Prosp.* 13, 173–88.

Buselli, G. 1980. Electrical geophysics in the U.S.S.R. *Geophysics* 45, 1551–62.

Conaway, J. G., Bristow, Q., and Killeen, P. G. 1980. Optimization of gamma-ray logging techniques for uranium. *Geophysics* 45, 292–311.

Dakhnov, V. N. 1962. Geophysical well logging. *Quarterly of Col. School of Mines* 57.

Doll, H. G. 1949. Introduction to induction logging and applications to logging of wells drilled with oil-based mud. *Trans. A.I.M.E.* 186, 148–62.

Doll, H. G. 1951. The laterolog, a new resistivity logging method with electrodes using an automatic focusing system. *Trans. A.I.M.E.* 192, 305–16.

Doll, H. G. 1953. The microlaterolog. *Trans. A.I.M.E.* 198, 17–32.

Freedman, R., and Vogiatzis, K. P. 1979. Theory of microwave dielectric constant logging using the electromagnetic wave propagation method. *Geophysics* 44, 969–86.

Gilreath, J. A. 1987. Dipmeter interpretation rules. In *The Technical Review*. Houston: Schlumberger Educational Services.

Glenn, W. E., and Nelson, P. H. 1979. Borehole logging techniques applied to base-metal ore deposits. In *Geophysics and geochemistry in the search for metallic ores*, P. J. Hood, ed., Econ. Geol. Report 31, Geol. Surv. Canada, pp. 273–94.

Hoyle, J. B. 1986. Computer techniques for the zoning and correlation of well-logs. *Geophys. Prosp.* 34, 648–64.

Jackson, P. D. 1981. Focused electrical resistivity arrays: Some theoretical and practical experiments. *Geophys. Prosp.* 29, 601–26.

Keys, W. S., and MacCarey, L. M. 1971. Applications of borehole geophysics to water resources investigations. In *Techniques of Water Resources Investigation*, Book 2, Ch. E1. Washington: U.S. Geol. Surv.

Labo, J. 1987. *A Practical Introduction to Borehole Geophysics*. Tulsa: Society of Exploration Geophysicists.

Mansinha, L., and Mwenifumbo, C. J. 1983. A mise-à-la-masse study of the Cavendish geophysical test site. *Geophysics* 48, 1252–7.

Moran, J. H. 1972. Discussion on radius of investigation in dc resistivity well logging. *Geophysics* 37, 542–3.

Moran, J. H., and Chemali, R. E. 1979. More on the Laterolog device. *Geophys. Prosp.* 27, 902–3.

Morris, C. F., Little, T. M., and Letton, W. 1984. Soc. Petr. Eng. 59th Ann. Fall Tech. Conf., paper SPE 13285.

Mwenifumbo, C. J., Urbancic, T. I., and Killeen, P. G. 1983. Preliminary studies on gamma-ray spectral logging in exploration for gold. In *Current research, Part A*, Geol. Surv. Can. Paper 83-1A, pp. 391–7.

Nickel, H., Sender, R., Thierbach, R., and Weichart, H. 1983. Exploring the interior of salt domes from boreholes. *Geophys. Prosp.* 31, 131–48.

Paillet, F. L., and White, J. E. 1982. Acoustic modes of propagation in the borehole and their relationship to rock properties. *Geophysics* 47, 1215–28.

Pascal, H. 1983. Further discussion of attenuation and dispersion of electromagnetic wave propagation in fluid-saturated rocks and applications to dielectric constant well logging. *Geophysics* 48, 1373–80.

Pickett, G. R. 1970. Applications for borehole geophysics in geophysical exploration. *Geophysics* 35, 81–92.

Pinnington, D., ed. 1981. *Well Evaluation Conference, Abu Dhabi*. Ridgefield (CT): Schlumberger.

Pirson, S. J. 1970. *Geologic Well Log Analysis*. Houston: Gulf Publishing.

Roy, A., and Dhar, R. L. 1971. Radius of investigation in dc resistivity well logging. *Geophysics* 36, 754–60.

Roy, J. 1984. Electrical methods in mineral well logging. Ph.D. thesis, McGill Univ., Montreal.

Salt, D. J. 1966. Tests of drill-hole methods of geophysical prospecting on the property of Lac Dufault Mines Ltd., Dufresnoy Twp., Quebec. In *Mining Geophysics*, vol. I, pp. 206–26. Tulsa: Society of Exploration Geophysicists.

Schlumberger 1972. *Log Interpretation I – Principles*. Houston: Schlumberger Ltd.

Schlumberger 1986. *Log Interpretation Charts*. Houston: Schlumberger Educational Services.

Schlumberger 1987. *Log Interpretation Principles / Applications*. Houston: Schlumberger Educational Services.

Schmitt, D. P., and Bouchon, M. 1985. Full-wave acoustic logging: Synthetic microseismograms and frequency-wavenumber analysis. *Geophysics* 50, 1756–78.

Segesman, F. F. 1980. History of geophysical exploration: Well logging method. *Geophysics* 45, 1667–84.

Seigel, H. O. 1979. An overview of mining geophysics. In *Geophysics and geochemistry in the search for metallic ores*, P. J. Hood, ed., Econ. Geol. Report 31, Geol. Surv. Canada, pp. 7–24.

Sheriff, R. E., and Geldart, L. P. 1982. *Exploration Seismology*, vol. I. Cambridge: Cambridge University Press.

Silva, J. B. C., and Hohmann, G. W. 1981. Interpretation of three-component borehole magnetometer data. *Geophysics* 46, 1721–31.

Snyder, D. D., and Fleming, D. B. 1985. Well logging – a 25 year perspective. *Geophysics* 50, 2504–29.

Tittman, J. 1986. *Geophysical Well Logging*. New York: Academic Press.

Tixier, M. P., and Alger, R. P. 1970. Log evaluation of non-metallic deposits. *Geophysics* 35, 124–42.

Wagg, D. M., and Seigel, H. O. 1963. IP in drill holes. *Can. Mining Jour.* 84, 54–9.

Wahl, J. S. 1983. Gamma-ray logging. *Geophysics* 48, 1536–50.

Worthington, M. H., Kuckes, A., and Oristaglio, M. 1981. A borehole induction procedure for investigating electrical conductivity structure within the broad vicinity of a hole. *Geophysics* 46, 65–7.

Wyllie, M. R. J. 1949. A quantitative analysis of the electrochemical component of the SP curve. *Trans. A.I.M.E.* 186, 17–26.

Wyllie, M. R. J., Gregory, A. R., and Gardner, G. H. F. 1958. An experimental investigation of factors affecting elastic wave velocities in porous media. *Geophysics* 23, 459–93.

Zeitz, I., Eaton, G. P., Frischknecht, F. C., Kane, M. F., and Moss, C. K. 1976. A Western view of mining geophysics in the USSR. *Geophysics* 41, 310–23.

Zemanek, J., Caldwell, R. L., Glenn, E. E., Holcomb, S. V., Norton, L. J., and Strauss, A. J. D. 1970. The borehole televiewer – a new logging concept for fracture location and other types of borehole investigation. *Jour. Petr. Tech.* 21, 762–74.